Development of horizontal memristive devices and their potential application as memsensors

Dissertation

zur Erlangung des akademischen Grades

Doktor der Ingenieurwissenschaften

(Dr.-Ing.)

der Technischen Fakultät

der Christian-Albrechts-Universität zu Kiel

Eric Alexander Victor Petar Kaidas

Kiel

22.06.2017

Erstgutachter: Prof. Dr. rer. nat. Rainer Adelung

Zweitgutachter: Prof. Dr. Lorenz Kienle

Datum der mündlichen Prüfung: 27.07.2017

Abstract

Since their invention sensor devices have become widely used in modern technologies. Their broad range of possible applications have made them crucial and mandatory in various areas for today's life to ensure safety and comfort. As demonstrated by ongoing research for augmenting devices, i.e. by enhancing efficiency or reliability, there is still room for further improvements, as for instance the gas sensors that are employed in solvent cabinets for safety reasons. The challenge in such environment is to attain the sensors functionality as it is continuously exposed to a certain amount of solvents and will therefore always show a bias concentration. This might lead to an oversight of sudden leaks or alike and thus to false conclusions. An improvement in this kind of application area can be achieved by implementing memristive sensors. These devices provide the opportunity not only to detect gases as common sensors do, but can become acclimatized to the atmosphere of a solvent cabinet, comparable to a human nose. This memory potential facilitates much safer and more accurate sensing and would only issue an alarm when certain gas compositions could result in a harmful event such as an explosion. The scope of this thesis is the development of an easy to fabricate and reliable memristive sensor. The presented devices work on the nanometer scale and follow an easily contrivable horizontal approach. The first one is novel and based on metal oxide needles bridging two gold contacts with highly promising gas sensing and memristive capabilities. The second and new device consists of a plain microchip (with gaps in the size between 1 and 10 µm) decorated with CNTs (carbon nanotubes) and Au (gold) and Ag (silver) clusters, bearing the potential of an excellent sensing device due to its high detection area to device volume ratio and simple production possibility. These two approaches will be investigated by means of electron microscopy and in their current – voltage characteristics by performing hysteresis measurements. In the end the advantages and disadvantages for these devices will be discussed and compared.

Since the second approach is entirely new the application of different CNT dispersions for the sample preparation will be discussed in more detail. The pros and cons of various deposition techniques will be investigated such as simple drop and spray coating and the differences between swiping and tipping a dispersion droplet for the resulting CNT network on the sample, as well as the impact of treatments with acids, bases or an applied electric field on the needed sparseness of the network. In addition the crucial influence of different thin coatings on the chip and the temperature during deposition will be examined. The generation of silver clusters is carried out by cluster sputter deposition; their deposition was monitored in situ through the electrical resistivity over the gap. Furthermore the effect of the addition of differently applied gold clusters, as well as their resulting forms, will be investigated in the course of this thesis, as well as working mechanism will be analyzed with the help a Monte Carlo simulation, resulting in a memristive switching device.

Kurzzusammenfassung

Seit ihrer Erfindung haben sensorische Geräte große Anwendung in modernen Technologien gefunden. Ihre große Bandbreite an Anwendungsmöglichkeiten hat dazu geführt, dass sie aus Bereichen unseres täglichen Lebens zur Gewährleistung von Sicherheit und Komfort nicht mehr wegzudenken sind. Andauernde Untersuchungen zeigen, unter anderem durch Verbesserung der Effizienz oder Wiederholbarkeit, dass es noch viel Raum zur Verbesserung gibt, wie zum Beispiel bei der Verwendung von Gassensoren die aus Sicherheitsgründen in Lösemittelschränken eingesetzt werden. Die Herausforderung hier ist es die Funktionalität des Sensors zu bewahren, da er ständigem Gasaustritt ausgesetzt ist und daher immer ein hohes Level an Hintergrundrauschen zeigen wird. Dies kann dazu führen, dass plötzliche Gaslecks übersehen werden oder es zu anderen falschen Rückschlüssen kommt. Eine Verbesserung kann daher in diesem Bereich die Verwendung von memristiven Sensoren darstellen. Diese Systeme ermöglichen nicht nur die Detektierung von Gasen wie herkömmliche Sensoren, sondern können sich der Atmosphäre in einem Lösemittelschrank, ähnlich wie eine menschliche Nase, anpassen. Diese Möglichkeit der Anpassung/Erinnerung ermöglicht ein sehr viel sichereres und genaueres Erfassen der Atmosphäre und würde nur einen Alarm auslösen, wenn es Aufgrund der vorherrschenden Gaskomposition zu einer Explosion käme.

Der Fokus der vorliegenden Arbeit liegt auf der Entwicklung eines einfach herzustellenden und verlässlichen memristiven Sensors. Die präsentierten Bauelemente arbeiten auf der Nanometerebene und basieren auf horizontalen und einfach umzusetzenden Ansätzen.
Der erste ist neuartig, zeigt vielversprechende Fähigkeiten in der Detektierung von Gasen, sowie memristive Fähigkeiten und basiert auf der Verwendung von Metaloxidnadeln, die zwei Goldkontakte miteinander verbinden. Das zweite neue Bauelement besteht aus einem einfachen Mikrochip (mit Lücken zwischen 1 und 10 µm) der mit CNTs (Kohlenstoffnanoröhrchen) und Gold- und Silberclustern dekoriert ist und aufgrund seiner hohen detektierfähigen Oberfläche, sowie der Möglichkeit einer einfachen Herstellung, das Potential eines hervorragenden sensorischen Bauteils besitzt.
Diese beiden Ansätze werden mit Hilfe von Elektronenmikroskopen untersucht, sowie auf ihre Strom-Spannungs-Charakteristika in Hinsicht auf Hysteresemessungen. Am Ende der Arbeit werden ihre Vor- und Nachteile diskutiert und verglichen.
Da der zweite ein komplett neuartiger Ansatz ist wird die Verwendung von unterschiedlichen CNT-Dispersionen zur Probenherstellung mehr im Detail erfolgen. Die Vor- und Nachteile von verschiedenen Auftragungsmethoden wie einfaches Aufträufeln und Aufsprühen, sowie der Unterschied zwischen drüber streichen und drauftippen des Dispersionstropfens wird in Hinsicht auf das resultierende Netzwerk, sowie dem Einfluss von Säuren, Basen und erhöhten Spannungen

untersucht. Darüber hinaus werden der erhebliche Unterschied von unterschiedlichen Dünnschichten und der Einfluss der Temperatur während der Auftragung untersucht.

Die Herstellung der Silbercluster erfolgt durch Kathodenzerstäubung; während ihre Auftragung durch Wiederstandsmessungen über die Lücken in situ vermessen wird. Darüber hinaus werden der Effekt der Hinzufügung von unterschiedlich aufgetragenen Goldclustern, sowie deren unterschiedlich resultierende Form, im Zuge dieser Thesis näher beleuchtet. Der Arbeitsmechanismus der Proben wird mit Hilfe der Monte Carlo Simulation untersucht und resultiert schlussendlich in einem memristiv schaltbaren Bauteil.

Contents

1 Introduction

The scope of this thesis is the fabrication of a simple to analyze and easy to fabricate memristive device and its potential application as a memristive sensor.

Sensors are electrical components, which are used to detect changes in their environment. They are commonly used as tactile sensors in touch displays, as pressure sensors in gauges, which are established in the vacuum technology or as detectors to determine changes in a gaseous atmosphere or differences in the intensity of light.

The aim for many scientists is to make devices as small as possible. One reasoning for this is to reduce the material costs, but another big advantage of the miniaturization of the sensor is its size-dependent influence on the system. Therefore devices built up from nanowires became the focus of attention (*1–3*), likewise due to their increased sensitivity and quick response times. However, some of these devices exhibit a large cross sensitivity meaning that the device is not sufficiently selective to quantitatively detect one specific gas. Lupan et al. (*4*) reported earlier about gas sensors based on CuO nanowires which at specific temperatures experience the same selectivity for hydrogen as for carbon monoxide. To achieve a good proportionally responding sensor it is feasible to functionalize them to increase their sensitivity as well as their selectivity (*5*). In nature such complex selective sensors are present as well, i.e. in the human body. It contains many systems capable of sensing and therefore possesses the ability to detect changes in pressure, temperature, sound, odor and many more. While most of the engineered sensors respond in a proportional way do the sensors in the human body work differently and become used to their surrounding as temperature or odors, as for example the nose becomes used to certain smells and will only detect changes when they are occurring. This adjusted sensing behavior referred to as habituation helps to avoid a signal overflow of the brain by reducing the amount of sensor responses and information which gives the human body the possibility to focus on other tasks. This adaptability is essential for us. The sensing capability of becoming habituated to certain conditions can be comprehended as some kind of memorization and therefore might be understood as a memristive detection method.

A device which is capable of memorization is the so called memristor (or sometimes referred to as memristive device). The memristor itself is one of the four fundamental electrical components beside the resistor, capacitor and inductor. Initially it was postulated by Chua in the year 1971 (*6*) and realized for the first time in the labs of Hewlett Packard in 2008 (*7*). Characteristic for a memristor is its memristance M, which is defined as the change in the magnetic flux (Φ) divided by the change of the amount of electrical charges (q) (*6*). Therefore a typical memristor is directly linked to the change of the magnetic flux, while commonly fabricated devices are depending on the number of charges that have flowed through it, which leads to a change in its resistance corresponding to the direction of flow. These devices are therefore called memristive devices due to this difference. The phenomenon these devices are based on is called resistive switching, which is the abrupt change of the resistance of a dielectric process. The devices are divided into different classes, depending on the mechanism of their switching process. Some of the classes make use of the movement of anion vacancies (i.e. oxygen movement (*7*)), rely on the change in their atomic arrangement (i.e. in a thin film of vanadium dioxide (*8*)) or cation ion movement (i.e. copper ion movement (*9*)). (*10*)

The combination of memory and sensing is not always beneficial as it is for the human body, but could be the superior choice for a sensing system if used in an environment which is exposed to a high and changing gas concentration as a chemical storage or cabinet. Here a changing level of gas concentrations is always present since the solvent containers are not always perfectly sealed. In these cases an alert notification is mostly unwanted since the fluctuation could still be below the critical atmosphere level and might therefore neither be harmful nor potentially explosive. Hence it is more convenient to use a memristive sensor which launches an alert notification if certain levels of gas concentration are exceeded. Scientists are already working on projects that deal with the fabrication of what they call electronic nose. However, these systems bear the drawback of having a higher level of complexity than a circuit which includes a memristive sensor. Recent work of F. Puppo (*11, 12*), Olumodeji (*13*) and Massoud (*14*) already show first attempts in the fabrication of such a memristive sensors. But most of the published results fall short in regards of their repeatability or that they are limited to the sensing of just one parameter like the pH-value, leaving much room for improvements in regards of their repeatability, reaction times and their capability of what to sense.

To achieve a working device two different approaches will be presented in the scope of this thesis. The first is a novel one and relies on the fabrication and utilization of metal oxide needles and is used to investigate the potential of the future appliance, while the second follows a completely new approach.

It is known that the memristive effect occurs on the nanometer scale. For this reason vertical memristive structures make use of very thin films since here the effect is the strongest (*15*). To realize such nanometer sized gaps for a horizontal arrangement thin needle like structures (*16*) or e-beam lithography designed samples (*17*) are quite often used.

Therefore, the metal oxide approach is based on the fabrication and usage of iron oxide needles bridging gold contacts. The here presented approach does not only show outstanding reaction times and gas sensing capabilities for different analytes, but as well a recurring memristive properties. Because this behavior already shows the great potential of this approach and will be discussed further in this thesis.

To realize the fabrication of a new horizontal memristive device different organic molecules (for example drugs and conjugated polymers) are applied to a chip architecture (bearing several gold gaps) as a 3D dielectric structure, with carbon nanotubes (CNTs) – used as alternative to the dielectric matrix – showing the most promising results. The devices based on CNT networks fabricated and investigated in the course of this thesis rely on the movement of silver ions - following the results of Jo et al. (*18*) who already discussed this mobility phenomena - by forming asymmetric contacts (*19*). In the course of this thesis the influence of various deposition techniques and as well of different surface coatings on the network formation will be discussed. Furthermore, it will be investigated to what extent it is possible to manipulate such nanotube network by applying different acids or high voltages in order to increase its sparseness.

Additionally the advantages and disadvantages of the deposition of silver cluster from solution and sputter deposition will be examined, as well as the possible tuning of the system by introduction of gold clusters to the system to enhance its properties. While validating the working principle on which the device is based via Monte Carlo simulation and resulting in a working device by following this new approach.

All prepared devices presented in this thesis were investigated by performing hysteresis measurements and tuned by applying different voltage pulses dependent on the outcome of the hysteresis. Furthermore due to the bottom-up approach used here, they were examined by observing their topographical structure with a SEM.

This thesis is structured as follows: fundamental theoretical elements of the memristor as well as the applied techniques will be discussed in Chapter 2. Subsequently, the explanation of the working routines used for the depositions and respective setups is covered in Chapter 3. Chapter 4 deals with the results and discussion for the metal oxide device as well as the CNT deposition and manipulation of the network of the new approach and likewise with the deposition of the silver as well as the gold clusters and analysis of the Monte Carlo simulation carried out. Finally Chapter 5 will give a summary of the presented work, a discussion and comparison of the presented devices and an outlook for future works.

2 Theory

2.1 Memristors and Memristive Devices

Like almost every other introduction dealing with memristors or memristive devices this one cannot do otherwise but to mention that the concept of these devices was first postulated in the early 70's by Chua (*6*) and generalized later further with the help of Kang (*20*). Following his assumption there must be one missing element connecting the four fundamental circuit variables (indicated in Figure 1 by the added circle). While the Current (I) and the electrical charge (q) and the Voltage (U) and the magnetic flux (Φ) are connected to each other by the integral of the time, the other ones are connected by two-terminal circuit components. The resistor connects the current and the voltage by the Ohmic law ($R = \frac{dU}{dI}$), which results in a linear behavior as shown in Figure 1b. Both the capacitor as well as the inductor are energy storage devices in which either the voltage lags behind the current phase by 90° or vice versa for the inductor (see Figure 1c, d). These elements can be described by $C = \frac{dU}{dq}$ and $L = \frac{d\Phi}{dI}$ respectively. To maintain the symmetry Chua postulated that the missing element must connect the flux and the charge like $M = \frac{d\Phi}{dq}$(*6*). He described M as being the memristance and named the element memristor, being a hybrid of the words memory and resistor. He added as well that these devices not only show a pinched hysteresis (*21*) but that all switching memories are memristors (*22*). In his first mathematical approaches Chua assumed that the changes for a plot of charge over flux would result in spontaneous increase (or decrease depending on the direction) of the curve (*6*). Though these changes are sometimes not as drastically pronounced as indicated in Figure 1e. In contrast to the capacitor and inductor the memristor is not an energy storing but rather an information storing element. The resistance of the device is not constant and depends on its history. This means that the resistance of the device depends on the amount and direction of electrical charge carriers that have flowed through it. This change in resistance induced by the electrical charge carriers remains even after the power supply was shut off, resulting in a device that possesses

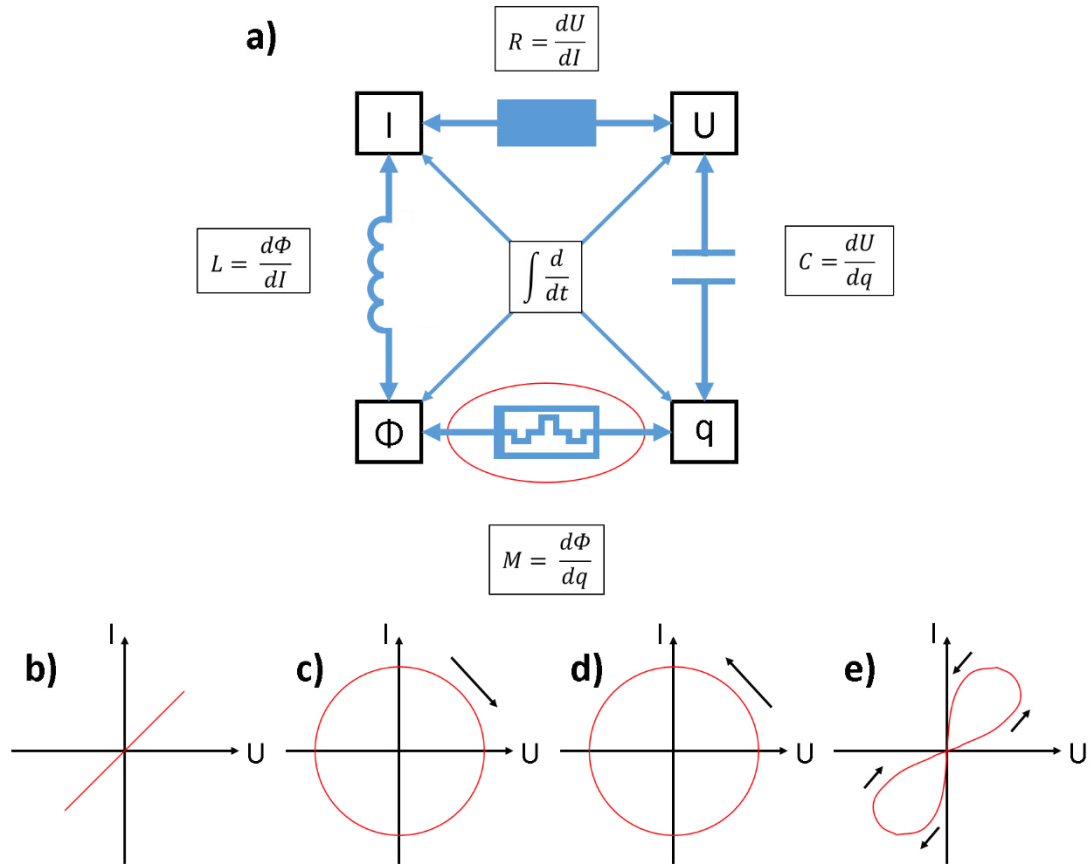

Figure 1: a) The relation between the four fundamental two-terminal circuit elements and their resulting IV curves (b) resistor, c) capacitor, c) inductor, d) memristor) (images based on the following sources (6, 7)).

a memory of its past. The classical memristor links therefore the charge with the magnetic flux having the resistance as the proportionally factor. Most of the practical memristors work in a slightly different way than the postulated one. For this reason the term memristive device was introduced. Its definition is changed slightly from that of the memristor in that the resistance of the device is depending on the number of flown charges through it and its resulting state. For this reason the word memristive device will be used more frequently than memristor in the course of this thesis.

Some years were needed before this concept sparked the interest of the topic memristors in the science community. In 2008 Hewlett-Packard Labs received an U.S. patent (*23*) and Strukov et al. of HP labs published a Nature paper claiming that they found the missing device, the memristor (*7*). This was the beginning for the rise in numbers of papers published on this topic. The first memristor utilized TiO_2 as memristive material. The TiO_2 layer consisted of two regimes with one enriched with oxygen vacancies and showing a higher conductivity. By

applying a voltage it was possible to change the size of the enriched regime and therefore changing the resistivity of the device (*7*). Scientists proved that the memristive effect could not only be addressed with the movement of vacancies. Papers were published showing that the effect could be found in spintronic based devices (*24*), phase-transition systems (*8*), tunnel devices (*25, 26*) or filamentary growth based ones (*27–29*) to name only a few. Different systems were tried, not only the metal/metal oxide, but also bio material (*30, 31*) or polymer (*32, 33*) based ones. Carbon nanotube based systems showed memristive switching behavior (*34–36*) and will be part of this thesis as well.

The possible applications for memristors range from nonvolatile elements like RAMs (*37*) to integration into neuromorphic circuits to mimic learning systems (*38, 39*) up to memristive sensors (*40–42*).

2.2 Lithography

Lithography is a process where, under the usage of a resist, an optical mask and an UV source, desired patterns or parts of thin films up to integrated circuits can be produced (*43*). In a first step a semiconductor surface (e.g. Si wafer) is coated with a thin layer photoresist. There are two different kinds of resists: positive and negative ones. While the polymer chains of the negative resist get strengthened under the exposure of UV light, the ones of the positive resist get weakened. One uses optical masks in order to illuminate only part of the sample. Optical masks consist of a quartz glass plate with a pre-pattern of chromium on top, which shows already the desired structures or a negative image of them (depending on the resist used). A simplified sketch of the process and the corresponding outcome can be seen in Figure 2. The figure shows in part a) the coated wafer being exposed to the UV light while covered by an optical mask. Depending on the resist used it leads to either a positive or negative image of the pattern. By using a developer the parts of the film softened by radiation get removed, as displayed in b. In a next step the open spaces created on the wafer are filled via sputtering (for example) with the desired metals (see Image c). In a last step (Image d) the remaining resist gets removed by bathing the wafer in an appropriate solvent like acetone or N-Methyl-2-pyrrolidone (NMP) and sonicating it afterwards.

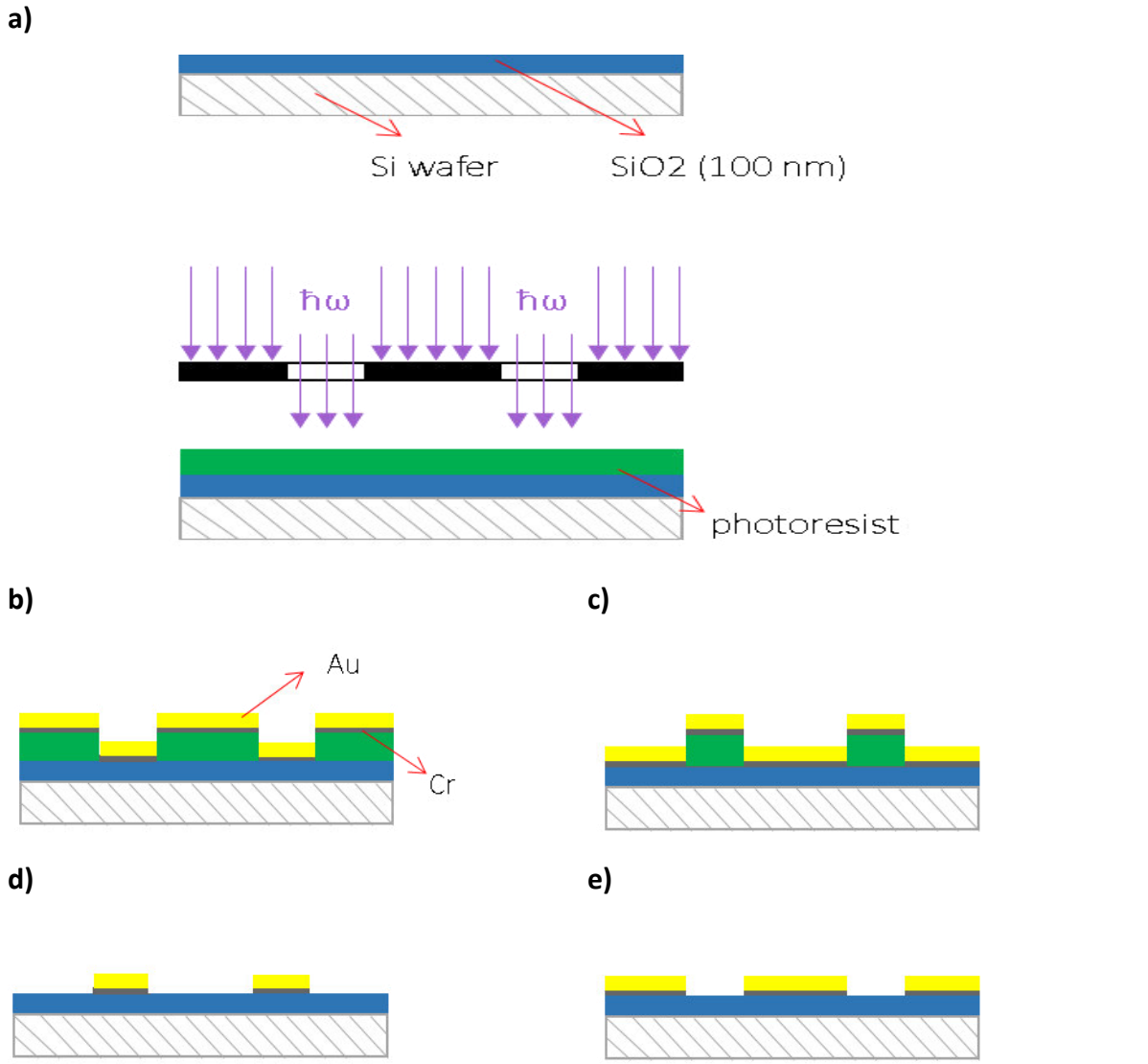

Figure 2: Schematics of sequential steps in a typical optical lithography process a) coating and exposure of the sample b)+c) deposition of the electrodes d)+e) lift-off.

The outcome of the resolution is dependent on the quality of the resist used as well as the wavelength of light used for radiation. The dependence of the resolution on the wavelength can be calculated by using the following formula (*44*):

$$CD = k1 \cdot \frac{\lambda}{NA} \qquad (1)$$

CD stands for the minimum feature size or critical dimension so therefore the maximum resolution. The k1 factor (k1) is a coefficient which represents the process related factors and

is depending on the imaging and the resist system itself. λ is the used wavelength and NA the numerical aperture of the lens in front of the to be structured wafer. Most common values for k1 are around 0,4 whereas values for NA are ranging from 0,25 to 1,7 (*44*). In this thesis a halogen lamp with a wavelength of around 400 nm was used as UV light source.

2.3 Silanization

Silanization belongs to the surface modification methods and describes the addition of silane compounds on the surface. It is widely used either to make the sample surface more attractive for the attachment of biomolecules (*45, 46*) or to make the surface more hydrophobic. The latter one is the desired property for this method in this thesis. Different kinds of silanes can be used for the silanization, leading to a variety of reactions that can take place during the binding of the silane. In Figure 3 a very simplified sketch of this reaction is shown. The sketch shows a reaction of the silicon bearing one organic group (R) and three active reaction groups (X) which can be hydrolyzed. Depending on the number of the active reaction groups it is

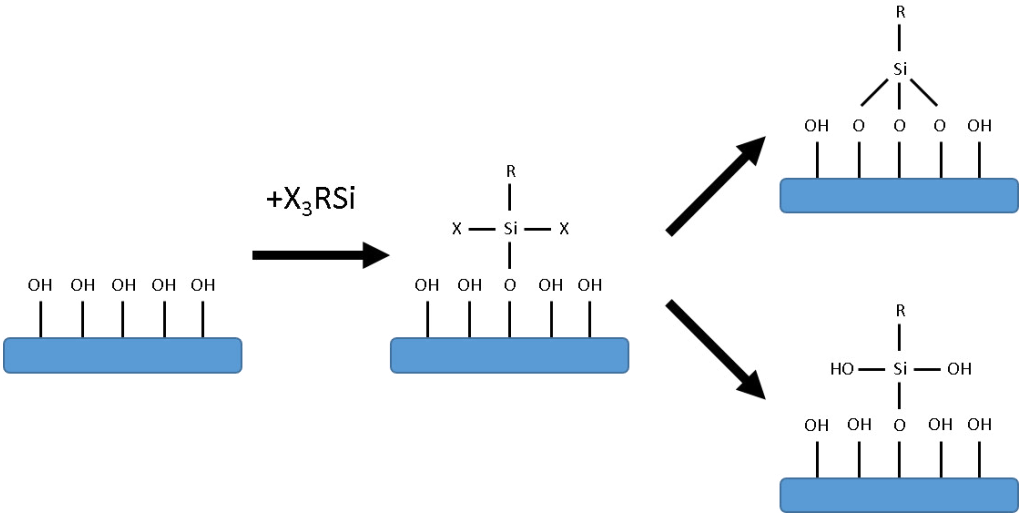

Figure 3: Simplified sketch for a silanization process (47, 48).

either possible that the silane molecule forms up to three bonds with the sample (as indicated in the figure) or the reactive groups get substituted by –OH groups. This reaction step takes place under the influence of water, which can be adsorbed at the sample surface prior to the reaction. Intermediate states are possible as well, where the molecule is double bonded to

the sample surface while one of its side arms is substituted. In addition to the described reactions the formation of siloxane groups where silane groups react with each other is possible as well. In this case a vertical polymerization takes place, leading to a monolayer of the silane on top of the sample. (*47*–*49*)

2.4 Sputtering and percolation

Sputtering in general belongs to the class of physical vapor deposition techniques (PVD). The working principle is that inert gas atoms get ionized by an applied electrical field and accelerated in the direction of the target to be sputtered. Caused by their high kinetic energy at the impact the bombardment of the target with the ions leads to erosion and extraction of material from the target. The extracted material condenses either at the walls of the vacuum chamber or at the sample surface. This technique is commonly used for the deposition of thin films. There are different forms of sputtering like AC (Alternating Current), RF (radio frequency) or reactive sputtering and many more. In this thesis a Haberland cluster gas aggregation source with DC unipolar magnetron sputtering (*50*) was used. The usage of such a cluster source enables the possibility to form clusters without using a wet chemical approach, which would increase the amount of formed silver oxide and therefore lower the potential for cluster migration in the presence of an electrical field.

As mentioned for the Haberland cluster a DC signal is applied and the chamber is flooded with Argon. For the sputtering process the target and the substrate are placed on an electrode respectively. Once the signal is applied there is an inelastic interaction of accelerated electrons and the argon atoms resulting in the formation of a plasma. The deposition rate itself depends on the target used and can be adjusted by changing the pressure in the chamber or by increasing or decreasing the used power. Due to collisions of the extracted atoms there is the formation of aggregates ranging from a few atoms up to thousands. The resulting structures are called clusters and as mentioned used in this thesis. After their formation and growth the clusters pass through an aperture and are directed onto the substrate. This allows the selection of the cluster size, which can be manipulated by changing the pressure in the chamber. The clusters condense afterward on the samples surface. (*51*)

By using an electrically conductive target material it is possible to monitor the change of the resistivity over the sputter time. The sputter time represents the amount of deposited clusters, as long as the sputter rate is kept constant. The resulting shape of such a resistance over time is depicted in Figure 4. It can be seen that the process starts off with a very high resistance since there is no material in

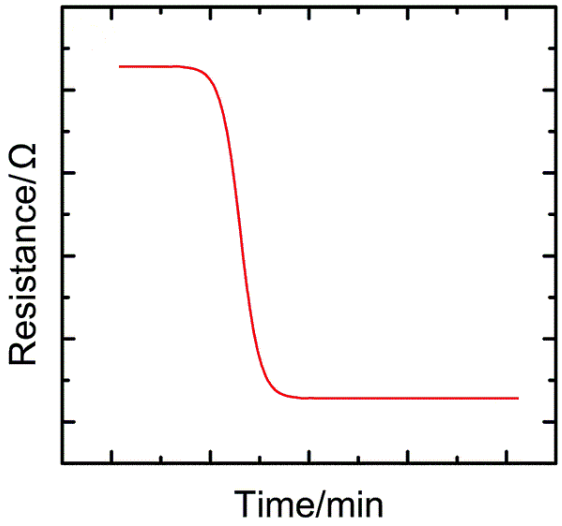

Figure 4: Sketch of a standard sputter experiment.

between the two contacts, which could lead to a conduction. After a specific time a sudden and drastic drop in the resistance occurs, which stops at a certain resistivity and returns to linear behavior. This resistivity level is the electrical resistivity of the sputtered material. The sudden change occurs due to the fact that the deposited material is dense enough to enable an additional phenomena called electron hopping. By increasing the density of the deposited material further the probability of hopping is increased. In some regions it can reach direct electrical contact. This process continuous until an amount high enough to cover the samples surface homogenously is reached.

2.5 Plasma Etching

All of the Au particles prepared in solution presented in this thesis needed to get plasma etched after deposition to remove their organic coating to ensure that these coatings would

not interfere with the later deposited clusters. In addition they show a capacitive behavior while performing IV-measurements, making them unusable for the task dealt with in this thesis.

A plasma is one of the four states of matter and is defined as a mixture of electrons and positive charged gaseous ions. One common way to generate such a plasma is generating electrons by applying an electromagnetic field, which collides with present atoms or molecules and ionize them by knocking out one of their electrons. For the setup used in this system the etching process can be described by the following: in the first step the gas used for the etching process is introduced to the chamber. The process gas can range from gases with a high fluorine amount like tetrafluoromethane (which follows a dissociative ionization with attachment: $CF_4 + e^- \rightarrow CF_3^+ + F^- + e^-$) and is used for removal of silicon dioxide or gases like oxygen (which is either simple ionized $O^2 + e^- \rightarrow O_2 + 2e^-$ or forms radicals $O_2 + e^- \rightarrow 2O + e^-$) and argon ($Ar + e^- \rightarrow Ar^+ + 2e^-$) which are used for resist or removal of organic remnants. Oxygen will react with the carbon bonds, making it more of a plasma enhancer, whereas the argon will not tend to react with the sample. By applying a voltage to the top electrode of the chamber the plasma is ignited which leads to the creation of the reactive particles (described previously).

Plasma etching was utilized for removal of the organic coatings on the clusters. The capability of the oxygen gas to attack carbon bonds, on the other hand, made it impracticable to use after CNT deposition since this would just crack and remove the nanotubes.

2.6 In-situ investigation of the sputter experiments (setup V1 + V2)

To develop a better understanding of a produced sample it helps to get an insight into its formation processes. To gain an insight into what is going on during the sputter process is difficult and for that reason an in situ measurement setup (later on called V1) and a later upgraded version (later on called V2) was build.

A sketch for setup V1 is shown in Figure 5. The red lines indicate the actual connections between the different components, whereas the black arrows indicate the communications

and interactions of the components among each other. The V1 consists of an Arduino Nano, which is connected to a SD-reader and an UI (user interface). On the SD-reader a file is located

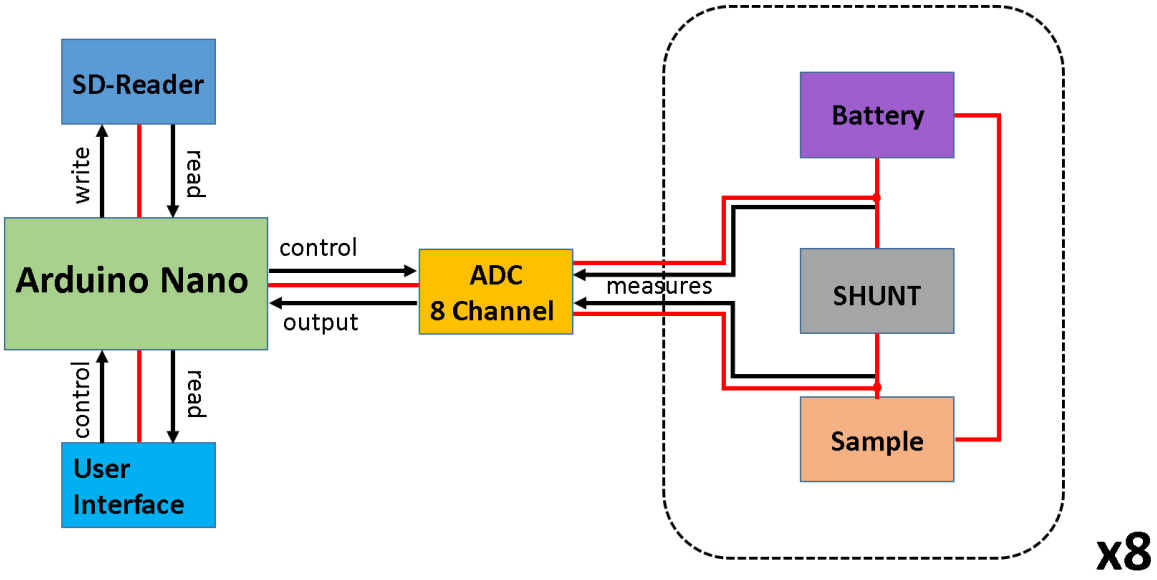

Figure 5: Process sketch of the sputter in situ measurement setup V1 ℕŜI·ťłÎI·úł2Y´2Ŧ úKŜ ăŜúdzLJ ǿłúK úKŜ KŜťLJ 2Ŧ 5ℕ℗ {℗ YI·LJă.

containing the parameters which are needed for the upcoming experiment, such as measurement intervals or delays between each measurement. This information are loaded into the Arduino Nano by using the UI which can be controlled by pressing the integrated buttons to scroll through the menu displayed on it. The loaded file can either be configured before starting the experiment by rewriting it at a computer or right at the start by scrolling through the UI displayed menu and making the needed adjustments there. The Arduino Nano is connected to two 4 channel ADCs (Analog-to-Digital-Converter) resulting in an 8 channel ADC element. This element is connected to a system consisting of a resistor R_{SHUNT}, a permanent power source (being a 3V button cell) and the sample itself. There are eight arrangements like this for which reason eight ADC entries are needed for the conversion of the data. The resulting measurement values were then passed to the Arduino and written on the SD-card. The resulting and changing resistivity of the sample during the sputter process can be monitored by assuming the circuit in Figure 6, a parallel circuit of the resistors R_{ADC} and R_{SAMPLE} in series with R_{SHUNT}, and using the equation (2). The setup follows the rule of the voltage divider from which the equation (2) originates. The resistance of R_{SHUNT} defines in

which regime the calculations of the resistance of the sample are the most precise ones. For this reason a shunt resistance of 1 MΩ was chosen. The reasoning behind this is to have a low power consumption a device must have a high resistance. This fact indicates that the later produced memristive sensors need to be of high-resistance. An additional factor is as well that the setup used for the subsequently following measurements has a reliable detection limit in the 10^9-10^{10} Ω regime making the selection of the 1 MΩ a good choice.

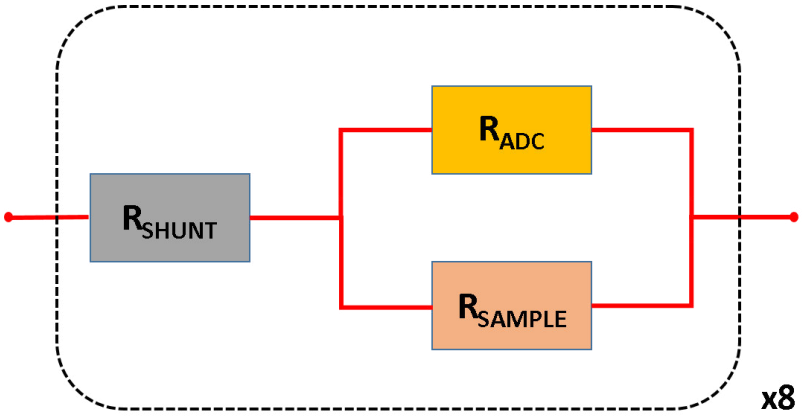

Figure 6: Circuit diagram for the voltage calculation for V1 ℕŜI·ßÎI·úÅ2Y´2Ŧ ÚKŜ ăŜÚdzLJ ǿÅÚK ÚKŜ KŜŁLJ 2Ŧ 5ℕ℗ {℗ YI·LJă.

$$U_2 = \frac{R_P}{R_{shunt}+R_P} \cdot U \text{ (with } R_P = \frac{R_{ADC} \cdot R_{sample}}{R_{ADC}+ R_{sample}}\text{)} \qquad (2)$$

During a series of sputter experiments and the interpretation of their measurement results one came to the conclusion that the setup needed to be upgraded. For this reason the improved version V2 was build, the process sketch of it is shown in Figure 7. The centerpiece of the in situ setup is again an Arduino, but for the version V2 the Arduino Due. While a SD-reader is directly attached to it and used for loading the measurement file into the Arduino or writing the data on the SD-card.

In contrast to the previous setup version there is no UI attached. The measurement results are not displayed during the experiment. The reasoning behind this is that the process of displaying the results on an UI takes time and therefore slows the following measurements down. One way to improve the speed is to abdicate the display. As a consequence is the experiment controlled by an additional computer unit. The other computer unit is an

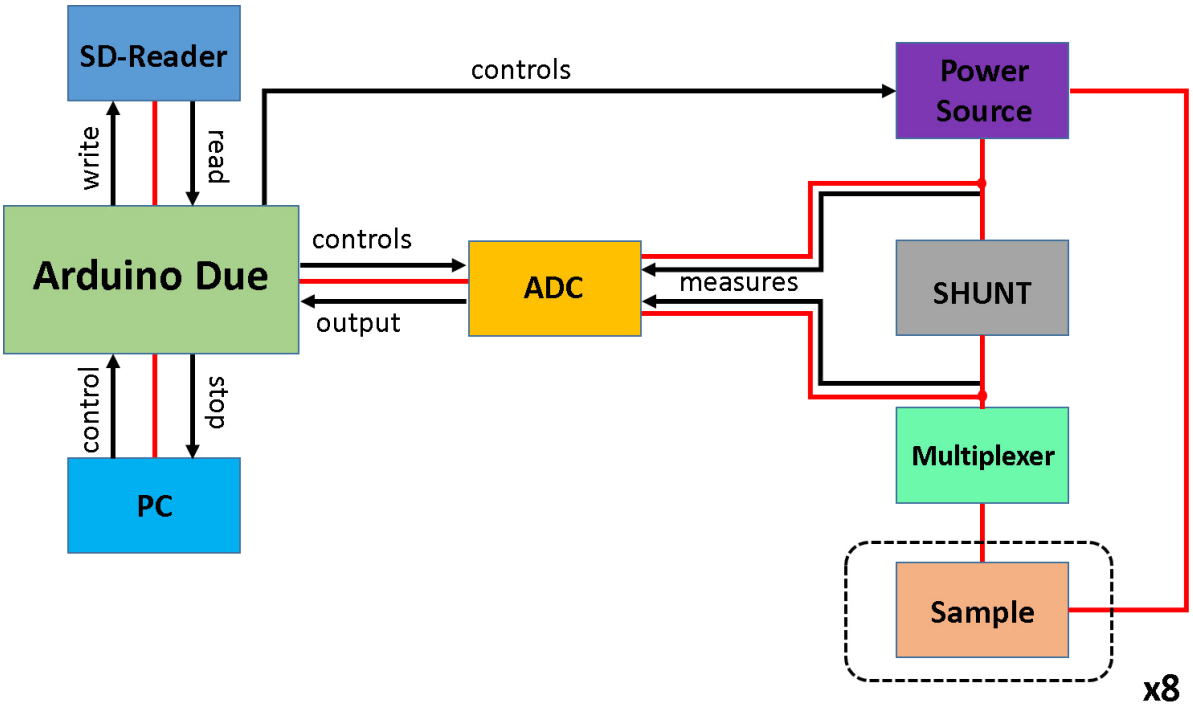

Figure 7: Process sketch of the sputter in situ measurement setup V2 ₪ŜĬ·ƭìÎĬ·úλ2ƴ2ŦúKŜ ăŜúdzLJ ǿλúK úKŜ KŜfŁJ 2Ŧ 5₪Φ {Φ YĬ·LJă.

additional Arduino Due which controls the sputter chamber. By using a communication program like CuteCom it is possible to load measurement files on the V2 Arduino, to manipulate them as desired and to run the measurement controlled by the other Arduino. The break conditions for the experiment can be specified in the measurement file and consist of a threshold resistance and a number of channels which have to fulfill this one. For example if the threshold value is set to 10^5 Ω and 3 channels the sputter process will stop at the moment when 3 or more channels show a resistance ≤ 10^5 Ω, making the experiments more sample orientated. The Arduino is again connected to an ADC which measured the voltage over the shunt. In addition a multiplexer is added between shunt and sample and is used to switch between all eight measurement channels individually. The usage of the multiplexer reduces the amount of shunt resistors and ADCs to just one. In addition is the applied voltage controlled by the Arduino Due, since it acts as a power source for the measurements. This lowers the influence of the measurement on the experiment as well. Furthermore the voltage is not applied constantly to the sample but rather in small measurement pulses.

The upgrades made to this setup make the measurements more controllable and individual. In addition to this is it possible to speed up the measurement cycles in contrast to V1 by using

a better routine and not displaying the results. This results in a decrease of the measurement for one loop (all eight gaps) from over 2 s to roughly 200 ms.

2.7 Organic materials for dielectric background

In the scope of this work several different organics are examined for their suitability as dielectric coating. It is intended to infiltrate these organics with silver particles as mobile species, motivated by the researches of Jo et al. (*18*). Therefore, since organic molecules have a way lower density than metal oxides can their switching times be lower than for already present devices (*52*). Organics like: acetylsalicylic acid, ethacridine lactate, polyacrylamide, P3HT (poly(3-hexylthiophen)), PPT (poly(thiophene-alt-pyrrole)) and tetracyclin-HCl are tested. These organics are either drop coated or applied by thermal evaporation under vacuum. Regardless of the way of application of the used organics the electrical measurements are rather unemployable for the selected memristive approach. To fulfill the foundation of being able to move silver particles by employing an electrical field the used dielectric matrix needs to have a remote conductivity. However, the mentioned organics fall short in these regards, since they show a too high or too low conductivity or bear additional

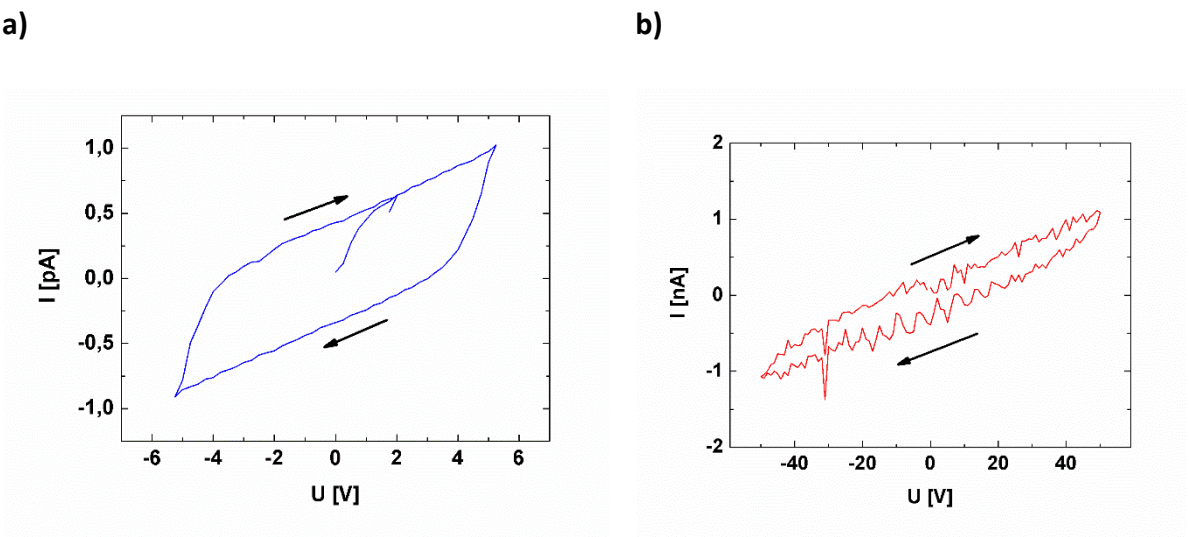

Figure 8: Examplary hysteresis measurement (a) acetylsalicylic acid with a maxi applied voltage of 5 V, b) ethacridine lactate with a max applied voltage of 50 V) for the investigated organic molecules.

unwanted side effects like capacitive behavior. Two exemplary hysteresis measurement for acetylsalicylic acid and ethacridine lactate can be seen in Figure 8. It is shown for both that they have a fairly low conductivity and capacitive behavior. This can be best seen for the acetylsalicylic acid since its measurement curve is broadened up the most, shows an initial curve and does not go back through the origin. Ethacridine lactate shows a seemingly higher current (compare ~1 pA for acetylsalicylic acid with ~ 1 nA for ethacridine lactate) but only since these experiments are conducted with a significantly higher voltage of 50 V. In addition to its low conductance does this drug show slight capacitive behavior as well.

In a further approach carbon nanotubes are introduced to the system instead of the dielectric matrix, which have been already in the focus of memristive researches. It was previously reported of the successful fabrication by coating of CNTs with gold islands (*34*), by compressing (*36*) or applying voltages (*35*) on bundles of nanotubes via STM tip resulting in memristive behavior.

CNTs can be synthesized in example by laser ablation (*53, 54*) or different CVD processes (*55, 56*). The drawback of the energetically more efficient methods is the much higher defect rate of the resulting structures and the subsequent difference/disparity of their properties (*57*). CNTs can be imagined as one or multiple layered and rolled up graphene sheets which form a quasi-one-dimensional structure with a diameter in the nanometer range. The carbon atoms in the nanotubes are arranged in a honey-comb structure. The single-walled cylindrical structures are called single-wall carbon nanotubes (SWCNTs) and the multi-walled are called multi-walled carbon nanotubes (MWCNTs). Similar to graphene individual CNTs bear outstanding chemical and physical properties. The Young's modulus of a single nanotube exceeds the one of stainless steel (E_{steel} = 180 GPa (*58*), E_{CNT} = 1 TPa (*59*)) and they have with 10^{-4} Ωcm (*60*) a very low resistivity making them a very good conductor. The high conductivity of the carbon nanotubes made them feasible to use as conductors for the concept presented in this thesis. By applying the CNTs on the prior mentioned chips it is possible to form a network with gaps in the nanometer range. As explained before, this miniaturization (from µm gaps of the chips to nm gaps in the network) is necessary to increase the memristive effect. In the present work it is attempted to influence the deposited CNT network and its resulting gaps via exposure to acids and bases, strong voltage pulses or by manipulation of the carbon

nanotubes during the process application. All of these different approaches and techniques will be further discussed in the course of this thesis.

2.8 Scanning Electron Microscopy

The scanning electron microscopy (SEM) is an imaging technique to get a magnified image of the surface of a sample and is commonly used in the materials science. This technique is not only limited to the examination of non-organic samples. Biological samples can be investigated as well by coating them with a thin conducting layer (i.e. gold) and using low acceleration voltages. The commonly applied voltages range depending on the sample between 2- 30 kV. For the emission a field emission gun is used and the resulting beam is firstly collimated by using a Wehnelt cylinder. The beam passes afterwards a system of a condenser and objective lens which demagnify the beam. The demagnefied beam than hits the sample surface where elastic and inelastic scattering effects of the incoming electrons with the sample occur. Elastic scattering is the deflection of the incoming electrons by mostly the core of the atoms of the sample while inelastic scattering refers to events where the electrons collide with electrons from the sample. This leads to the formation of secondary electrons, X-rays, Auger electrons and others. Specific detectors are used to capture the resulting electrons which are later on shown as maps on the computer screen. Depending on the mass of the atoms in the sample, defects or geometrical aspects a variation of the signal and therefore of the resulting image occurs. The resulting image is only a pseudo 3D image of the samples surface and has to be interpreted carefully. The scanning of the sample is achieved by either moving the generated electron beam over the samples surface by using scan coils or in newer systems by digitally controlling the beam position itself. This method is mainly used in the course of this thesis to get a closer look on the deposited CNTs and clusters and their treatment results. (*61, 62*)

2.9 Transmission Electron Microscopy

Transmission electron microscopy (TEM) is a versatile tool for analysis on the nanoscale, widely used in material science. In this thesis TEM is utilized to examine the structure and size of the clusters for specific sputter experiments. Comparable to SEM, TEM can be used for imaging samples, but with higher resolution. However, thin samples with thickness below 100 nm is a prerequisite to obtain reasonable high resolution data. For imaging the electrons are extracted from the electron gun and accelerated to an energy above 100 keV. After the electrons are extracted from the electron gun (commonly field emission guns are used as sources) it gets directed by a Wehnelt cylinder. The following condenser lens system is used to align the beam in parallel. The collimated beam is directed on the sample. Due to the high energies of the electron beam and the low thickness of the sample the electron beam is transmitted through the specimen. As a result of the collision process a large variety of processes occur, which can be used for detailed analysis e.g. energy dispersive x-ray spectrums (EDX). The transmitted beam is further magnified by the objective lens system. The resulting image is then projected onto a fluorescent screen. Image recording nowadays is routinely done by CCD cameras.

Due to the complex interaction of the transmitted beam several contrasting formation processes have to be considered or facilitated. For this thesis bright field images were used most commonly to identify the particle size of the nanoclusters. In bright field the electrons get preferentially scattered at thicker regions or regions with high atomic mass and consequently appear darker on the imaging medium. (*63, 64*)

3 Experimental

3.1 Chip Preparation

The fabrication of the microchips was carried out in the cleanroom (Nanolab) of the technical faculty of Kiel University. The patterning is achieved by using a standard photo lithography process. The used wafers are 4 inch in diameter and consist of p-type (Boron) <100> oriented Si with a thickness of 525 ± 25 µm, one side polished, has a resistivity of 1 – 10 Ohm·cm and are coated with a 300 nm thick SiO_2 layer (MicroChemicals GmbH). For the first use no precleaning is nesseccary. In the case of the recycled ones (from previous deposition experiments) the cleaning is done as follows: First the chips are ultrasonicated in acetone for at least 5 min, afterwards for the same time in isopropanol, rinsed with deionized water and in a final step dry spun and blown. The last step is performed to get rid of the last aqueous remnants. The clean wafers are mounted on a spincoater and further processed as described in the following. First a homogenous resist layer is applied by adding a volume of 3.5 ml of the photoresist AZ 5214 E to the wafer (using an Eppendorf pipette) at a rotation speed of 3000 rpm, resulting in a resist layer of 1.4 µm (*65*). The following step is a prebake carried out on a hotplate preheated up to a temperature of 110 °C for 50 s. Afterwards the coated wafer is structured by using the Süss MicroTec MA6/BA6 mask aligner and a clear field mask with the respective pattern. The mask aligner is set on hard contact mode to guarantee sharp edges. The exposure time is 2.1 s to ensure enough energy (at least 200 mJ/cm²) to make the film soluble. Afterwards a 90 s reversal bake step at 120 °C on a hotplate occurs and then subsequently a flood exposure for 7.0 s to generate photoactive compounds in absence of the previous used mask. For the resist removal are the processed wafer immersed into AZ 726 MIF developer for 60 s. The wafers processed this way are rinsed with deionized water and spin dried to get a clean surface. By sputtering (which counts to the Physical Vapor Deposition (PVD) techniques) utilizing the Ardenne CS 730 S thin layers of 10 nm of chromium and 100 nm of gold are deposited on the wafer. The chromium layer is used as an adhesion promoter between the gold and SiO2 and chosen due to its ease in handling, inertness and good conductivity. A side view sketch of the resulting chip is depicted in Figure 9. In a last step the

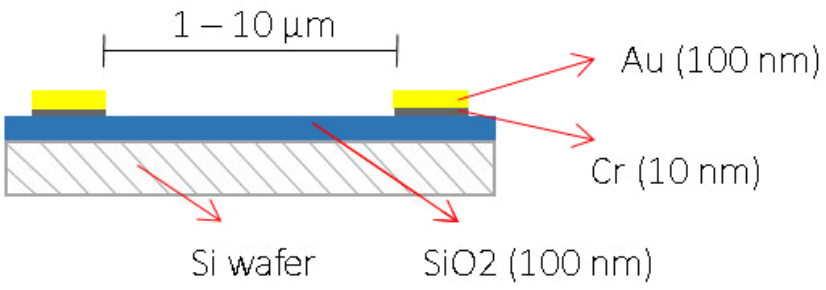

Figure 9: Side view of the produced chips. Consisting of a Si wafer coated with a SiO_2 (100nm) layer provided with gold (+ chromium added as adhesion promoter) contacts separated by a 1 – 10 µm gap.

resist which is hardened by the UV light of the mask aligner is removed. This is achieved by placing the wafer in an acetone bath for several hours to guarantee an easier lift off. The final step of the lift off is carried out by ultrasonicating the wafer in the acetone bath for a few minutes. To remove the last impurities from the surface the wafer is also ultrasonicated in isopropanol and rinsed with deionized water afterwards, following spin and blow drying. The chips are afterwards separated from the wafer by utilizing a diamond cutter, and one of

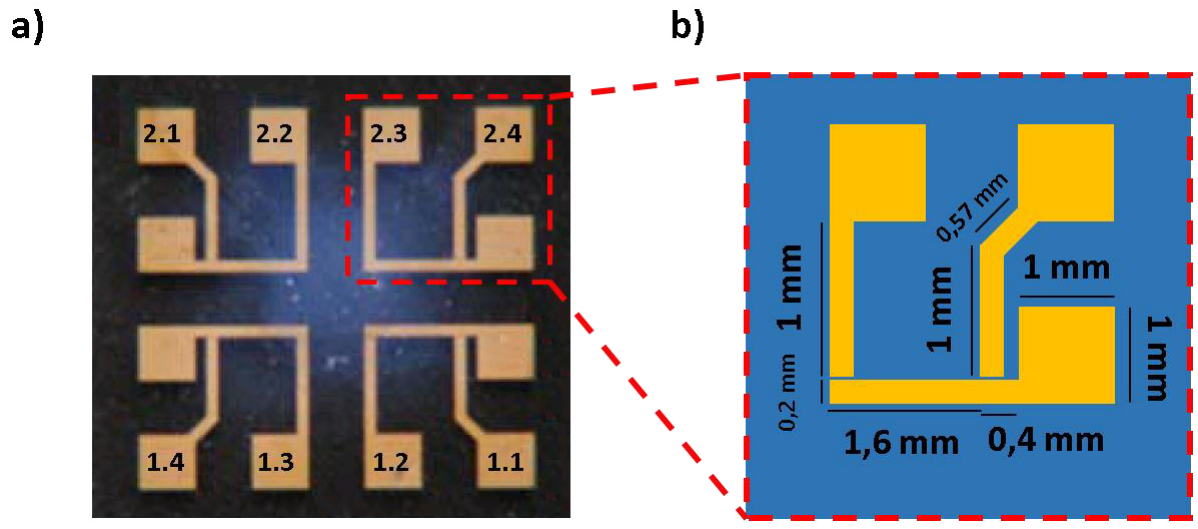

Figure 10: a) Produced chip with gap labeling, b) zoomed in view on the chip and its feature size.

the structured chips can be seen in Figure 10. The chip structure itself is shown as well as the labeling of the gaps. The chip consists of four times the same arrangement of three gold electrodes, which are separated by small gaps in the micrometer range. The individual gaps differ in their feature size ranging from 1 to 10 µm. Whereas the gaps referring to the numbers

1.1 – 1.4 have a size of 10 µm while the others range from 1 µm (2.1), to 2 µm (2.2), to 6 µm (2.3) and up to 8 µm (2.4). A sketch of a close up of one part of the chip is shown in Figure 10b. The design is chosen in such a way as to allow for different gap sizes, and gold contacts big enough to be contacted easily as well as having some electrical shielding effects with respect to the arrangement of the antenna setup (the contact arms).

3.2 Fabrication of the iron oxide needles and samples

As backbone for the preparation of the FeO samples a silicon wafer coated with iron particles is used. The iron particles (99.99% from Aldrich) are 1-10 nm in diameter and dispersed in ethanol. The application is achieved by adding 50 µl of dispersion onto a wafer and letting it dry in on a hotplate (T = 120 °C) under ambient conditions.

Subsequently different heat treatments are conducted with these samples. For this routine they are placed on a pre-heated hotplate (T = 255 °C) for several hours (12 – 24 h) under ambient conditions. The resulting µm long iron oxide needles are cut and transported using the integrated FIB of the SEM afterwards. The needles are fixed on pre-patterned Au pads on glass substrates using platinum.

The resulting devices were investigated on their current - voltage characteristics by performing voltage sweeps from 0 to +15 V, from +15 V to -15 V and back to zero. Additional gas sensing measurements were carried out by exposing the sensor to defined amounts of gas (H_2, NH_3, acetone, ethanol) to measure its response and later tested on its reaction times after being exposed to acetone vapor in an amount of 5 – 100 ppm.

3.3 CNT Deposition and Manipulation Techniques

3.3.1 Dilution of CNT dispersion

To get a proper CNT network a large number of different deposition experiments have been carried out. In the following chapter the different technics will be described and further commented on.

For this thesis different CNT dispersions in water were tested with regard to how easily they can be applied on the surface of the chip structure and on their usability for memristive experiments. The multiwall CNT dispersions used were CarboDis TN (FutureCarbon GmbH), CarboBYK-9810 (BYK-Chemie GmbH), Aquacyl (Nanocyl) and for additional testing purposes a single-wall CNT dispersion, namely Tuball Ink (OCSiAl). All of the multiwalled CNT dispersions are diluted in a ratio of 1:3200 in a first step by weighing a small amount of the master dispersion and adding deionized water for further dilution. Additionally an ultrasonic disperser (SONICS by Vibracell) is used to prevent any agglomeration. Therefore, the samples are homogenized by placing the ultrasonic disperser into the solution for 5 min and applying pulses of 20 kHz with a length of 2 s and a resting time after each pulse of the same length at a power of 200 W. If needed is the intermediate dispersion diluted even further in the same way using the disperser and deionized water up to a ratio of 1:200000. Each dispersion is prepared prior to the deposition to guarantee that the nanotubes are distributed nicely before they are used further. The Tuball Ink tends to precipitate very quickly for which reason the weighed solution is agitated and applied to the chip right away.

3.3.2 General measurement of the nanotube network

All electrical measurements, except the in-situ ones, are carried out by using a Keithley 6517B electrometer in the two-point mode. Two tungsten needles are placed on the gold pads as displayed in Figure 11, exemplarily for the 1.2 gap shown. One of the needles is used to apply the voltage to the gap to be measured while the other needle is placed on the respective ground contact accordingly. For the regular hysteresis curves the applied voltages ranges from +/-0.5 to +/-5 V over a series of 48 measurement steps for a whole measurement.

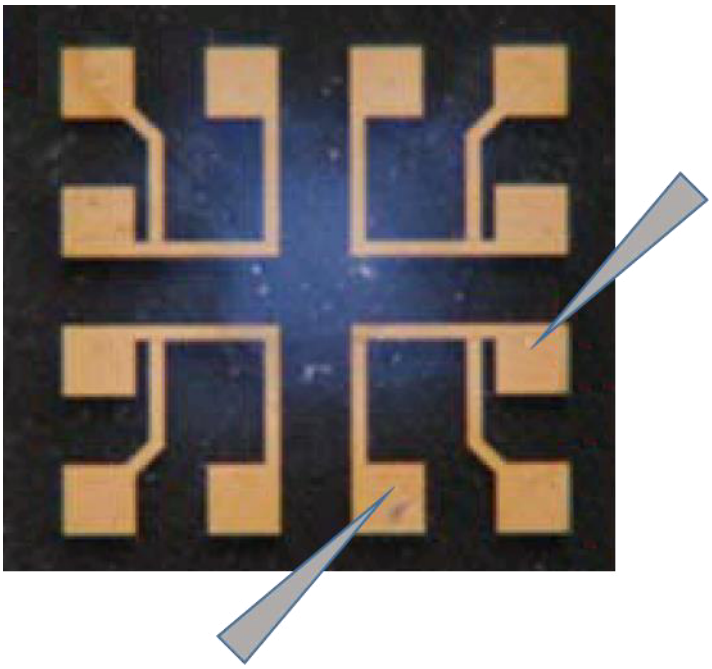

Figure 11: Sketch for the needle arrangement for the"two point probe" measurement on the used chip layout.

A hysteresis cycle always starts at 0 V. The voltage is then increased to the maximum set value and decreases back to zero. Right afterwards an additional negative measurement is carried out in the same manner, closing the cycle this way. Concluded from the resulting hysteresis curves the subsequent scan pulses are applied accordingly. As soon as one of the resulting parts of the measured hysteresis loop is significantly smaller than the other one, has the subsequently applied pulse the same polarity as the smaller loop. This means that in case that the loop in the negative regime of the hysteresis curve is smaller the next following scan pulse will have a negative voltage applied. The voltage pulses used are greater than 1 V and go up to several volts. The pulse length is dependent on the sample and is varied between a few seconds up to several minutes. In addition for some of the experiments carried out the pulse length and the number of pulses is varied as well.

3.3.3 Manipulation techniques post deposition

3.3.3.1 Manipulation of the nanotube network with high voltages

For the manipulation of the CNT network by using different voltages following the idea to burn some of the interconnections the same setup as described prior for the hysteresis measurements is used. While the applied pulses range from 0,1 s to up to 120 s and voltages of up to 120 V are applied. For these experiments only a positive voltage is used. The result of the prior conducted hysteresis measurement, which is carried out to compare the old with the new result, is not taken into account here any further. The pulse heights are varied and increased subsequently from 5 V to the already mentioned maximum voltage.

3.3.3.2 Manipulation of the nanotube network via ultrasonication

The experiments conducted to influence the applied nanotube network by using an ultrasonic bath are carried out by placing the sample to be treated (using the CARBOBYK dispersion in a ratio of 1:8000) in a beaker and putting it into a standard ultrasonic bath. The samples stay in the ultrasonic bath for 5-10 min and are measured afterwards using the later described procedure for the hysteresis measurements.

An additional series is carried out utilizing the ultrasonic bath and is carried out by placing a beaker filled with DI water into the bath and dipping the sample for a short moment into the water.

3.3.3.3 Manipulation of the nanotube network by temperature treatment

In a second approach different temperature treatments are carried out post deposition. For all samples the dispersion CARBOBYK in a ratio of 1:8000 is used. The CNTs were applied by using the drop coating method and letting the droplet dry in at ambient conditions. For the high temperature treatment is the sample placed on a hotplate for 3 hours at a temperature

of 150 °C controlled by an attached temperature sensor to the surface of the hotplate. For the low temperature experiment liquid nitrogen is used, in which the sample is placed for a few minutes.

3.3.3.4 Manipulation of the nanotube network and Ag clusters with acids and bases

The manipulation experiments in which acids and bases were used are simply carried out by placing a droplet of the respective fluid on the CNT coated chip. It is made sure that the whole structure is covered with liquid. The samples are kept like this in ambient conditions for up to one hour to ensure enough time for the chemical reaction of the carbon bonds and the acids used to take place. The resulting samples are afterwards rinsed off carefully with deionized water and like all prior discussed manipulation experiments re-measured to check for any changes occurring in the resulting hysteresis.

3.3.4 Deposition techniques

To manipulate the deposition of the CNTs several changes to the deposition technique were investigated. One of these deposition methods was carried out by simply placing a droplet of the desired dispersion on the chip by using a one-way 3,5 ml LDPE pipette (Reichelt) and letting it dry in ambient conditions (see Figure 12a). To accelerate the drying process a vacuum oven (VT 6025 from Thermo Electron LED GmbH) is used later. The oven is set to 60 °C at a low vacuum leading to an evaporation of the droplet in a timeframe of roughly 1 h instead of several ones in ambient conditions. A further variation is the change of the deposition temperature. Therefore chips are placed on a glass slide on a hotplate before deposition to guarantee that they are heated evenly. The temperature is raised stepwise to up to 120 °C and is controlled by using a temperature sensor which is placed in the center of the plate. The deposition of the droplet is performed like described prior by using a one-way pipette (see Figure 12b).

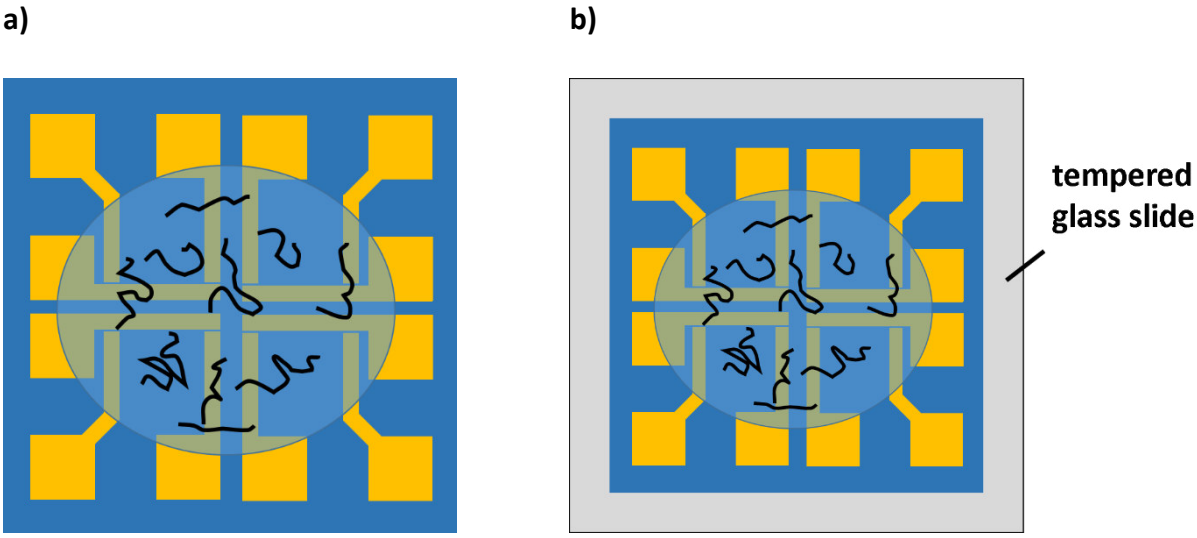

Figure 12: Sketch of the simple deposition technique by drop coating a) without and b) with tempered substrate.

3.3.5 Deposition techniques with altered chip surfaces

To investigate the effect of the surface on the deposition of the droplet and the containing CNTs samples with different coatings (instead of the SiO_2 from the used chips) were tested. The samples used are pieces of Si coated with 40 nm of ZnO, with 40 nm of Al_2O_3 and coated with an 80 nm thick AZO (Al doped ZnO) layer respectively. The deposition is carried out as well by using a one-way pipette and a hotplate.

A further modification of the surface is achieved by silanating it. This is done by placing the chip in a small desiccator and exposing it over night to Trichloro(1H,1H,2H,2H-perfluorooctyl)silan. To do so an additional vessel containing one droplet of the fluid is placed in the desiccator and for 5 min an attached rotary vane pump is switched on to generate a vacuum. The system stays like this and results in a homogenous monolayer. The subsequent CNT deposition is carried out in different ways after the silanated samples are gently rinsed with acetone to remove remaining residue. Either way, the droplet is dragged across the chip from one corner to another or just tapped several times on the surface of the sample. These procedures will be discussed separately in this section. During the procedure is the silanated chip heated using a hotplate up to 115 °C.

Aerosol experiments are carried out by using regular perfume atomizers which are cleaned carefully beforehand. The chips are put on a hotplate at 115 °C while the concentration of

CNTs in the experiments is varied. The amount of dashes varies according to the used concentration, while the spray distance is set to approximately 15 cm away from the sample guaranteeing that the formed atomizer mist covers the sample evenly (see Figure 13a). With silinated samples on a hotplate additional deposition experiments are performed. For the first ones is the droplet formed not dropped on the surface to let it dry in there, but rather dragged across the surface slowly at a uniform speed utilizing a one-way pipette. Each swiping process starts in one of the corners and ends at the diagonally located corner dragging the droplet all the way. This process is repeated several times depending on the dispersion used (see

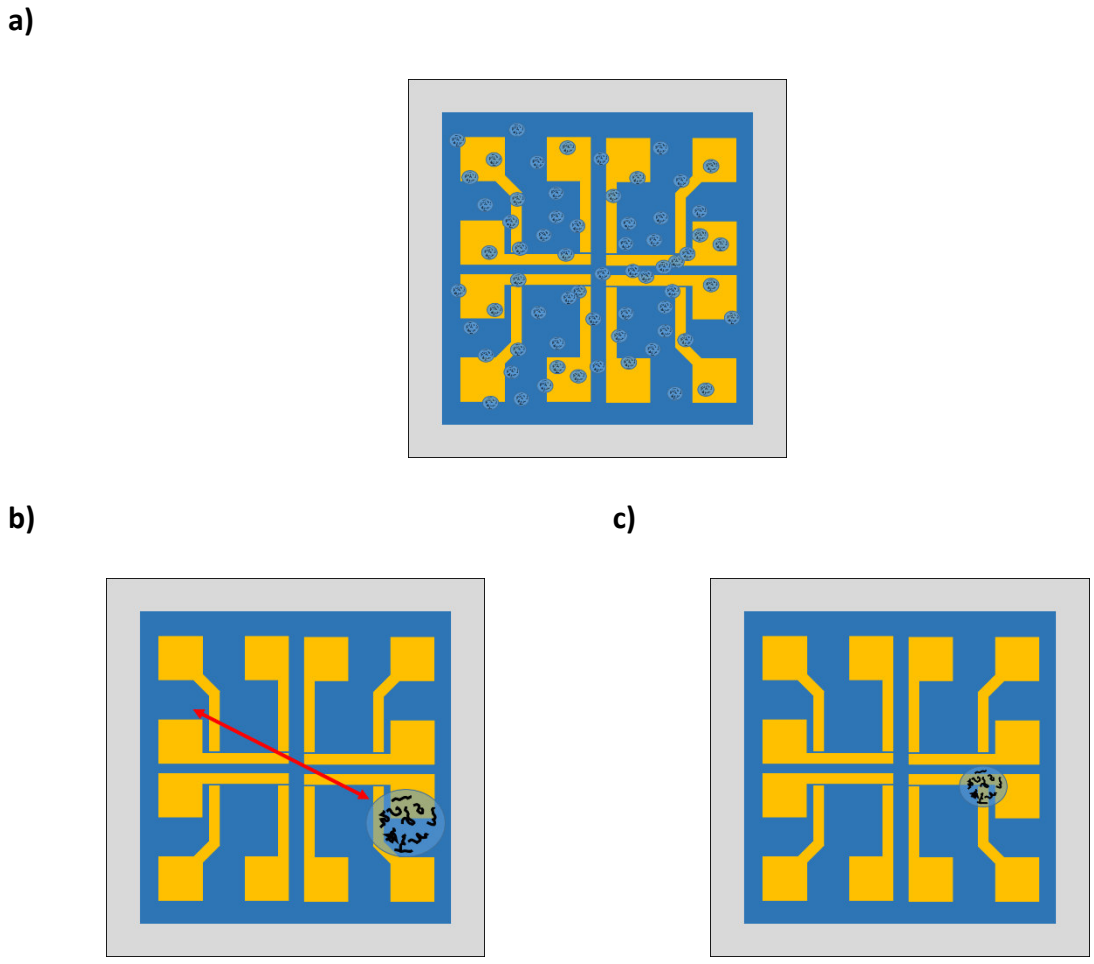

Figure 13: Sketches of additional deposition techniques for tempered chips: a) spray coating of the CNT dispersion on the chip, b) dragging of the droplet across the chip (with one directional indication), c) tipping the droplet (it was made sure to only cover the to be coated gap).

Figure 13b). In another approach is the droplet not dragged over the surface but rather just tapped on the gaps several times. For this reason an Eppendorf pipette is used with a volume of 5 µl (10 µl as max. volume for the pipette) to form droplets small enough to cover only the desired gap and not the whole sample. The droplet is formed at the tip of the pipette and pushed gently onto the chip surface for 2 s. This process is repeated six times for each gap and

every time with a new volume of CNT dispersion (see Figure 13c). To make sure that the droplet does not form at the side of the pipette, which makes it hard to handle proper, is the tip wiped off with a Kimtech wiper to remove remains which stay at the tip after dipping it into the dispersion to refill the pipette with new dispersion. As well the tips are renewed after some depositions since they tend to bend due to the heat of the hotplate making it hard to tap the droplet repeatable on the surface.

3.4 Cluster deposition

3.4.1 Deposition of the Ag clusters

The silver cluster depositions were carried out in two different ways. Either by deposition out of dispersion or by sputtering. The dispersion was fabricated following the approach of Slistan-Grijalva (*66*), in which he suggests to dissolve 13,5 g of PVP 75 ml ethylene glycolin and adding 0,30 silver nitrate to 50 ml of this dispersion in order to generate silver clusters. For the dispersion deposition a simple droplet of it is placed on a preheated sample by drop coating. To perform the in situ measurements the sample has to be mounted on a special circuit board. For the bonding a 5430 from the company F&S Bondtec with an attached MS 5 microscope from Leica is utilized. The result of a bond process can be seen in Figure 14. To connect the gold pads of the chip with the copper pads of the circuit

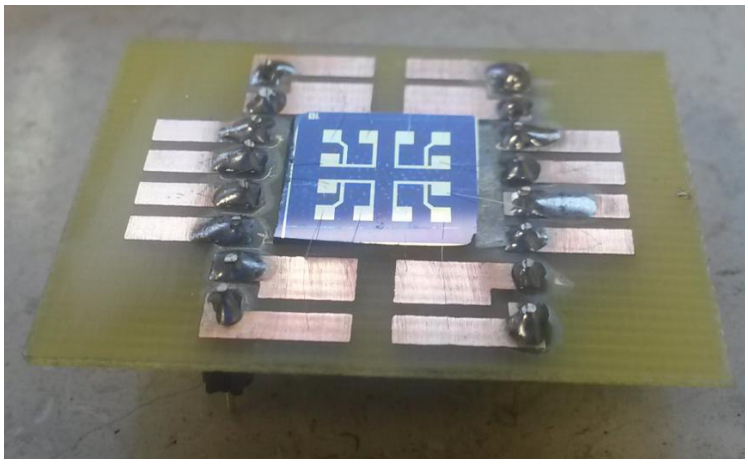

Figure 14: Wire bonded Si-chip (AlSi 1% wire used 25 µm thick using ultrasound welding).

board a 25 µm thick AlSi 1% (aluminum containing 1% of silicon) wire is used. The bonding is always carried out in the same pattern. While the copper pads on the side, which are aligned in a row, are used to bond the centered gold pads to ground are the other stacked ones used to contact the other ends of the gaps. It is mandatory to always follow the same pattern to ensure that the resulting measurement results are saved correctly in the measurement file created.

The samples are placed after the bonding process on a Teflon sample holder in the center of the sputter chamber. Teflon is used for the reason to prevent a possible short circuit between the sample and the sample holder/chamber since this would lead to false results. The sample holder is then connected to the measurement setup enabling the monitoring of the followed sputter experiments in situ.

The deposition of the metal clusters is carried out by sputtering using a custom Haberland gas aggregation source with DC unipolar magnetron. Before any of the sputter experiments are carried out is the pressure in the chamber pumped down until a value of 10^{-5} mbar or below is reached. Depending on the used target Ag or AgAu different parameters are used. For the Ag sputtering the applied power to the magnetron is set to S_{Ar} = 40 W (255-257 V) and the Ar flow to $F_{Ar} = 0.4 \frac{mbar \cdot l}{s}$ leading to a final pressure at the cluster source of $p = 5 \cdot 10^{-3}$ mbar. For the AgAu sputtering the Ar flow is set to $F_{Ar} = 0.8 \frac{mbar \cdot l}{s}$ resulting in a pressure at the cluster source of $p = 6 \cdot 10^{-3}$ mbar, while the power at the magnetron stays the same but with a slightly higher voltage of 277 V. The sputter times varied for each measurement depending on the starting resistivity of the used chips and therefore the quality of the network in its gaps. Over the time two different setups of the custom made in situ measurement setup for the sputtering process were used. For this reason are the Ag experiments carried out with the first setup version and the AgAu experiments with the latter one. For the older version a constant voltage of +3 V is applied to each gap individually and the termination criterion was deduced from the sputter time of the prior made experiment and was mostly at a deposition time of 205-230 s. For the later used setup is the sputter time mostly around 150 s depending on the time needed for change in the output current, while the termination criteria are selected differently. The experiments are not finished after a specific time, but rather after a prior set

number of gaps resistance drops below a certain threshold value. This value varied through the series of experiments and ranged from 10^2 - 10^4 MΩ. These values were chosen after examining the sputter curves in regards of their shape. By checking for the point of inflection and taking a slightly higher value, one ensured that there is a sufficient number of clusters in the gap but that it is still below the percolation threshold, which would just lead to conductive paths through the device, making it unusable. The shutdown of the cluster source is initiated automatically by the setup as soon as the set termination criterion is fulfilled. The voltage applied for the measurements is applied individually at every gap during the measurement and set to 0,7 V to influence the clusters as little as possible.

3.4.2 Au particle deposition from solution

Besides utilizing Au particles formed by cluster sputtering were Au particles formed in an aqueous solution also used. For this purpose 1,6 ml of a 0,02 M $HAuCl_4$ solution are added to a 200 ml solution containing deionized water and 1,0812 g β-D-glucose. The solution is stirred for 75 min using a magnetic mixer and then a 0,05 M solution of NaOH is added slowly to it until the pH reaches a value of 9,2 (resulting in a total used volume of 5 ml). The NaOH is added to control the size of the resulting Au particles. The size of the particles is later determined by using an UV/VIS/NIR Spectrometer Lambda900 (from the company PerkinElmer) in transmittance mode. Following this is the solution centrifuged at a speed of 6000 rpm for 60 min. The resulting pellets are diluted afterwards with 2 ml deionized H_2O. The dispersion is deposited on the chips by spin coating. The accelerations used varied from 700 to 1500 with an end speed of 1000 and 1500 rpm. Since the Au particles are encapsulated with glucose a further cleansing step using a plasma etcher is mandatory. For this process a TePla 100 plasma system (from the company PVA) is used. As reactive gas a mixture of oxygen and argon is used in a ratio of 2:1 at a pressure of 0,4 mbar and power of 300 W for 60 min.

Another approach of adding Au particles to the surface was to use Block Copolymer Micelle Nanolithography (BCML) (*67*). The procedure as described in the paper is the dissolution of Poly(styrene-b-2-vinyl-pyridine) (PS(110000)-block-P2VP(52000), 4 $\frac{mg}{ml}$, Polymer Source, Canada) in toluene and to add tetrachlorogold(III) acid trihydrate (from Sigma-Aldrich) in a molecular ratio of 0,4. The produced solution is deposited on the sample by either spin-coating

at speeds ranging from 3000 to 5000 rpm or by dip-coating at dipping speeds of 10 $\frac{mm}{min}$ to 25 $\frac{mm}{min}$. Afterwards, to remove the micelle polymer are the samples placed in a plasma etcher and treated for 60 min with a mixture of hydrogen and argon in a ratio of 1:9 at 0,4 mbar and a power of 300 W.

The SEM imaging of the samples was mostly carried out using the InLens mode and an acceleration speed of 8 keV. For this purpose the EM XL30 from Philips was used. The TEM images were captured using a Tecnai G2 F30 S-TWIN (300 kV, FEG) equipped with a Si/Li-EDX detector (EDAX).

4 Results and Discussion

4.1 Investigation of the FeO samples on their current - voltage characteristics

The results presented and discussed in this sub-chapter are the results of an already published paper (*68*) which originates from a cooperation which was conducted in the scope of this thesis.

After the iron particle coated samples were temperature treated, like in section 3.4 described, did this result in several nanowire structures consisting of Fe_2O_3. Results for an exemplary sample are shown in Figure 15. The SEM images show the temperature grown needles, which

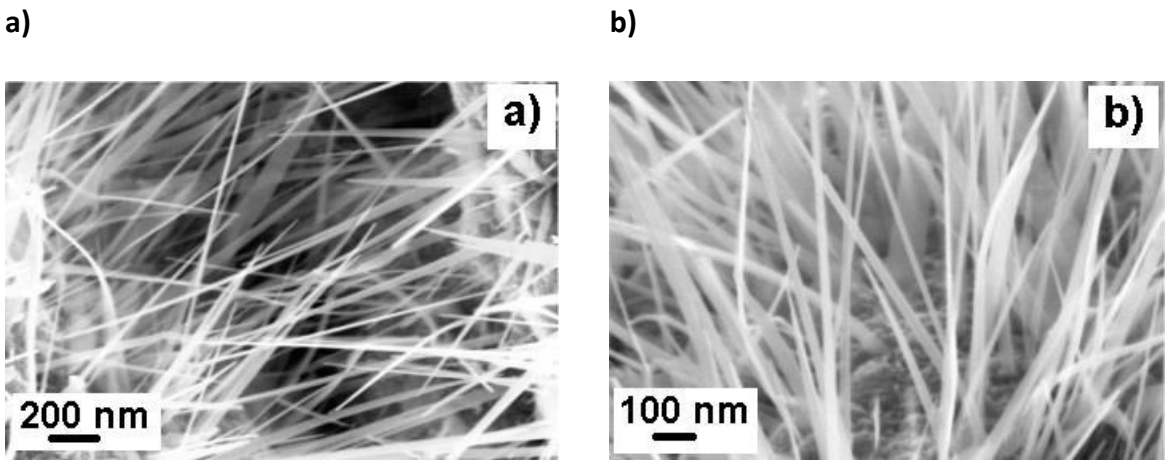

Figure 15: SEM results for a temperature treated Fe sample resulting in numerous nanometer thick iron oxide needles (68) (printed with permission of the co-authors).

reached a length of up to several µm and range in diameter from 30 to 50 nm. It is notable that out of a single micro-particle many oxide needles branch, resulting in a dense arrangement of them. Figure 16 shows a resulting device with one of these needles being attached to two platinum pins which are attached to gold contacts (not shown in the image). The transfer was carried out using a FIB. An occurring disadvantage for these kind of devices can be the low resistance of incompletely oxidized iron. For this reason, the annealing times were chosen as 12 and 24 h to ensure that the system had enough time to completely

transform into iron oxide. In addition were several needles attached to a single gold contact, to establish at least one working device for each contact.

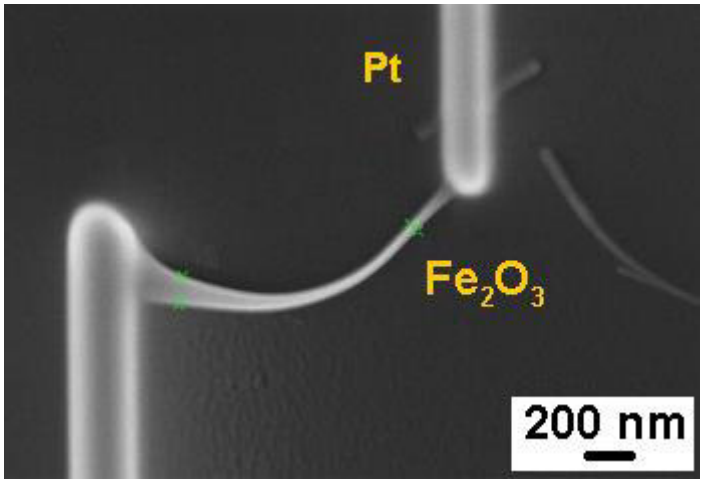

Figure 16: SEM image of a fabricated FeO memsensor based on a single Fe_2O_3 nanowire with a diameter of ~50 nm, being connected to a Pt pin (and not shown to an Au contact) (68) (printed with permission of the co-authors).

The sensorial properties for the FeO device are shown in Figure 17. In Figure 17a the capability of the demonstrated device to different gases at elevated temperatures is shown. It can be seen how the device responds to four selected gases individually indicating the presence of some sort of cross sensing capability like it quite often occurs for sensors (*4*). The gas response rate ($\frac{\text{Rgas}}{\text{Rair}}$) for the FeO sensor is the lowest for H_2 with 2,9, quite similar for NH_3 (18,8) and ethanol (24) and superior for acetone (125). Hence, this sensor shows a quite high selectivity to acetone vapor in the conducted experiments. Which can be attributed to the reaction of

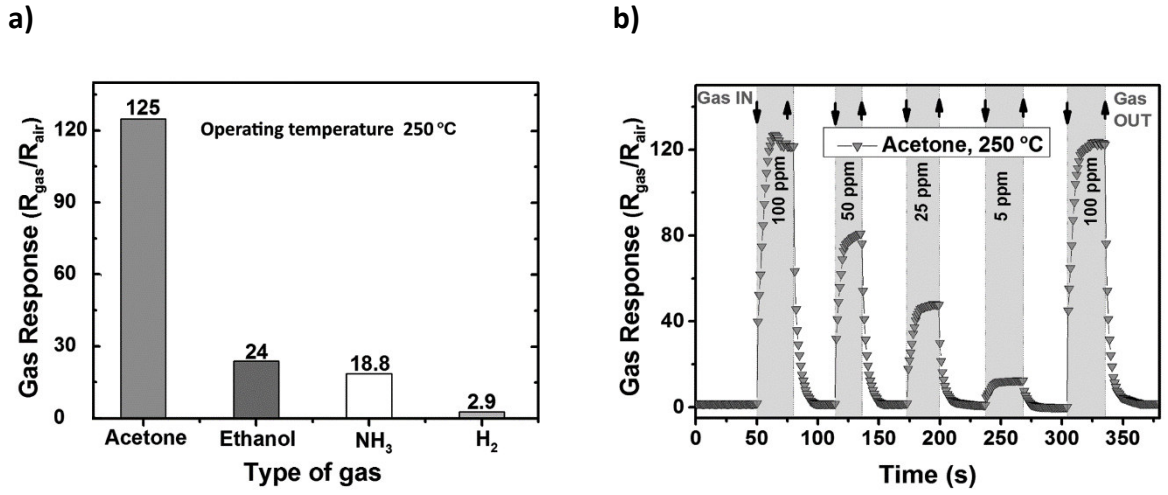

Figure 17: Sensorial results for the presented FeO sensor. a) gas responses for acetone, ethanol, NH_3 and H_2 at T = 250 °C, b) gas response rate for acetone one different amounts (68) (printed with permission of the co-authors).

the acetone with on the surface adsorbed oxygen atoms to CO_2 and H_2O. This leads to a reduction of the amount of generated holes, which are formed because of the adsorbtion of oxygen on the surface, and therefore due to electron-hole recombination to a decrease of the bending of the band structure, resulting in a lowering of the conductance of the system (*69*). The dynamic response of the system was tested and the results are shown in Figure 17b. It can be seen that the response of the sensor to the exposure of 5 – 100 ppm of acetone is very rapidly and as well repeatable, since the shape of the curves is fairly sharp. In addition the sensor recovers completely and goes always back to its initial electrical baseline, proving again its promising repeatability. The response time, which is the time the system needs to change its resistance by 90 % in case it is exposed to a gas or the exposure was stopped, is estimated to be 8 s for a response to acetone vapor and 7 s for a recovery of the system. These times are exceptional and superiorly shorter than for other reported metal oxide devices (*70, 71*) and can be assigned to the high porosity of the system. This porosity ensures a rapid diffusion and adsorption (*72, 73*) as well as dissociation (*4, 74*) of the analyte gas.

The hysteresis measurements for the iron oxide samples were conducted as described in the experimental section. The results of these measurements are shown in Figure 18. Here the differences of the voltage – current characteristics of a sample annealed for 12 h and one for 24 h at T = 250 °C are shown. It can be seen that the resulting graphs not only differ in their shape but as well in the maximum of current measured. While the maximum current for the shorter annealed sample results in a value of 1,5 A the one of the longer annealed one is with 80 mA significantly lower. Both kind of samples show a non-linear shape of curvature, however a broadening of the curve is detectible for the longer annealed one (see Figure 18b) hinting to a memristive behavior additionally to its already gas sensing capabilities. The memrisitive behavior is not only described by the broadening of the curve but as well by the pinched hysteresis curve and as well the altering of the direction how the current follows the voltage, resulting in a high and low resistive state, respectively. Similar results are reported for other metal oxide systems earlier (*75, 76*), whereby these devices are based on the usage of films, in contrast to the approach presented here, which is needle based. The memristive behavior for this sample can be attributed to the same phenomena, which is as well responsible for the switching in titanium oxide based samples, the movement of oxygen vacancies (*77*). Due to the earlier mentioned high porosity of the samples a high density of interface states and vacancies between nanowires and particles can be present (*76*), which

opens the possibility of vacancy movements. The fact that for these samples 15 nearly identical voltage sweeps for several samples were performed indicates as well their great reproducibility.

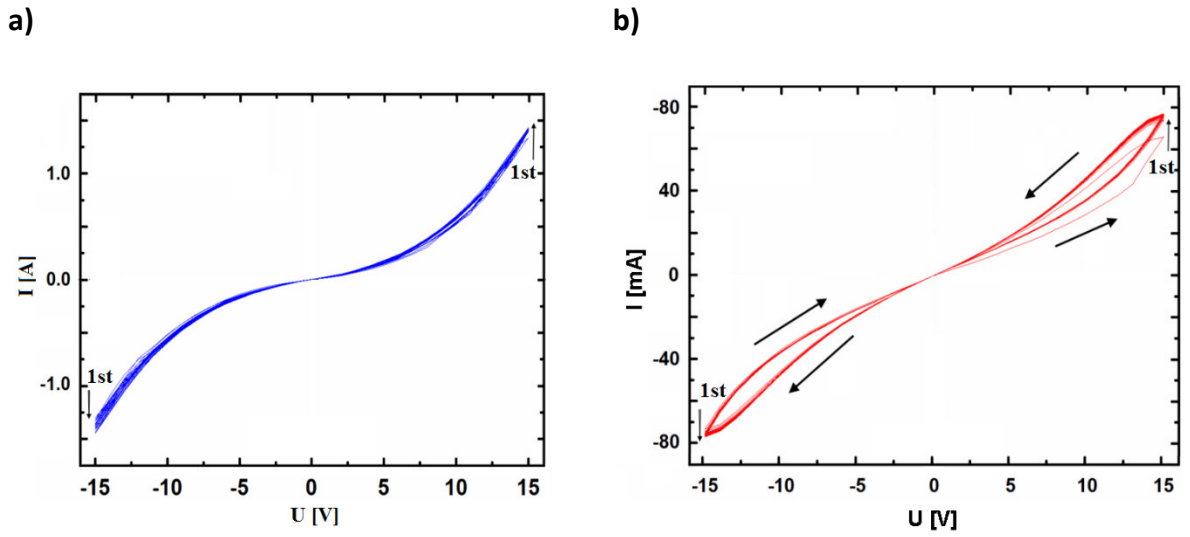

Figure 18: Hysteresis measurement results for a FeO memsensor after 15 cycles and a maximum voltage of 15 V(a) for a device with a annealing temperature of T = 255 °C for 12 h, b) for a device with a annealing temperature of T = 255 °C for 24 h) (68) (printed with permission of the co-authors).

The here presented results for the FeO samples do not only show sensing for various gases, but also memristive switching capabilities. The advantage of the presented system lies as well in the fact that it can be easily altered between the two states of simple sensing and memristive behavior by a longer temperature treatment. It can from this be concluded that these samples bear the potential to be utilized as memsensors. Such memsensors can be found in literature (*11, 78, 79*), whereas these devices need to be functionalized to show memristive switching and are in contrast to the here presented system based on Schottky-barrier memristive silicon nanowires.

Since the presented system does show both sensing and memristive behavior should it be possible to fabricate a memsensor device by further investigation and optimization of the present design. However this will not be part of the present thesis.

4.2 Results for the simple deposition of different dispersions following various techniques

It is important to get a reasonable CNT network that is bridging the gold contacts, but still contains enough nanometer gaps between the CNTs to provide the possibility for a memristive switching network when the metal clusters are applied. In the literature different approaches can be found to deposit or coat devices with CNTs. Ranging from using CNTs dispersed in an aqueous solution (*80*) as a starting point, growing the CNTs on the surface (*81*) or even by growing and transferring them directly onto the sample (*82*). Due to the fact that only a small area (the gap) should be covered and a non-periodical arrangement is a beneficial approach, it was decided to use nanotubes dispersed in an aqueous solution. The non-periodical arrangement was needed so that the effects occurring did not cancel each other out. For this reason different CNT dispersions and several deposition techniques have been investigated and will be discussed in this thesis.

4.2.1 Investigation of the deposition results of different multi-wall and single-wall dispersions

In the course of this thesis four different CNT dispersion (three MWCNT and one CNT dispersion) were investigated on their applicability to deposit them on the surface, the way they distributed on the surface and if the dispersion contained too many unwanted additives.

The first to be presented dispersion is an aqueous one called CarboDis TN of the company FutureCarbon GmbH. This dispersion consists of 2 wt% of MWCNTs dispersed in deionized water with the aid of an electrically neutral surfactant. The starting solution was diluted to a ratio of 1:10 and even to 1:100000 following the prior described method. Afterwards it was applied to the chip as one droplet by using a 3 ml disposable pipette. The droplet was dried in ambient conditions and the resulting network is shown in the SEM image in Figure 19. While both SEM images show a dispersed CNT network, the concentration for the 1:100000 ratio (see Figure 19a) seems to be too low while for the 1:1000 sample (see Figure 19b) it appears

a) **b)**

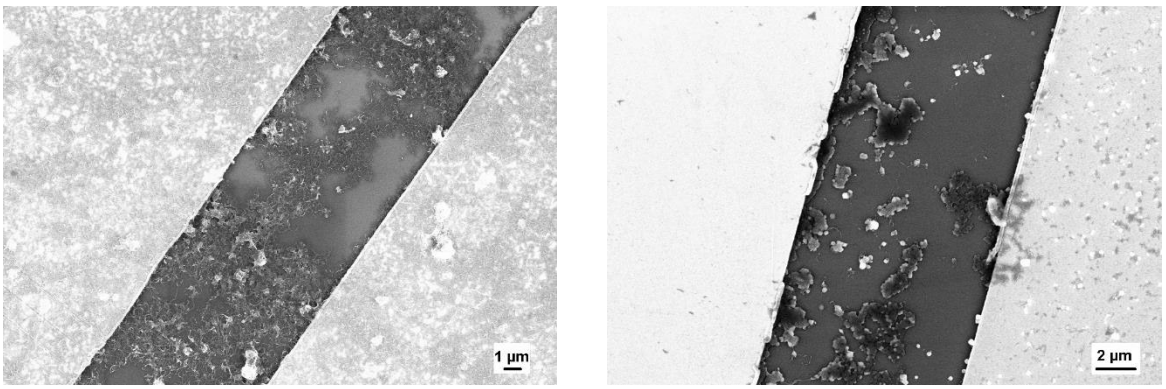

Figure 19: SEM images of a dried in dispersion of CarboDis TN in the ratio a) 1:100000 and b) 1:1000, with both of them showing unwanted impurities.

to be too high. In addition further impurities can be identified that most likely arise from the surfactant of the dispersion, since the chips produced were clean beforehand and did not receive further treatment except the application of the dispersion droplet. For the fabrication of a suitable sample it is highly important to have as little impurities as possible, since they can lower the influence of the electrical field, block clusters sterically and under certain conditions react chemically with parts of the system, especially when an electrical current is applied. In summary because of impurities occurring the CarboDis TN dispersion is unsuited for further experiments.

Aquacyl AQ0302 provided by the company Nanocyl is the second here presented product. This CNT dispersion contains 3 wt% of MWCNTs and an anionic surfactant to provide higher dispersability of the nanotubes in deionized water. The dispersion was diluted stepwise by using the former described ultrasonic disperser method. A ratio of 1:24000 regarding the master solution was chosen to make it comparable to other investigated dispersions. The dispersion selected for comparison was chosen to be the CARBOBYK-9810 since it was a suitable reference dispersion. The ratio was set to 1:64000 for this product resulting in the same as for the Aquacyl since this product contains 3 wt% in comparison to the 8 wt% of the CARBOBYK dispersion. Figure 20 shows SEM images of the resulting deposition on 10 µm gaps for this sample. It can be seen that the amount of CNTs as depicted in both images is too small to form a network. This problem could be easily approached by increasing the amount of

nanotubes by using a less dilute dispersion, but the deposited CNTs in the image display as well that they tend to form agglomerations rather than spreading out over the surface individually. The increased entanglement of the CNTs can be assumed to be caused by the surfactant itself. The surfactants concentration might not have been high enough to hold the nanotubes completely dispersed or that it did not cover the whole CNTs leaving free space to let them physically interact with each other. But since this is not part of this thesis was this aspect not further investigated.

The fact that the CNTs tend to form agglomerates for the dispersions with low concentrations indicate that for the dispersions with higher concentrations the possibility of forming more and bigger agglomerations should increase, due to the higher number of nanotubes. For the reason that a thin network rather than agglomerates of CNTs are needed makes this dispersion unsuitable for further researches. Furthermore the dispersion seems to contain some impurities, in addition to the apparent distribution problems. This impression occurs since the resulting structures not only consist of filamentous parts (the CNTs), but appear to contain broader structures as well. For example the structure shown in Figure 20b (middle right) which could not further be specified, making it impracticable for further usage since these might disturb the later fabricated device.

a) **b)**

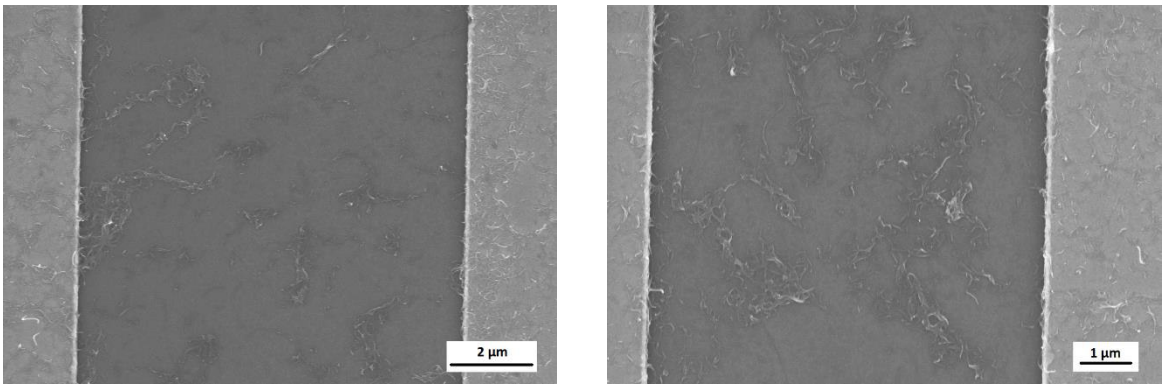

Figure 20: SEM images of a dried in dispersion of Aquacyl in the ratio 1:64000 for two 10 µm gaps. The results are not sufficient in regards of network formation and because of present impurities and agglomerations.

CARBOBYK-9810, a product provided by the company BYK-Chemie GmbH, is the last here MWCNT dispersion presented in this work. It contains 8 wt% of CNTs coated with 2-

methoxymethylethoxyl propanol as a surfactant for dispersion in deionized water. The master solution was diluted following the same procedure as for the CarboDis TN by utilizing the ultrasonic disperser. The outcome of a dried in dilution of 1:40000 is shown in Figure 21 and it can be seen that the CNTs are not widely dispersed across the surface, but are not completely clumped up either. The main advantage for this type of dispersion compared to others (i.e. the one from FutureCarbon) is the absence of additional impurities.

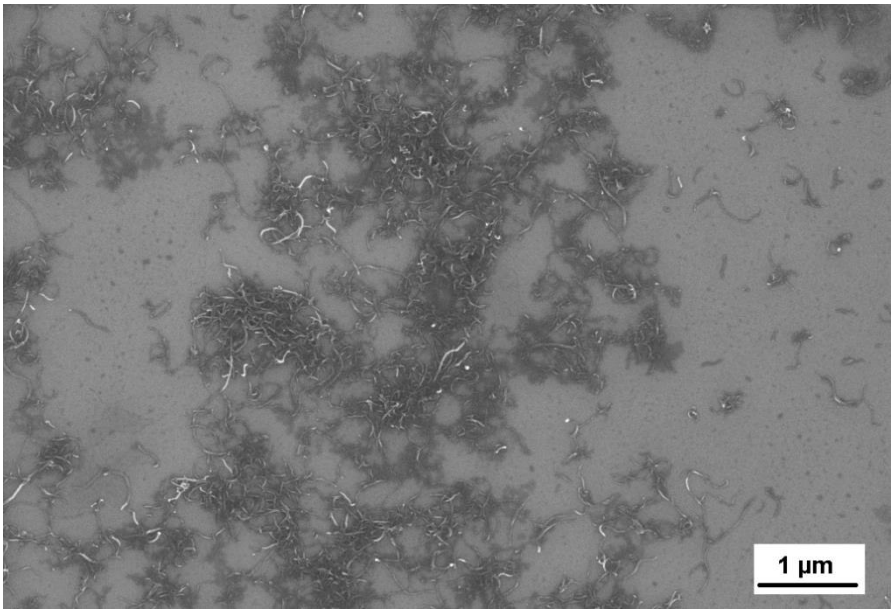

Figure 21: SEM image of a dried in dispersion of Carbobyk-9810 in the ratio 1:40000.

In addition to the MWCNT dispersion a SWCNT dispersion was investigated as well, to be able to compare these two different types of CNTs in regards of their applicability and the way they tend to deposit on the surface. The chosen CNT dispersion was Tuball Ink (product of the company OCSiAl). Tuball Ink contains 0,2 wt% SWCNTs and an electrically neutral surfactant to stabilize the CNTs in the deionized water and to prevent them from agglomeration. The deposition was carried out by repetitively placing one small droplet on top of the gaps as earlier described in the experimental section. Although it is challenging to disperse the diluted CNTs the respective SEM image demonstrates a quite nice distribution on the surface (see Figure 22). The image indicates that the CNTs were distributed quite evenly during the deposition. This sample does not show larger agglomerations of CNTs, in contrast to many of the other investigated dispersions. Some of the nanotubes in the image show a more dense arrangement but are overall quite evenly distributed. In addition no remnants of any kind of

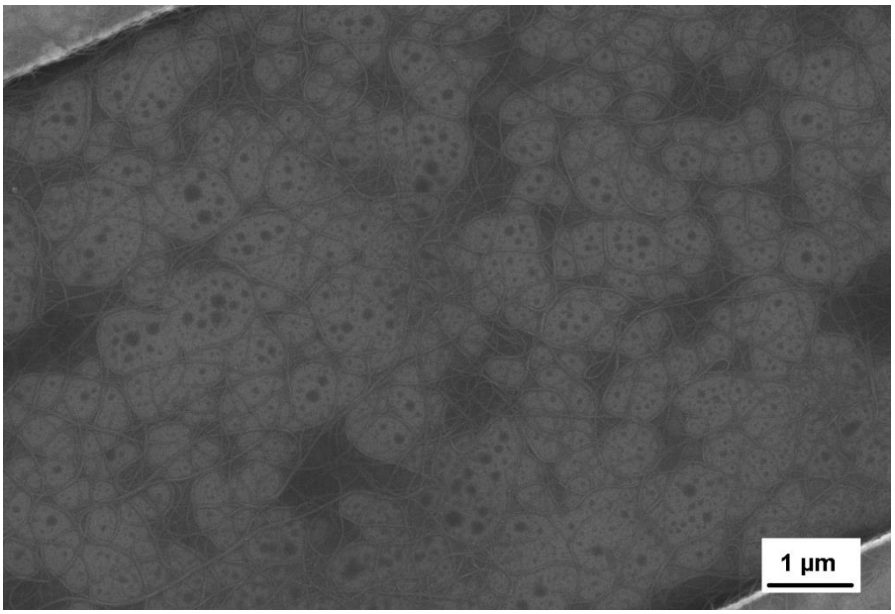

Figure 22: SEM image of SWCNTs of a dried in dispersion of Tuball in the ratio 1:64000.

the surfactant or other impurities are visible, making this dispersion in this regard suitable for further investigations. However, the general investigations were carried out using a MWCNT dispersion since their handling and the dispersing of them is easier than for the SWCNTs. Thus the further results presented in this thesis were achieved by using the CARBOBYK-9810 product.

4.2.2 Influence of the resting time on diluted dispersions

It is important to note that the quality of the dispersions used depends not only on how easy it is to disperse nanotubes, but as well on how old the dispersion is, as it has been already indicated in the experimental section. For which reason this sub-chapter will deal with a further experimental series on the influence of time on the distribution of the CNTs in solution. Therefore the influence of being allowed to rest or kept in steady motion was tested for the dispersion. To keep the samples in motion they were placed on a self-built man conveyor. The quality of the resulting samples was judged on the dispersity of the nanotubes on the surface, which was examined using the SEM.

The outcome of this series is that it has a significant influence on the quality of the distribution of the CNTs on the sample if the dispersion was freshly fabricated or a few days old and just

re-dispersed by using the ultrasonic disperser. There is also no noticeable influence on the dispersion detectable if the solution was kept resting or in movement. The quality of the fresher dispersion is always superior. A possible reason is that during dilution of the dispersions the amount of surfactant is reduced as well, leading to easier agglomeration of the nanotubes in the diluted solution. The influence of the re-dispersing step on the agglomerates to separate them again is therefore limited. An investigation of this connection has to be part of future investigations. For this reason all of the used dispersions were freshly produced to decrease their resting time as much as possible.

4.2.3 Discussion of various simple droplet deposition techniques

The deposition by simple drop coating of different Carbobyk-9810 dispersions in various ratios leads always to the formation of agglomerations on the sample surface similar to the ones shown before. Since this phenomena occurred for different dilutions it can be concluded that the CNTs tend to aggregate more than to spread over the surface, which can be attributed to the fact that the added dispersion droplet is too voluminous. It is assumed that the CNTs can move around freely in the comparably large droplet until they form an agglomeration big enough to sink down onto the surface of the chip or until too much water is evaporated hindering them to move further. To investigate this phenomena various deposition techniques as well as surface coatings were examined to form an agglomeration free sparse CNT network, which will be discussed in this section.

4.2.3.1 Untreated surface

One of the approaches to overcome this issue of the formation of CNT agglomerations was to increase the spreading of the droplet over the surface of the chip. This was done by adding a small amount of isopropanol to the droplet which further decreases the contact angle by 15 – 20° compared to the untreated one. The outcome for this experiment can be seen in Figure 23, which shows that the CNTs tend to agglomerate in certain areas (see Figure 23b) leaving broad areas empty (see Figure 23a). The reason for this behavior is the influence of the solvent on the surfactant of the nanotubes. The addition of isopropanol to the solution

can lead to a partial removal of the surfactant which results in a stronger aggregation of the CNTs.

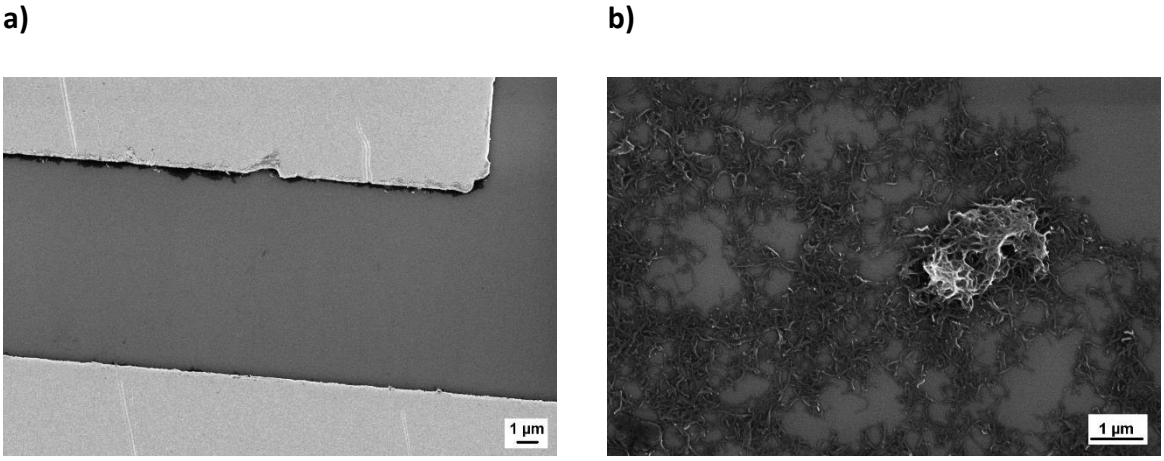

Figure 23: Experimental result of dispersion droplet + isopropanol resulting in a) empty areas and b) aggregations in others.

The second here presented approach, which focuses as well on the acceleration of the evaporation speed, involves the rise of the temperature of the substrate. Therefore a series of experiments is conducted in which the samples were placed on a hot plate during the application of the droplet. An exemplary result of this series can be seen in Figure 24 after letting a droplet of a dispersion with the ratio 1:64000 dry on a T = 90 °C hot sample. It can be seen that this temperature treatment results in the formation of circular stains consisting of

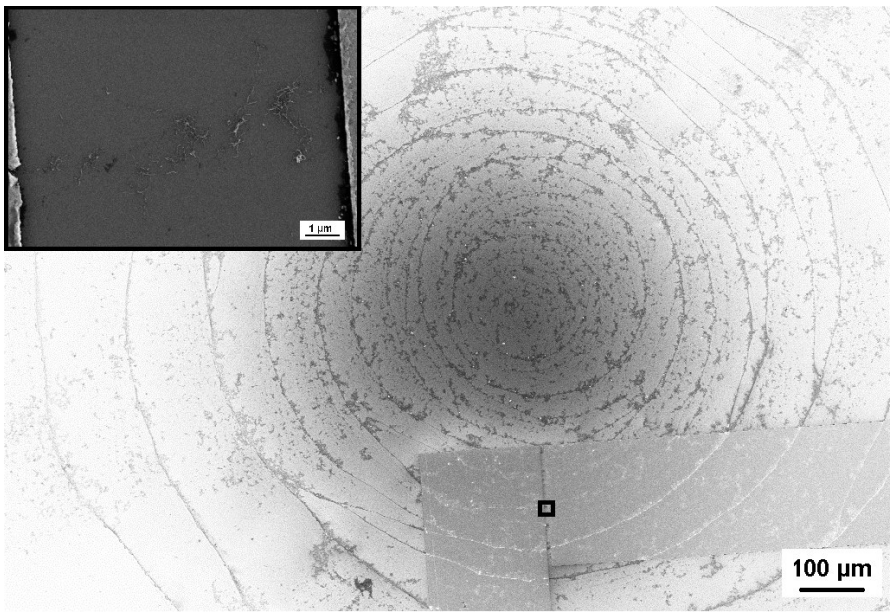

Figure 24: SEM image of a dried in dispersion droplet (ratio 1:64000) on a pre-heated (T = 90 °C) hot plate.

CNTs, which can be concluded from having a closer look at the magnified image. These stains can be explained quite easily with the way a droplet tends to dry in. This effect of leaving stains behind is called coffee-ring or coffee stain effect and was further investigated by Y. Li et al. (*83*), R.D. Deegan et al. (*84*) and P.J. Yunker (*85*). The reason for this phenomenon is that the formation of the rings occurs due to the low evaporation rate of the droplet. This low rate in combination with present capillary forces leads to a particle enrichment at the edges of the droplet and results in the end with this edge growth process, since it does evaporate stepwise. Further temperature increasements above a temperature of 115 °C result in a rise of gas formation inside of the droplet due to a too sudden evaporation, making the droplet instable in its position. In

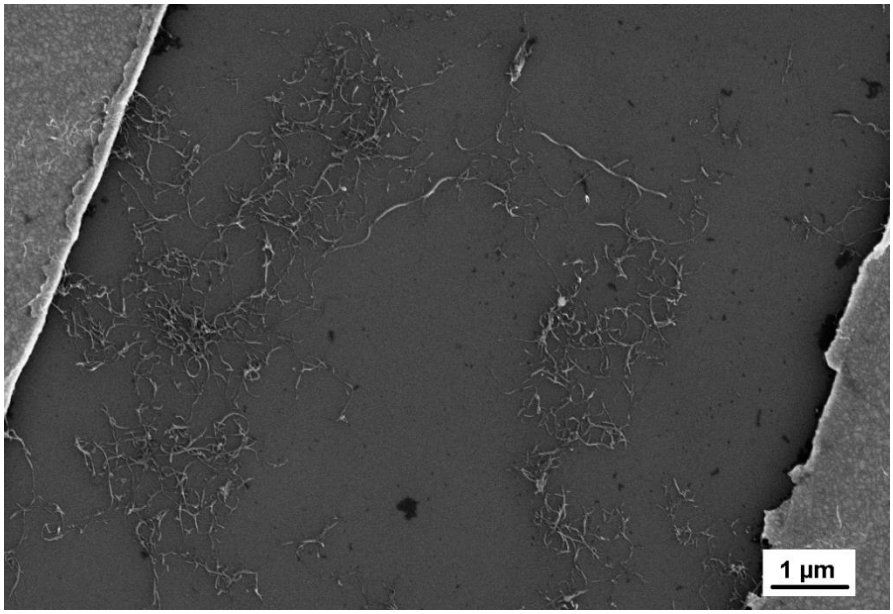

Figure 25: SEM results for a drying in experiment using a substrate temperature of T = 115 °C and a dispersion with the ratio 1:64000.

Figure 24 the outcome of the deposition of a dispersion droplet with the ratio 1:64000 on a 115 °C hot sample surface can be seen. It is noticeable that the result does not show the formation of stains anymore. Furthermore the CNTs do not tend to form agglomerations and are in contrast to prior presented results partly well distributed. During the experiments with elevated sample temperatures it was investigated that the contact angle of the droplet was increased in comparison to droplets applied to samples at room temperature. Therefore it can be assumed that a tuning of the shape of the droplet has a remarkable influence on the way

the CNTs tend to deposit on the samples surface. One reason for this behavior can be that the increased contact angle leads to a smaller probability for formation of the stain effects due to a smaller contact area between droplet and surface. Since when the droplet dries in the system tries to keep the volume in contact with the hot surface as low as possible, resulting in a more uniform deposition of the nanotubes.

In a further attempt to avoid the formation of stains, CNTs were applied by spray coating. Since the nozzles of perfumes are very fine, perfume atomizer samples were used for the spray coating after several cleansing steps were carried out beforehand. The samples to be coated were placed on a 100 °C warm hot plate to increase the evaporation rate of the small droplets even further. The samples were sprayed numerous times and different dispersion concentrations were tested. Figure 26 shows the results of a spray coating experiment carried out with a dispersion of 1:64000 while the dispersion was applied ten times. The SEM pictures show that a decrease of the droplet size and an increase of the surface temperature still lead to the same results as in prior experiments. The sample shows coffee stains going along with areas with an increased amount of carbon nanotubes next to areas with a decreased number of nanotubes. It can therefore be concluded that the use of smaller droplets and an elevated substrate temperature does not lead to a reduction of the stains, but increases the speed of this process resulting in similar outcomes.

a) **b)**

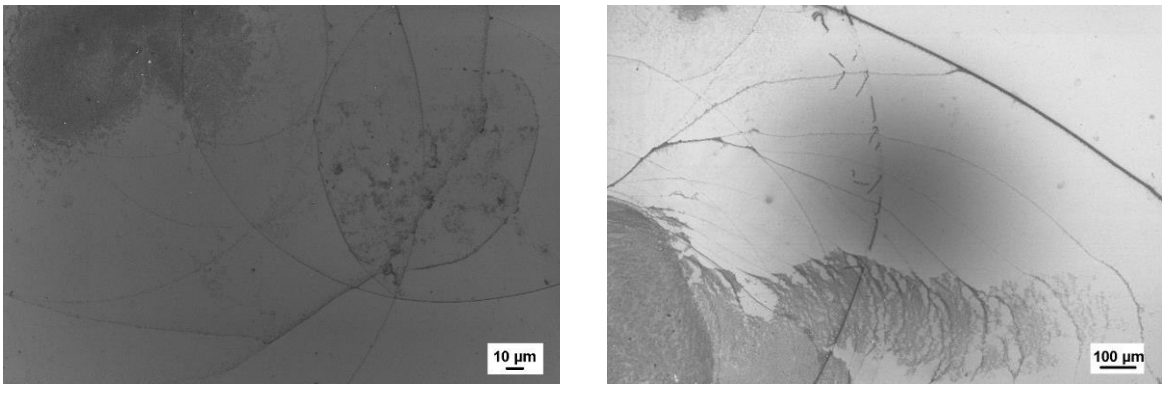

Figure 26: SEM image of the experimental result for an aerosol experimental utilizing an atomizer and a dispersion with the ratio of 1:64000.

4.2.3.2 Treated surface

For another experimental series conducted in the course of this work coated substrates were tested to investigate the influence of contact angle on the CNT deposition. These samples consisted of Si coated with 40 nm of ZnO, Si coated with 40 nm of Al_2O_3 and Si coated with AZO (Al doped ZnO). For the reason that their results are quite alike only the results for the ZnO (Figure 27a+b) and Al_2O_3 (Figure 27c+d) samples are shown. The results displayed here were again produced by using a dispersion with the ratio of 1:64000. The estimated contact angles for the individual sample and the dispersion droplet were all smaller than the one from the original SiO_2 sample, but not by much. Furthermore, all of the SEM images presented in Figure 27 are similar to each other, showing that the CNTs tend to form agglomerations and do not cover the surface evenly. In addition, by having a greater overview of the samples, it is clearly visible that the droplets do not evaporate evenly, as circular shaped stains are visible.

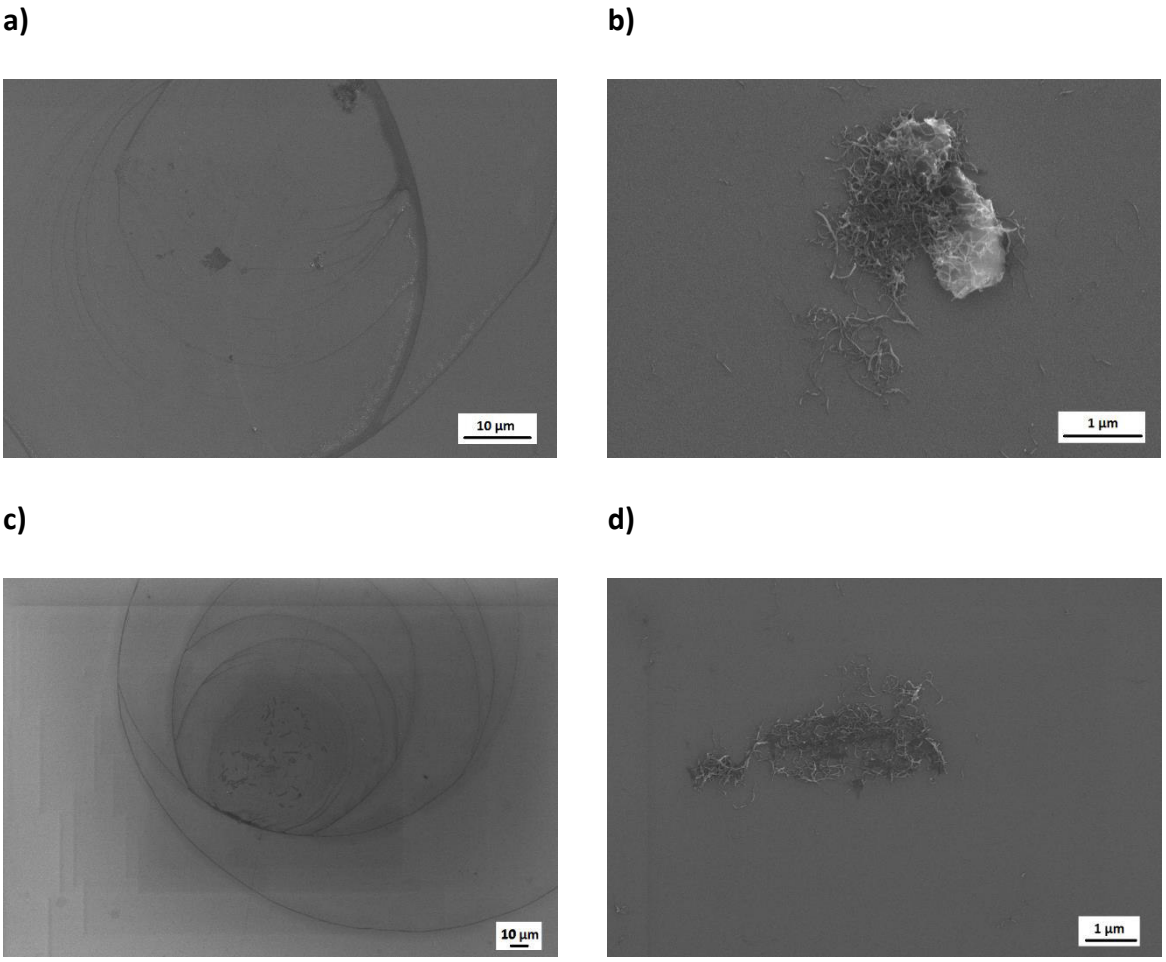

Figure 27: SEM images for the dried in samples a+b) on Si coated with ZnO and c+d) Si coated with Al_2O_3 using a dispersion with the ratio 1:64000.

Moreover silane as potential surface coating was investigated as well. For this reason chips were coated with a thin silane layer as discussed in the experimental section. Furthermore the temperature of the substrate is increased stepwise to examine both influences on the CNT deposition. The most promising results are achieved at a surface temperature of 115 °C and a dispersion ratio of 1:64000 and are shown in Figure 28. By looking at the SEM results in Figure 28 it can be seen that it is possible to form a quite homogenous network over some gaps (see Figure 28a) on the one hand, although other gaps indicate that this is not possible for the whole sample (see Figure 28b). Since experiments carried out at slightly lower surface temperatures show similar results, only differing in the homogeneity of the network for the outer gaps, does this lead to the conclusion that the not only surface coating and temperature influence the nanotube deposition but as well the way the droplet is applied. It still appears that by letting the droplet dry in on the sample's surface that this results in unevenly distributed CNT networks.

a) **b)**

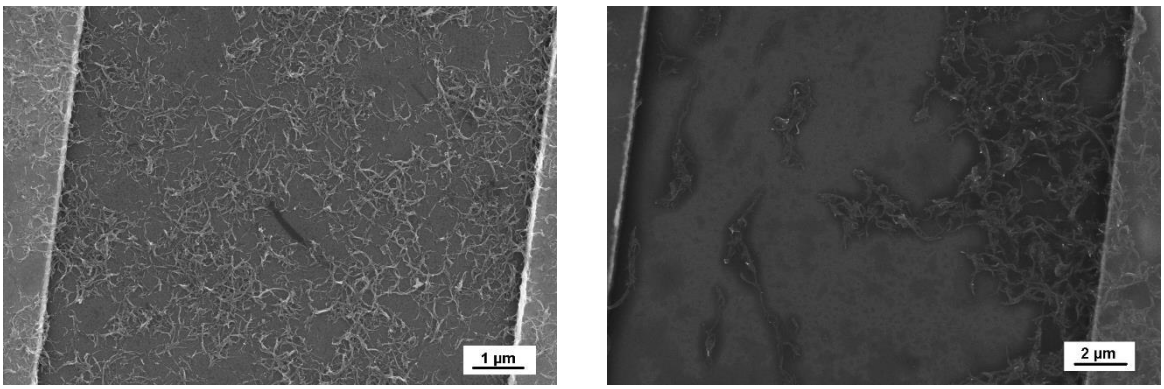

Figure 28: SEM image of a silanized sample decorated with CNTs (dispersion ratio 1:64000) and a substrate temperature of T =115 °C.

Investigations on alternative types of droplet deposition were carried out by either sweeping the droplet over the sample or by tipping it onto the surface. Results for the sweeping approach can be seen in Figure 29. While the used technique is further described in the experimental section lies the difficulty in the execution of it, since one has to make sure that the same number of wipes are performed over all of the sample area and not to lose the droplet during the process. The idea of this technique is to apply the CNTs out of the droplet like the ink out of a ball pen. The in Figure 29 shown sample results are produced by swiping and using a dispersion with the concentration of 1:6400. In Figure 29a it can be seen that the

experimental result shows in some areas a more widely homogenous network, but again leaving some of the gaps nearly uncovered (see Figure 29b). For the sample shown it can be concluded that the increased density of the network presented in Figure a results from the higher concentration of the dispersion used. It can be noticed as well that the gaps in the middle of the chip architecture are the least coated ones. Therefore it is assumed that the problem here is that most of the CNTs are preferably deposited at the surface along the outer areas of the chip, leaving too few CNTs in the droplet to cover the inner gaps homogenously as well. This results in an oversaturation of the outer and undersaturation for the more central gaps. Even by trying different swiping approaches it is not possible to get a more homogenous result. Therefore it can be concluded that this result is caused by the effect that by applying

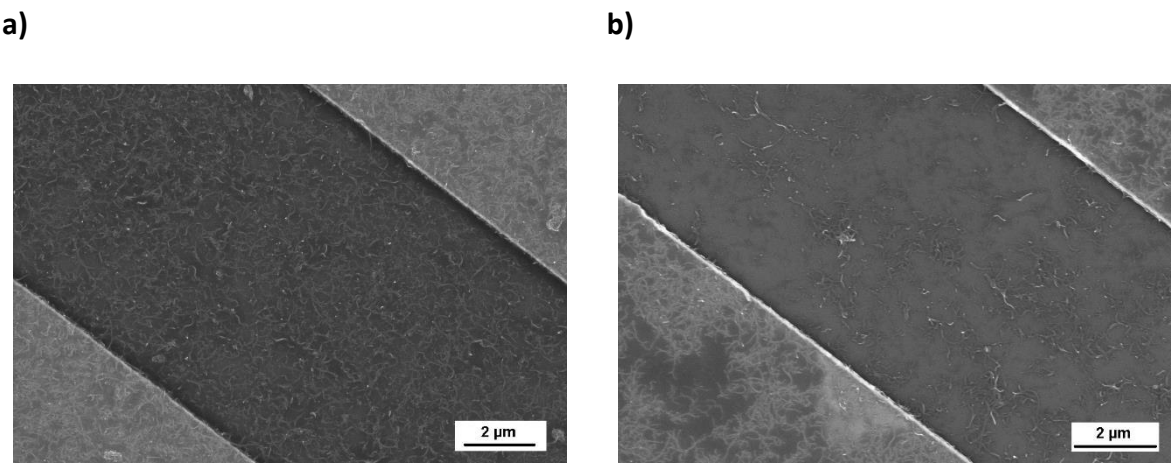

Figure 29: SEM image of silanized sample after swiping a dispersion droplet (ratio 1:6400) over the pre-heated surface several times.

the droplet only the CNTs at the surface of the droplet get attached to the surface of the sample (like a stamp). For the other remaining nanotubes it is more favorable to stay inside of the volume of the droplet in solution than to move to the outside of it and getting attached to the sample surface, resulting in a decrease in the amount of deposited CNTs while moving the droplet. An additional factor is that as soon as the droplet is applied the temperature of the samples surface decreases. Therefore in the first moment the droplet is applied the temperature is significantly higher, which results in a sudden evaporation of the tip of the droplet which is in contact with it. This leads to a first coating of the surface with nanotubes, since the CNTs at the tip of the droplet are unable to react fast enough to stay in the solution. Abdelaziz et al. (*86*) investigated such reaction of a cold droplet on a hot plate. They reported

that an immediate and spontaneous evaporation occurs at the contact area. Furthermore it is possible to detect conducted charge separation and a temperature gradient inside of the droplet. Hence it can be stated that the charge separation and as well the temperature gradient lead to a depletion zone in regards to the CNT concentration at and close to the contact area after the first tangency. This observation was as well proofed to be correct by research published by Elbahri et al. (*87*). They postulated further that a temperature gradient is present in the droplet. This gradient should for this reason be present in the dispersion (used for the here presented sample preparation) as well and would lead to a further induced upstream since the warm water rises in the direction of the colder area which results therefore in an additional upturned movement of the dispersed nanotubes. This leads to the conclusion that since the held and swiped droplet does not turn like the ball from a ball pen that this causes the lower deposition of CNTs for the more centered gaps.

The approach of tipping the dispersion droplet onto the sample surface several times was carried out with samples similar prepared to the ones for the just described sweeping technique. The outcome for this tipping approach can be seen in Figure 30. Presented is one

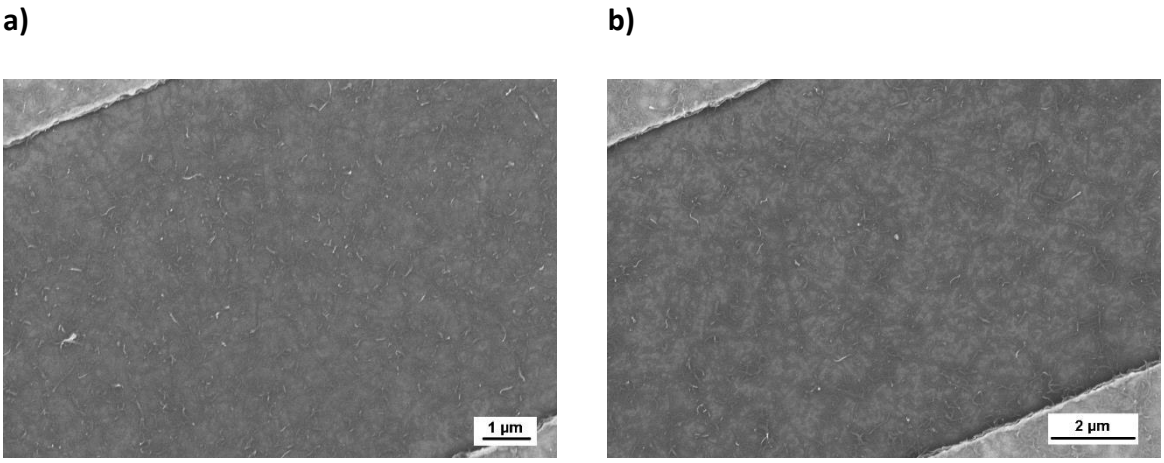

Figure 30: SEM image of silanized sample after tipping a dispersion droplet (1:64000) on each gap individually on the pre-heated samples.

of the outer gaps (Figure 30a) and one of the inner gaps (Figure 30b). It can be seen that the usage of the tipping technique results in a far more homogenous nanotube network over all of the gaps. This fact also proves the observation that the differences in the coating of the

gaps result from the application of the dispersion by swiping. Due to the technique of dipping the droplet onto the surface and always using a fresh droplet it is possible to form an excellent homogenous and as well partly sparse network, since a fresh layer is applied with each dip resulting in the present network.

The series of experiments presented here shows that the deposition of CNTs is not straight forward process if there is the need for a sparse and agglomeration free network. It was shown that it is important to use an appropriate CNT dispersion as well as that the resulting contact angle (influenced by coating and heating of the sample) have a positive influence on the resulting distribution of the nanotubes on the surface. Furthermore it was shown that by repetitive tipping of a dispersion droplet onto the surface it is possible to generate an excellent homogenous and reproducible sparse CNT network between two gold contacts without the usage of further additives.

4.3 Manipulation of the CNT network

In order to generate a homogenous and sparse network experiments were conducted with the aim to manipulate an already deposited dense CNT network in order to decrease the amount of interconnections and therefore to increase the number of nano gaps. For this reason various approaches were performed ranging from simple attempts to use ultrasonic – in order to move the nanotubes physically – up to chemical treatments with acids to etch the CNTs partly or to fuse them by applying voltages above 100 V. The different approaches carried out will be discussed in the following segment in regards of their practicability and influence on the deposited network.

4.3.1 Ultrasonication and temperature treatments

The first approach presented is the attempt to rearrange the deposited CNT network by wet and dry ultrasonication. These experiments were carried out as described in the experimental section. Some of the results of a series of experiments, after a hysteresis pulse with a heights of 0.5 V was applied pre- and post-treatment, are presented in Table 1 (for simplifications only the measured maximum values are noted). Notable at first glance are the large differences in the individual gaps. While the measured current for the large 10 µm gap is ~10^{-7} A, for the 1 µm gap it is up to 3 orders of magnitude smaller (~10^{-5} A). This might be due to the inhomogeneous deposition of the nanotubes. The outcome for the dry ultrasonication experiments, in which the samples were placed into the ultrasonicator for up to ten minutes, show no significant changes in the measured current values and is in the regime of measurement errors or noise. This indicates that the nanotubes are not only lying freely on the surface but are fairly strong bound to each other by weak forces such as van-der-Waals forces, making them immobile.

In the second part of the ultrasonic experimental series, samples were dipped in a beaker of deionized water which was placed in an ultrasonic bath. It is notable, by having a look at the measurement results in Table 1, that for several individual gaps no successful electrical

measurements can be carried out. From this it is followed that the present weak physical bonds are strong enough to hold the nanotubes in place during the dry ultrasonication, but

Table 1: Results for the ultrasonic experiments for different CNT concentrations after applying a voltage of 0.5 V.

	CNT Dilution	**gap (µm)**	**I [A] pre-treatment**	**I [A] post-treatment**
Ultrasonic (dry)	**1:170000**	**2.1 (1 µm)**	$1.7 \cdot 10^{-6}$	$1.8 \cdot 10^{-6}$
		2.2 (2 µm)	$7.3 \cdot 10^{-5}$	$7.6 \cdot 10^{-5}$
		1.4 (10 µm)	$1.7 \cdot 10^{-7}$	$1.9 \cdot 10^{-7}$
	1:120000	**2.1 (1 µm)**	$8.1 \cdot 10^{-4}$	$1.3 \cdot 10^{-4}$
		2.2 (2 µm)	$8.7 \cdot 10^{-5}$	$5.7 \cdot 10^{-5}$
		1.1 (10 µm)	$1.5 \cdot 10^{-6}$	$1.6 \cdot 10^{-6}$
		1.2 (10 µm)	$2.0 \cdot 10^{-9}$	$1.4 \cdot 10^{-9}$
		1.4 (10 µm)	$3.0 \cdot 10^{-7}$	$3.2 \cdot 10^{-7}$
Ultrasonic (dip)	**1:170000**	**2.1 (1 µm)**	$6.1 \cdot 10^{-8}$	$2.8 \cdot 10^{-8}$
		2.2 (2 µm)	$8.9 \cdot 10^{-6}$	$8.0 \cdot 10^{-6}$
		1.1 (10 µm)	$2.9 \cdot 10^{-9}$	----------
		1.3 (10 µm)	$2.2 \cdot 10^{-7}$	$5.1 \cdot 10^{-9}$
		1.4 (10 µm)	$2.6 \cdot 10^{-6}$	$5.6 \cdot 10^{-7}$
	1:170000	**2.1 (1 µm)**	$1.4 \cdot 10^{-5}$	--------
		2.2 (2 µm)	$2.0 \cdot 10^{-6}$	--------
		2.4 (8 µm)	$6.0 \cdot 10^{-10}$	--------
		1.1 (10 µm)	$1.0 \cdot 10^{-4}$	--------
		1.2 (10 µm)	$1.1 \cdot 10^{-6}$	--------

fail as soon as water is involved. It is therefore assumed that the CNTs are partly re-dispersed again into the deionized water due to the presence of the surfactant coating.

In order to investigate the influence of heat on the nanotube network the samples were heated above 150 °C, as described in the experimental section. The outcome of these experiments are shown in Table 2 for sample S6. The results of the pre-treated samples show a large difference in the measured values (ranging from ~10^{-6} A to ~10^{-8} A). This can be due to the random distribution of the nanotubes across the surface/gap while drying, since the networks were generated by drop coating of dispersions with a high concentration. The heat treated samples show a constant increase in the measured current by an order of magnitude

Table 2: Results for the heat treatment (S6) and cooling (S7) experiments measured with a voltage of 0,5 V.

	Sample S6		**Sample S7**	
gap (µm)	**I [A] (pre-treatment)**	**I [A] (post-treatment)**	**I [A] (pre-treatment)**	**I [A] (post-treatment)**
1.1 (10 µm)	$1{,}7\cdot10^{-6}$	$2{,}5\cdot10^{-5}$	$1{,}2\cdot10^{-6}$	$3{,}3\cdot10^{-8}$
1.2 (10 µm)	$2{,}2\cdot10^{-6}$	$2{,}3\cdot10^{-5}$	$7{,}5\cdot10^{-7}$	$9{,}4\cdot10^{-7}$
1.3 (10 µm)	$4{,}1\cdot10^{-6}$	$2{,}6\cdot10^{-5}$	$4{,}3\cdot10^{-8}$	$7{,}4\cdot10^{-8}$
1.4 (10 µm)	$3{,}8\cdot10^{-6}$	$3{,}0\cdot10^{-5}$	$2{,}0\cdot10^{-7}$	$1{,}1\cdot10^{-7}$

from 10^{-6} to 10^{-5} A. A plausible explanation for this phenomena is that due to the higher temperatures the carbon nanotubes start to fuse together (induced by Joule heating), forming better contacts and leading to a lower resistivity of the network. This phenomena was documented by Li et al. (*88*), where it is attributed to the increase of the temperature over a threshold value and a with it linked transition of the nanotube matrix from the solid to the liquid phase leading to an improvement of the interconnections. This point was proved as well by Lu et al. (*89*).

Not only was the influence of heat, but the general effect of temperature on the resulting network examined. For this reason the system was exposed to liquid nitrogen as described in the experimental section. At first sight the change for the liquid nitrogen treatment seems to have a large impact on the network (see Table 2, sample S7), since for the first measurement the difference between pre-treatment ($1{,}2 \cdot 10^{-6}$ A) and post-treatment ($3{,}3 \cdot 10^{-8}$ A) is in the range of two orders of magnitude. However, the further the measurement series for these gaps went, the smaller the difference between the respective measurements becomes. The reason for this is most likely that the sample acclimatizes during the course of the measurements leading to an increase in its temperature. The temperature of the liquid nitrogen is ~70 K (*90*) and the experiments were carried out at room temperature (roughly 298 K). While the sample might be close to the temperature of the liquid nitrogen after the immediate transfer from the nitrogen to the electrical setup the contacting of the needles and the measurement itself needs some time. This timeframe of transfer and contacting of around one minute is enough time for the sample to heat up, getting closer to room temperature again. This is indicated by the measurement differences between pre- and post-treatment since the resistivity decreases over the course of the survey of one chip. The influence of the temperature on the conductivity of CNTs was shown before as well by Singh et al. (*91, 92*), proving the correct assumption.

The experimental results presented in this section for the temperature and ultrasonication treatment of the deposited nanotube network does not lead to the wanted decrease of the interconnections. While the heat treatment results in a strengthening of the network, while the only influence monitored change in resistivity for the nitrogen treated samples is caused by a heating of the sample back to room temperature. Furthermore, dry ultrasonication experiments lead to no change in the system, while the addition of water results in a re-dispersion of the nanotubes. Making all of the presented approaches impractical for the wanted manipulation of the network.

4.3.2 Network manipulation with acids

Another approach to tackle the manipulation of the network is the treatment of the samples with acids to weaken the bonds between the CNTs. This was done by applying nitric and sulfuric acid individually or combined at different concentrations. These acids were chosen due to their ability to oxidize C=C bonds (*93, 94*), while the combination of these acids in oxidizing CNTs was studied by Lee et al. (*95*). The samples were rinsed carefully with deionized

Table 3: Results for the acid treated samples with HNO_3 (0,02 M) (S1), H_2SO_4 (0,05 M) (S3) and a mixture of both (S4) measured with a voltage of 0,5 V.

	S1		**S2**		**S3**	
gap (µm)	**I [A] (pre)**	**I [A] (post)**	**I [A] (pre)**	**I [A] (post)**	**I [A] (pre)**	**I [A] (post)**
1.1 (10 µm)	$7{,}9\cdot10^{-6}$	$3{,}2\cdot10^{-6}$	$1{,}3\cdot10^{-5}$	$3{,}4\cdot10^{-6}$	$3{,}7\cdot10^{-6}$	$1{,}2\cdot10^{-5}$
1.2 (10 µm)	$5{,}4\cdot10^{-7}$	$6{,}7\cdot10^{-8}$	$2{,}3\cdot10^{-8}$	$2{,}4\cdot10^{-7}$	$4{,}0\cdot10^{-7}$	$1{,}3\cdot10^{-8}$

water after the acid was applied for some time under ambient conditions to remove acid residuals from the surface, since they would participate in the electrical measurements carried out afterwards as well, distorting the results. The results for the application of the acids in low concentration can be seen in Table 3. Again there is a large difference in the measured current visible for the respective gaps already pre-treatment (same holds for results presented in Table 4 for which a higher acid concentration was used). This irregularity is attributed to the same

a) **b)**

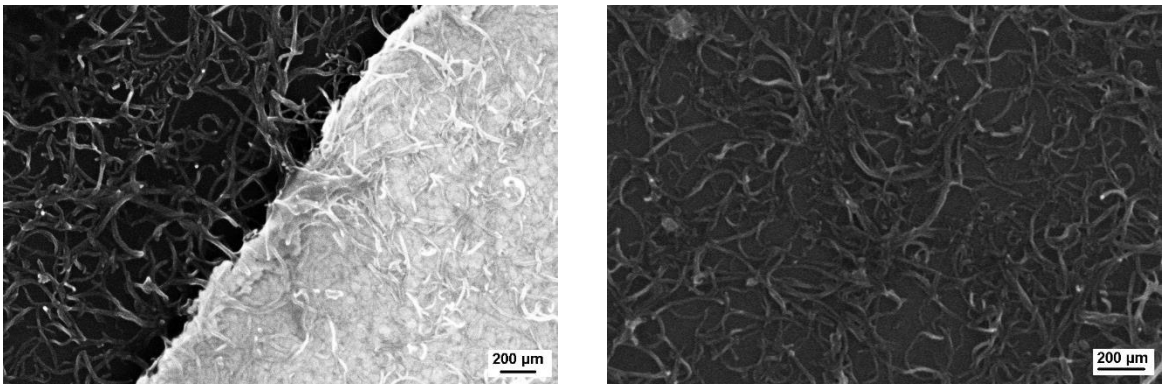

Figure 31: a) SEM image of S1 after treatment b) untreated CNT sample. Both samples were prepared using a 1:8000 CARBOBYK solution applied via drop coating.

cause as for Table 2 and not further discussed here. Almost every analyzed gap shows an increase in the resistivity in the order of one magnitude post treatment. The sample S1 shows the smallest change for the 1.1 gap with only a change of nearly half a magnitude (from $7{,}9 \cdot 10^{-6}$ A to $3{,}2 \cdot 10^{-6}$ A). By comparing Figure 31a (S1 after treatment) and Figure 31b (an untreated sample) no real differences can be told by comparing the CNT present networks.

The experimental results for the samples conducted with higher concentrated acids are shown in Table 4. The concentrations of the used acids were 60 times (for HNO_3) and 30 times (for

Table 4: Results for the acid treated samples with HNO_3 (1,3 M) (S4), H_2SO_4 (1,5 M) (S5) measured with a voltage of 0,5 V.

	S4		**S5**	
gap (µm)	**I [A] (pre)**	**I [A] (post)**	**I [A] (pre)**	**I [A] (post)**
1.3 (10 µm)	$2{,}4 \cdot 10^{-7}$	$8{,}0 \cdot 10^{-8}$	$2{,}3 \cdot 10^{-9}$	$1{,}0 \cdot 10^{-6}$
1.4 (10 µm)	$4{,}8 \cdot 10^{-6}$	$7{,}6 \cdot 10^{-7}$	$5{,}3 \cdot 10^{-9}$	$1{,}8 \cdot 10^{-5}$

H_2SO_4) higher than the prior used acid solutions. The outcome for the HNO_3 treated sample (S4) is a change of merely one order of magnitude and therefore in the same range as for the way lower concentrated experiment presented prior. In contrast to this doe the H_2SO_4 treated

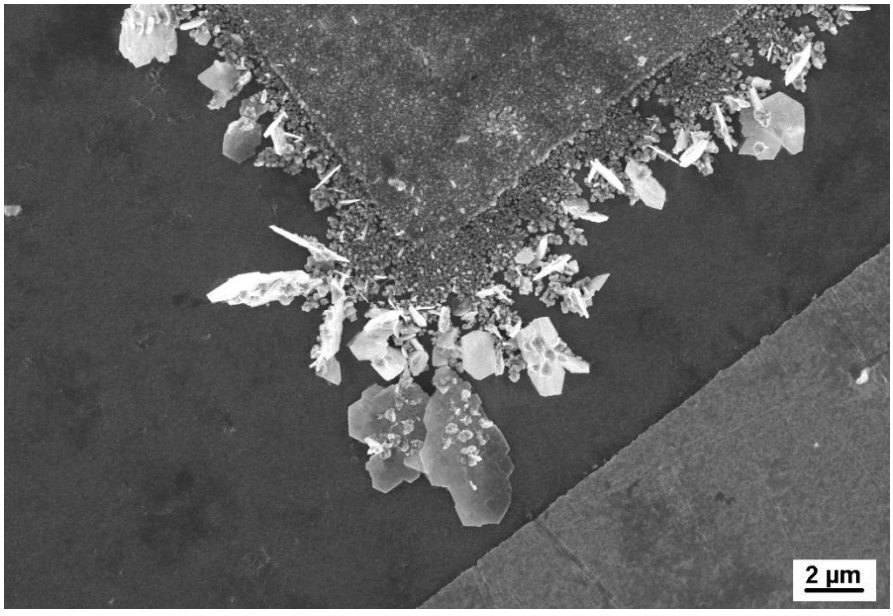

Figure 32: SEM image of sample S5 after sulfuric acid treatment. Showing some grown crystals.

sample (S5) show a major change in the measured current. Here the current changes from 10^{-9} to $10^{-6}/10^{-5}$ A. This result stands in contrast to the prior discussed ones, since the sulfuric acid should oxidize the CNTs causing them to break when the voltage is applied leading to an increase in resistivity, while here the treatment results in a decrease of it. A closer look at the SEM images (see Figure 32) give a clear indication on what causes this decrease. It can be seen that it comes under the influence of the sulfuric acid to a formation of crystals. These crystals span over the gaps, forming an additional path over to the opposing gold electrode resulting in a drop of the later measured resistivity. The cause of the crystal formation has not been studied further, but might be caused by impurities or a reaction with the surfactant of the carbon nanotubes or the nanotubes themselves.

Based on the results of the presented experiments no major change of the current measured can be attributed entirely to the oxidizing ability of the acids on the CNTs. Even the combination of nitric and sulfuric acid has no amplifying effect on the experimental outcome. Furthermore, since some of the experiments tend to the formation of unwanted crystal structures are these networks treatment not feasible for its manipulation

4.3.3 Applying high voltage pulses

By understanding the CNTs as electrical conductors, it can be assumed that it can be possible to fuse them like an ordinary cable by applying a voltage just high enough to burn them. This concept was tested in the scope of this thesis as a further approach of network manipulation and will be discussed in the following.

One exemplary series for the application of higher voltages can be found in Table 5. The samples presented were fabricated using a CNT dispersion with the ratio 1:40000. It can be seen that the treatment with a 10 V pulse, which is applied in the way it was described in the experimental section, does only result in a small deviation which can be caused as well by a measurement error. On the other hand, the higher applied pulses to the samples S8 and S9 lead to a more notable change in current, from $8{,}2\cdot10^{-6}$ A and $7{,}0\cdot10^{-8}$ A to $1{,}8\cdot10^{-5}$ A and

$2{,}4 \cdot 10^{-7}$ A, respectively. Similar to the previously discussed change in the conductivity this effect can be likewise addressed to the fusing of the CNTs (*88, 89*). Although this time the fusing is not caused by the direct heating (originating from the usage of the hotplate) but rather by the temperature increase that occurs as the charge carriers are passing through the nanotubes and for this reason resulting Joules heating.

Table 5: Results of sample S8 and S9 after different voltage pulses with a length of 40 s (measured with a voltage of 0,5 V).

Sample	I [A] untreated	I [A] after 10 V pulse	I [A] after 30 V pulse
S8	$8{,}2 \cdot 10^{-6}$	$9{,}1 \cdot 10^{-6}$	$1{,}8 \cdot 10^{-5}$
S9	$7{,}0 \cdot 10^{-8}$	$7{,}4 \cdot 10^{-8}$	$2{,}4 \cdot 10^{-7}$

The application of even higher voltages shows a different outcome as documented in Table 6. While the treatment for S10 consisted of a pulse of 100 V for a time of 16 seconds, a higher (150 V) but shorter pulse (0,01 s) was applied to S11. For both experiments a drastic decrease in the measured current and therefore an increase in the resulting resistivity of up to three orders of magnitude can be noted. One might jump to the conclusion that the drastic decrease and the networks conductivity are caused by the destruction of the CNTs or their interconnections, but the SEM pictures from similar treated samples show another cause.

Table 6: Results of sample S10 and S11 after different voltage pulses of different length (measured with a voltage of 0,5 V).

Sample	I [A] untreated	I [A] after 100 V pulse (16 s)	Sample	I [A] untreated	I [A] after 150 V pulse (0,01 s)
S10	$3{,}9 \cdot 10^{-6}$	$1{,}5 \cdot 10^{-9}$	S11	$1{,}3 \cdot 10^{-6}$	$8{,}0 \cdot 10^{-9}$

In both SEM images (see Figure 33a and Figure 33b) an overview of a CNT covered and treated gap can be seen. It is clearly visible that the change in the resistivity in Table 6 is not caused by the breaking of CNT interconnections, but rather by the destruction of the gold contacts themselves. According to what the SEM images show, the high voltage and therefore high number of charge carriers is enough to melt the gold contacts. In some areas in Figure 33b it even seems as if the molten gold film has partly exploded since droplet like structures are lying

a) **b)**

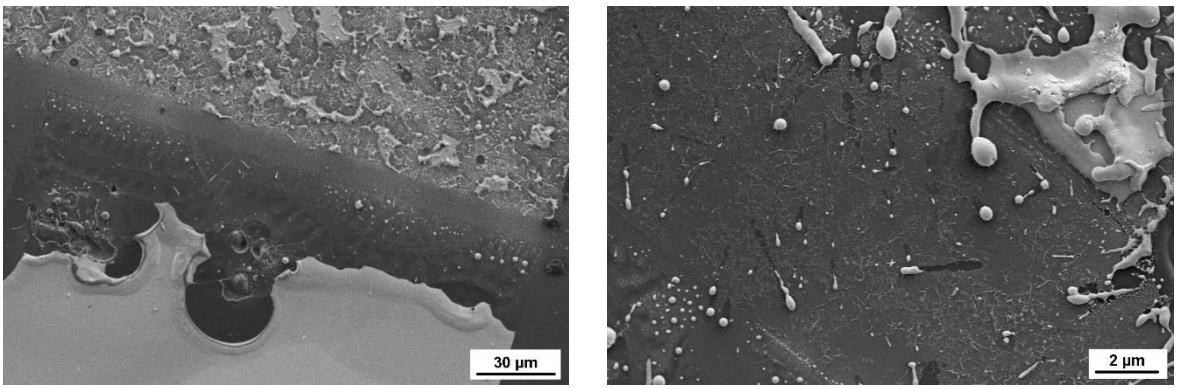

Figure 33: a) SEM image of S10 after the electrical treatment and b) SEM image of S11 after the electrical treatment. Both showing major damage on the gold contacts.

in the middle of the gap, where normally no gold can be found. In addition to the melting of the contacts an electrical breakdown can be seen. This is indicated by the small circles at the contacts in Figure 33a. These circles can be found as well at the positions where the sample was contacted with the help of the needles giving an additional hint that a break down through the underlying insulating SiO_2 layer occurs due to the high voltage. A further SEM image of the contact between gold pad and the tungsten contact needle can be seen in Figure 34. It is

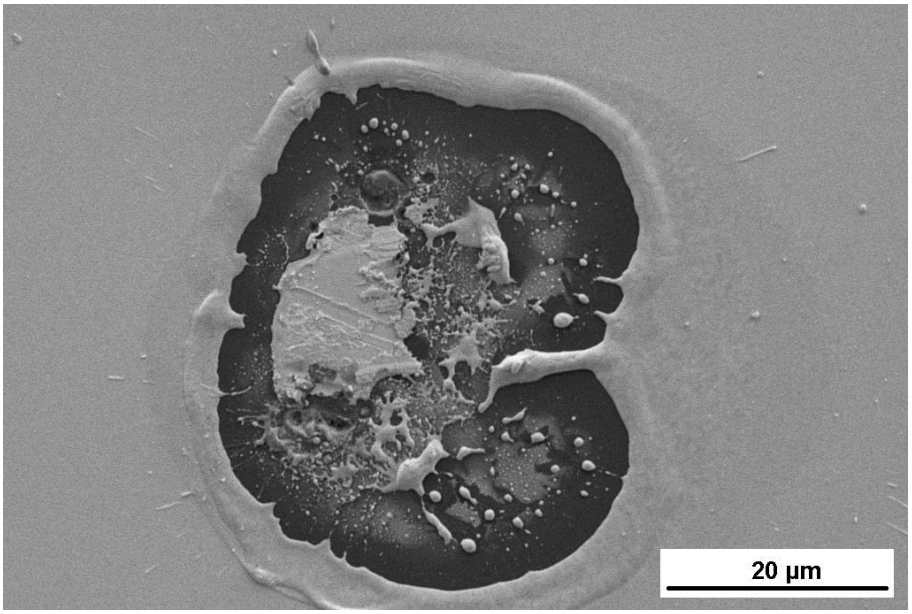

Figure 34: SEM image of one of the positions of the needles on the gold pad after applying a voltage above 100 V showing a major damaged gold pad.

shown that usage of such high voltages at these contact points induces a sudden fusing of the gold contacts. This indicates, on the other hand, that the observed fusing is not only a gap contact phenomena but does likewise occur at the needle contacts. Since the layer underneath the insulating layer is made of doped silicon it should be possible to induce a change in a measured current by exposing the sample to UV light. In case of an electrical breakdown does the influence of the UV light create additional charge carriers semiconductor (the doped silicon) resulting in an increase of the current. Experimental results for such an examination are shown in Figure 35. For this experiment a normal hysteresis with a maximum voltage of +/-0,5 V was run, while being exposed periodically to an UV source. One is able to identify easily when the switching of the UV source occurred. The switching results in sudden changes in the measured electrical current. This can be seen for example in the recorded measurement while having a look at the back swing of the first positive hysteresis curve. Here the UV source switches on at a voltage of 0,25 V and switches off around the 0 V mark. The system reacts directly with a current jump of 0,02 µA and decreases again in respective heights to the applied voltage when the lamp is turned off. Additional sharp jumps can be noted by having a closer look into the measurement results while all indicated the same behavior. For this reason it is inferred from this that the changes in current result from the breakdown of the insulating layer and therefore interaction of the underlying semiconductor layer underneath with the UV light, and not with other possible changes of the network.

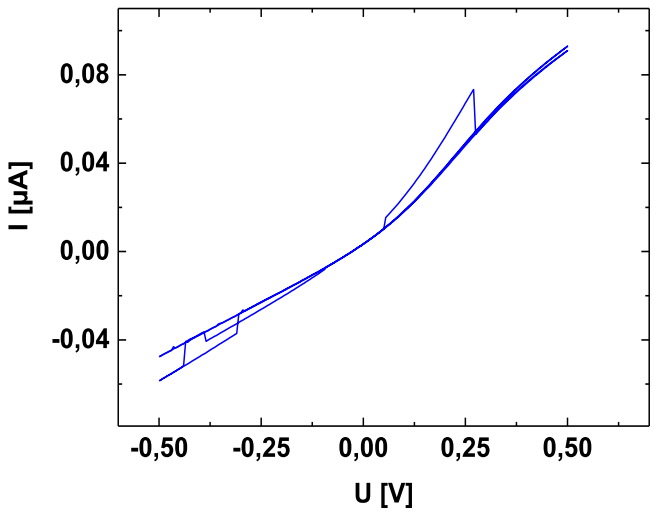

Figure 35: IV characteristic of a sample after experiencing a break down and being exposed periodically to UV light (maximum applied voltage 0,5 V).

Experiments carried out voltages below 100 V and above 30 V were carried out as well. Their results are not shown here, since they show little to no effect or only vary slightly from the already discussed results. Overall can be stated that higher voltages tend to fuse the CNTs, improving their conductivity, while even larger voltages above 100 V lead to a destruction of the gold pads. These results show as well that the used design of the device can at least withstand voltages of up to 70 V without being destroyed. Whilst using the here presented result one should refrain from voltages above 10 V to prevent the nanotube network from getting strengthened due to the reported fusing.

By having a look at the results discussed in this section, it can be seen that the manipulation of a carbon nanotube network is quite challenging. The use of acids (H_2SO_4 and HNO_3) does lead to a change in the resistivity, but induces the growth of some kind of crystal structures, which influence the conductivity measurements significantly. Ultrasonic and temperature treatments show little to no change in the network, only resulting in an increase of the conductivity for the heat treated samples. The voltage treatments show that the system can withstand voltages of 70 V without harm, but that it is not possible to burn the CNTs utilizing the Joules heating, since they are way more stable than the gold contacts, which ‘blow up’ if one applies voltages above 100 V.

4.4 Investigation and analysis of the formed CNT network

In order to get a working memristive device it is highly important to understand the device one is working with in order to get deeper knowledge of its working principles and to make adjustments if necessary. Therefore the following chapter will cover the examination of the chip decorated with carbon nanotubes in regards of its current – voltage characteristics.

4.4.1 Analysis of the formed nanotube network

To investigate the generated CNT networks were electrical measurements conducted. For the results shown in Figure 36 three voltage sweeps ranging from 0 V to +5 V to -5 V and back to the starting value were applied. The first cycle (indicated by the roman I) shows no significant change in measured current until a voltage larger than 2,5 V is applied. From here on the measured current increases by roughly 50 µA in the same voltage interval (indicated by the arrow). By decreasing the voltage again the curve follows another path than the one described prior and ends more in a straight line in the origin. The behavior in the negative direction is less pronounced and therefore the difference between the forward and backward direction

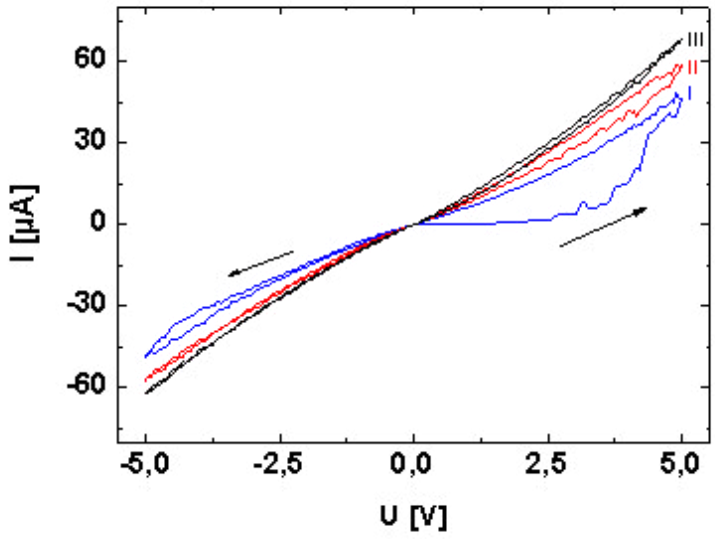

Figure 36: Result of the electrical investigation of the CNT network by applying a hysteresis of 5 V.

is not that large. The curve ends again after decreasing the voltage in the origin. For the second (II) and third (III) cycle the measured current maximum increases successively by around 10 µA. Furthermore the difference between the forward and backward direction is less and less pronounced and vanishes completely during additional cycles. The change in resistivity can be addressed again to the fusion of the CNTs (*88, 89*) as was discussed earlier in this thesis.

It can be concluded from these measurements that for the pure CNT network a hysteresis curve can be measured which differs in the forward and backward direction, but tends to decrease during additional cycles. In addition is the behavior of the curve symmetrical in positive and negative voltage direction to each other. One of the criteria for a memristor is the asymmetry between the two different voltage regimes. Therefore, the investigated device fails in these regards. The explanation for this kind of failing can be found in the already mentioned symmetry of the system. The memristor shows asymmetric behavior, while the investigated system behaved in the opposite way. By having a look in the structure of the different devices it becomes clearer why the individual systems behave the way they do. In Figure 37 a sketch of a TiO_2 memristor and for the used CNT device is shown. It is clearly visible that the presented CNT device shows a quite symmetric structure (independent of the point of view does it consist of two gold contacts bridged by a CNT network). While the one of the

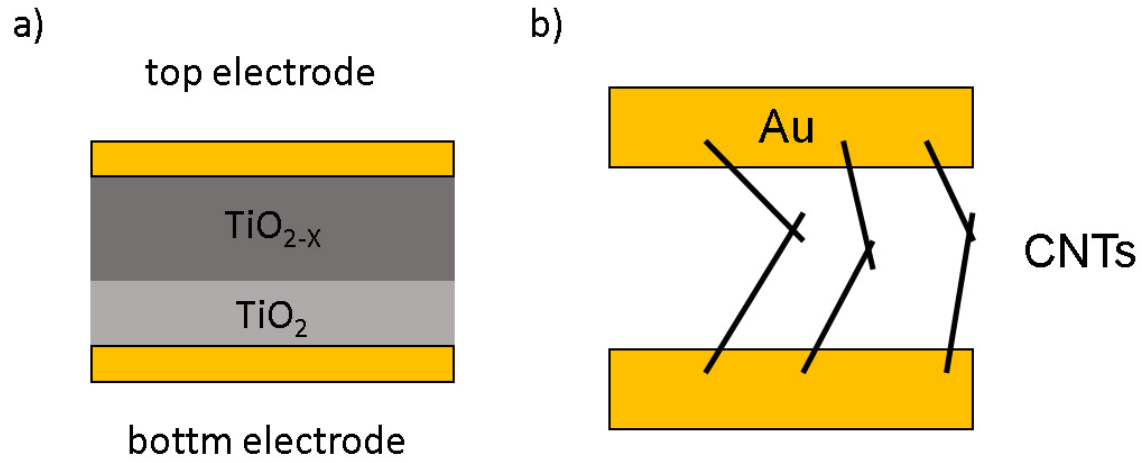

Figure 37: Sketch of a a) MO memristor and a b) CNT device.

TiO_2 memristor is a more asymmetrical one (here it depends on the point of view if the setup consists of a gold, TiO_2, TiO_{2-x}, gold or gold, TiO_{2-x}, TiO, gold design). Therefore it makes a

difference for the TiO_2 device in which direction the current flows, resulting in an asymmetric IV-characteristic. In Figure 37b this asymmetry is missing for which reason the outcome will always be the same independent of the direction the current flows. Here it just flows from one gold contact through the CNT network into the other gold contact in both directions. This link between the symmetry of the system and the resulting hysteresis indicates that it is not possible to fabricate a memristive device on the base of only gold contacts bridged by CNTs.

4.4.2 Discussion of the necessity of an asymmetric approach

Since it is not possible to achieve a memristive device with a symmetric approach will the following segment deal with the influence of an asymmetric contact on the characteristics of a CNT network. The results presented and discussed in this sub-chapter will soon to be published and were carried out in collaboration with the work in this thesis and deal with the effect between two 3D nanostructures when they are brought together and a voltage is applied.

To achieve an asymmetric contact a design consisting of a silicon microwire array and a 3D carbon network was chosen. The used silicon needles were fabricated by using anodically

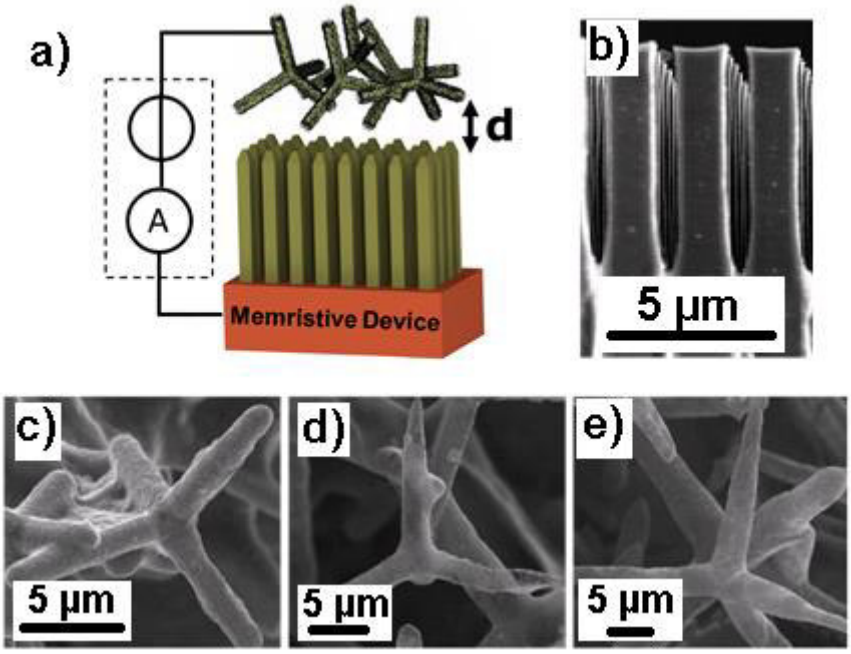

Figure 38: a) Scematic representation of the randomly arranged CNTs and the straight aligned Si wires, b) SEM image of the straight algined Si wires, c) 3D CNT nano architectures still containing ZnO, d) 3D CNT nano architectures without CNT, e) 3D CNT nano architectures without CNT and additional graphitic coating (19)(printed with permission of the co-authors).

etching. For this purpose a pre-structured p-doped silicon wafer was used. In different etching steps and by utilizing a copper substrate the fabricated needles were bonded. A SEM image of these structures is shown in Figure 38b. The 3D CNT structures were obtained by pressing tetrapodal shaped zinc oxide powder into cylindrical shaped samples with a density of 0,3 $\frac{g}{cm^3}$ followed by sintering step. The samples were afterwards coated with the same dispersion as used in this thesis (CoarboByk) by applying the dispersion drop wise onto the sample several times. The produced samples were either kept untreated, placed in low concentrated HCl, rinsed with ethanol and dried, or placed in a furnace with an additional carbon source to remove the ZnO. Resulting SEM images of the samples can be seen in Figure 38c-e.

The different samples are measured and brought together with a self-engineered micromanipulator Maerzhaeuser Wetzlar HS 6.3 setup with a precision of 10 nm. As source a source-meter by Keithley 6400 is used. By connecting the respective 3D structure to an

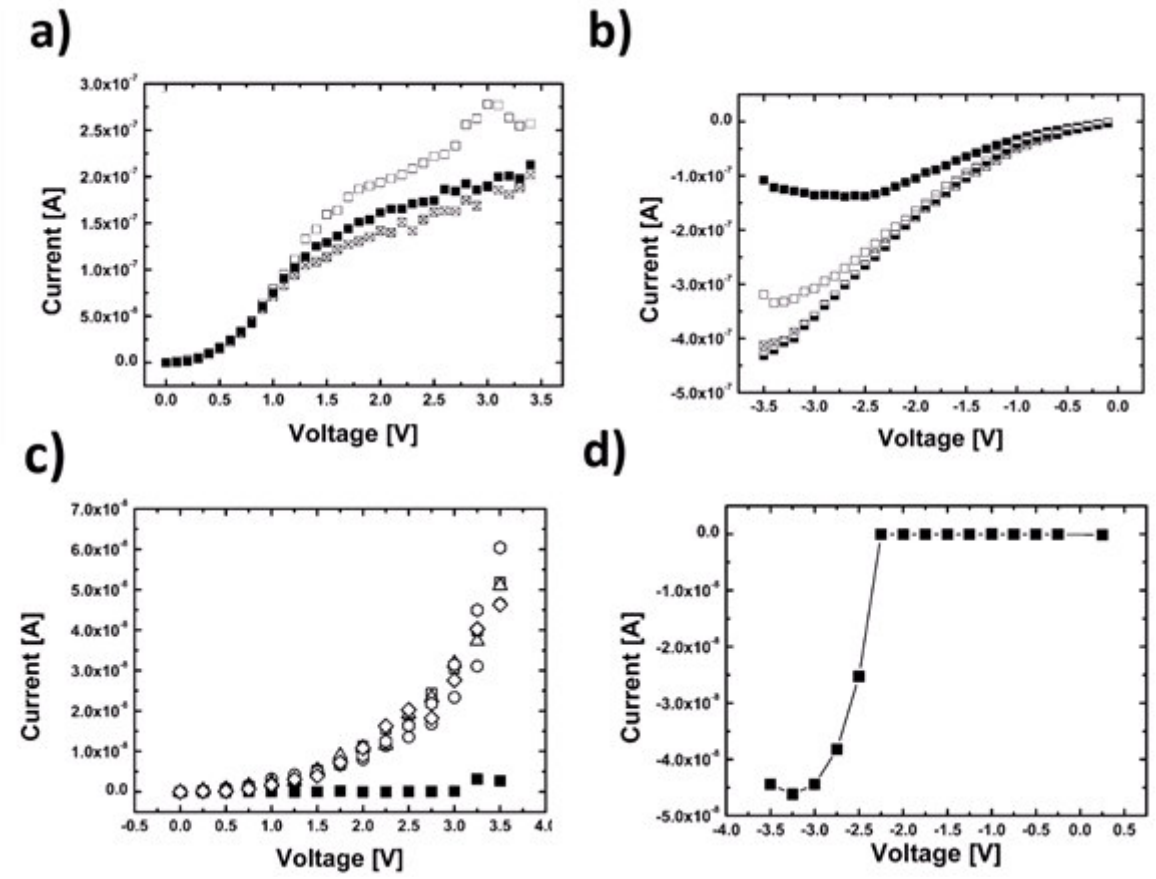

Figure 39: Characteristic switching for different CNT Si wire arrangements. a+b) relatively stiff CNT structure still containing ZnO for set (a) and reset (b) c+d) relatively flexible CNT structure with additional graphite and without ZnO for set (c) and reset (d) (19) (printed with permission of the co-authors).

electrode and bringing them in touch it is possible to measure the current-voltage characteristics of the asymmetric contact (formed by the tetrapodal arms and the Si needles) The design of this setup is shown in Figure 38a while the experimental results, for which voltages from 0 V to +4 V and -4 V to 0 V were applied, are shown in Figure 39. Figure 39 shows the two possible switching types for the respective systems, depending on the chosen carbon morphology. It can be seen that the rather stiff networks, which still contain the ceramic backbone, switch in a relay like manner (see Figure 39c+d). This abrupt reaction of the system can be explained by the limited flexibility of the system itself due to the still present metal oxide backbone. On the other hand the more flexible CNT structure, which is provided with an additional graphite coating and no backbone, show MOSFET-like memristive switching behavior while brought in contact with the Si needles. Here it is attributed to the higher elasticity of the system due to the missing backbone. It needs to be mentioned as well that each of the systems contains one fast and one slow switching process.

It is important to note that the memristive switching behavior is only present for the case when the two electrodes are just brought in contact with each other. The effect does not occur when the Si wires penetrate into the CNT structures and changes into a behavior similar to a diode as discussed in the paper.

More detailed information to this topic can be found in the soon to be published paper from Hansen et al. (*19*).

The discussion and interpretation of the presented results make clear that it is not possible to achieve a memristive switching device by only using carbon nanotubes, due to a lack of asymmetry. For this reason will be the influence of introduced silver clusters on the system as well as their movement be discussed in the next chapter.

4.5 Generation and interpretation of the memristive device

The last abstract showed the need for an asymmetric contact in a memristive device. To achieve the needed asymmetric contact silver particles were introduced to the system in the course of this thesis. Silver particles are suitable for forming an asymmetrical contact by adding the particles and moving them into specific positions by applying a voltage and inducing an electrical field. This approach is based on the reported movement of silver particles in an applied electrical field by Jo et al. (*18*).

Furthermore, it is mandatory to understand which kind of network is suitable for this idea, for which reason a closer look into it needs to be done. The way a nanotube network with no agglomerations forms it can be assumed as depicted in Figure 40. In Figure 40a a gap formed by two gold electrodes of the size of 2 µm is shown which is not perfectly bridged by a certain number of connections formed by CNTs (symbolized by the black crosses). To describe system mathematically the amount of not formed connections, either by the fact that the CNTs do

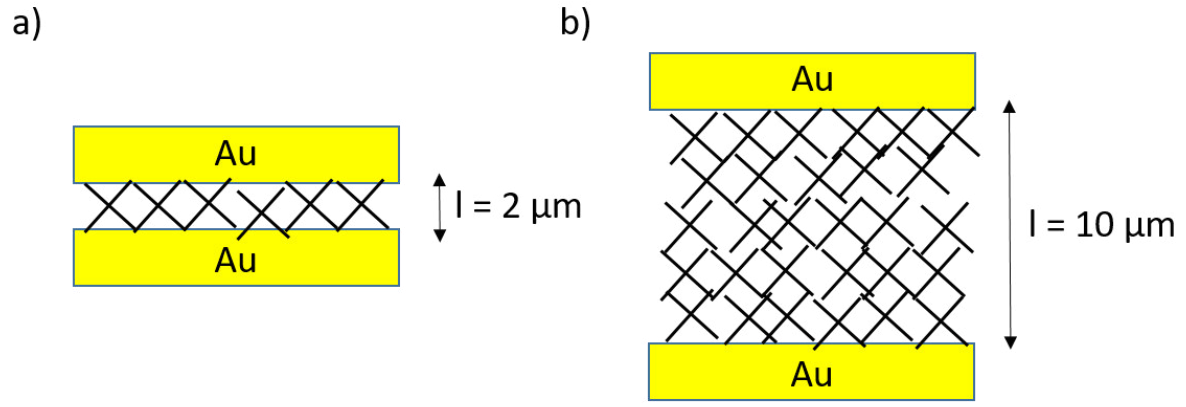

Figure 40: Showing a sketch of the CNT network for a) a small gap with a gap size of 2 µm and b) for a large one with a gap size of 10 µm.

not reach the other side of the gap or that the interconnection of the CNTs is not present, can be expressed by the value α (number of missing connections). Indicating the lower the amount of connections are present in the network the bigger this value becomes, while ranging from 0 (perfectly connected network) to 1 (no connections present in the network). By assuming that for a wider gap size additional 'layers' are simplified spoken added to the first one to fill

out the gap the value α will increase with the widening of the gap. This leads to a correlation of the gap size (l) and the number of missing connections (α) like follows: α^l. Therefore, the probability to achieve a connection path through the network decreases with the increase of the distance between the two separating contacts. This results in an increase in the resistivity for the CNT network presented. It can be concluded from this that the geometry of the formed network can be characterized by resistance measurements across the individual gaps.

4.5.1 Introduction and analysis of Ag clusters from solution and cluster source to the network

In the course of the here presented work two different approaches were executed to add silver clusters to the CNT network and will be discussed in the following.

The first approach carried out is the synthesizing of the silver particles in a glycol-silver nitrate-polyvinylpyrrolidone solution such as described in an earlier section of this thesis following the approach of Slistan-Grijvala et al. (*66*). The conducted electrical measurements for these devices result in a quite poor conductivity, which is most likely caused by the PVP coating of the particles. It is to assume that the PVP does not only cover the particles, but also parts of the CNT network due to its presence in the solution, leading to a partial isolation of areas of the network. A plasma or wet chemical approach to remove the coating is not possible for this system since the nanotubes cannot withstand such treatments, since they get oxidized or washed away during such process. Therefore, a more promising technique to introduce the silver particles is the cluster sputter deposition, which is a non-wet chemical approach and was prior described in the theory section.

The carried out sputter experiments were conducted as described in the experimental section utilizing a self-build Haberland gas aggregation source (*50*) and monitored using the measurement setup V1, which was introduced in the theory section. A typical outcome for such sputter experiment on CNT networks across different gaps can be seen in Figure 41. The shape of each curve is identical to the one presented in the theory section about sputter deposition, showing that the percolation process for these experiments is similar to the one presented in literature. One has to take into account before evaluating the graphs that the overall resistivity varies between the MΩ and kΩ regime, depending on the gap size. Since all of the networks end up at roughly the same resistivity indicates this, that by having the same

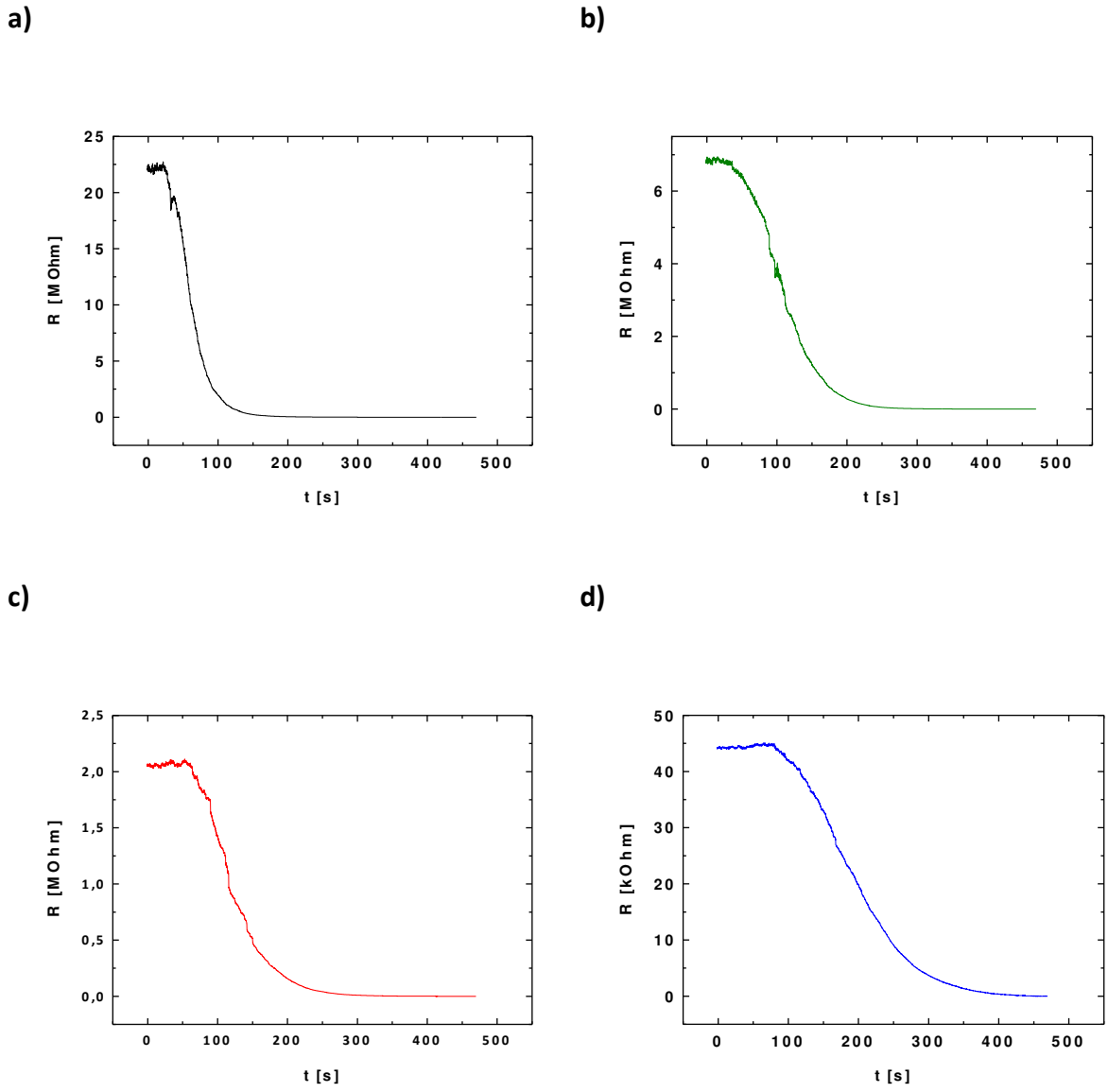

Figure 41: Ag sputter deposition on CNT networks across various gap sizes and their change in resistivity over the deposition time.

shape the drop in resistivity must be the most pronounced for the biggest gaps. This assumption is true, since the resistivity of the 10 µm gap drops in the first 50 s of the sputter process by 10 MΩ, the resistivity for the 6 µm gap just changes by 1 MΩ and for smaller gaps the resistivity changes even less. All these resistance measurements about the CNT networks and their change during sputter deposition can be summarized in the following formula:

$$R(l,t) = \frac{R_0}{l(1-(1-\alpha_0)\beta^{d(t)})^l} \qquad (3)$$

With R being the resistivity, while R_0 represents the resistivity of the initial network, l and α the gap size and the number of missing connections (such as introduced before), d(t) standing for the deposition of metal clusters versus time and β is a scaling factor for how effective the deposited metal clusters form connections in the interrupted CNT network. This formula takes into account the fact that the change in resistivity is mainly caused by the formation of new interconnections due to the added metal clusters by sputtering in the network and lowering of the α value rather than on the change of resistance by the clusters on the individual CNTs themselves. By further rearrangement of formula (3) it is possible to characterize the morphology of the network even further. By plotting the expression $ln\frac{1}{lR(l,0)}$ of formula (4)

$$\boldsymbol{ln\frac{1}{lR(l,0)} = llna_0 - lnR_0} \qquad (4)$$

$$\boldsymbol{\sqrt[l]{\frac{R_0}{lR(l,t)}} = 1 - (1 - a_0)\beta^{d(t)}} \qquad (5)$$

(which originates from formula (3)) against the gap size l is the result a slope as illustrated in Figure 42a. It is shown that there is a logarithmic dependency of the resistivity of the contact bridging imperfect CNT network. It is clearly visible that the resistance of the network follows a linear trend indicated by the added line of best fit. The linear relation indicates that the CNT deposition formes a homogenous network. By extrapolating the resulting graph to the gap size of 0 µm it is possible to determine the resistivity of the CNTs (in this case ≈ -8,5). Figure 42b shows the result for the expression $\sqrt[l]{\frac{R_0}{lR(l,t)}}$ of formula (5) (originating as well from formula (3)) versus the elapsed time for the sputter deposited networks. The resulting shape of the graphs for the corresponding gaps is almost identical, indicating that the network itself is homogenous in the start, but indicates that the sputter process is not completely homogenous across the whole sample.

a) b)

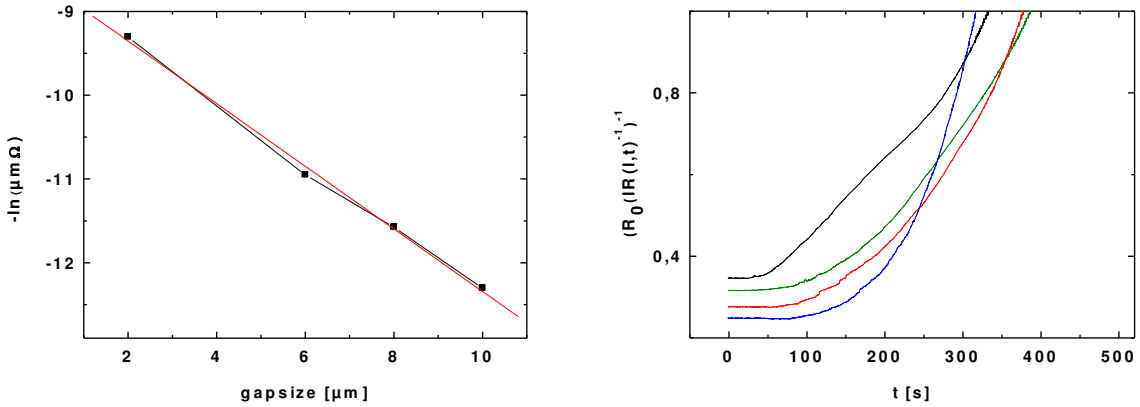

Figure 42: Gap size dependency for the initial resistivity of the bridging CNT network a) showing the linear dependency of the resistance of the network with the gap size b) resistance change with the addition of silver clusters (the variation indicates a certain.

This discussion shows what the needed condition is that a CNT network has to fulfill to be suitable for the planned devices, namely that the resistivity of the CNT network needs to be gap size dependend (following α^l).

4.5.1.1 Discussion and evaluation of sample S13

In Figure 43 a SEM image for a chip decorated with CNTs and Ag clusters deposited via sputter deposition is shown. The CNT concentration used for this sample was 1:100000 while the deposition itself was carried out via simple drop coating at room temperature as described earlier in this thesis. It can be seen that the nanotubes tend to form agglomerates which can be attributed to the gradual drying process in ambient conditions as discussed in section 4.2. The deposition experiment was carried out as described in the experimental section and monitored with the setup V1. For S13 an argon flow of F_{Ar} 0.4 $\frac{mbar \cdot l}{s}$ was chosen at a power of 40 W. The sputter process was terminated after a significant change in the measured resistivity was noticeable, which occurred after 205 s. In addition does Figure 43 display that the Ag clusters are deposited on the sample surface evenly and even on top of the CNTs (see Figure 43) which indicates that the physical bonds between the clusters and the nanotubes are relatively strong. The influence of the electrical field on the deposited silver clusters can

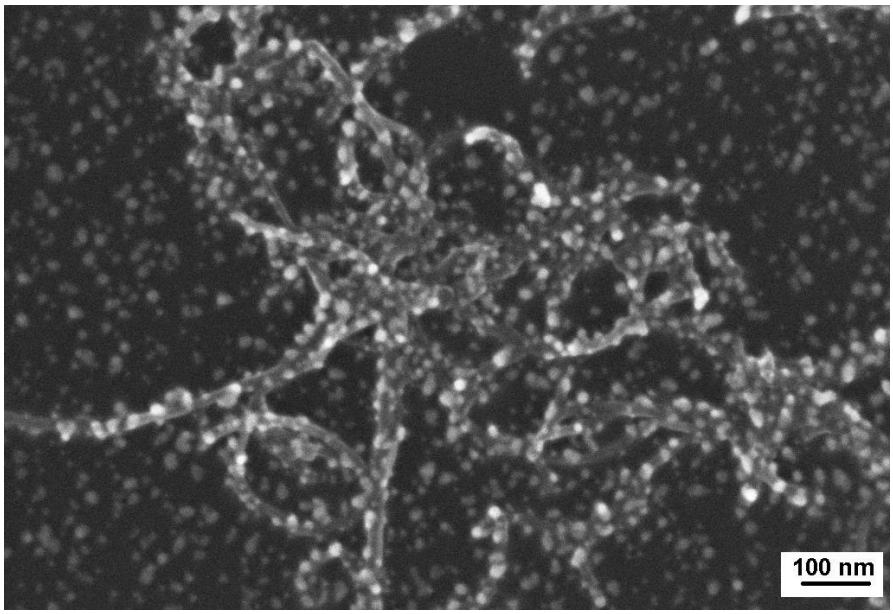

Figure 43: SEM image of S13, produced with a CNT concentration of 1:100000 and decorated with Ag clusters via sputter deposition.

be investigated by applying voltage pulses and further hysteresis measurements. To compare the results an initial virgin curve before further treatment is recorded. Figure 44 shows the virgin hysteresis curve of S13 for a 10 µm gap. Here the voltage is increased stepwise from 0 to +1 V, decreased in the same manner and repeated for the negative regime in the same step size until a voltage of 0 V is reached. The step size in which the voltage is incrementally increased or decreased is fixed to twelve steps in each direction. The arrows indicate the direction of increase and decrease of the current during the hysteresis. It can be noted that the current increases linearly with increasing voltage, but shows two stronger rises of the slope after a voltage of roughly 0,3 V and 0,75 V. The highest current value of 0,14 µA is reached at a voltage of +1 V. While the voltage is decreased back to 0 is the measured current slightly higher than for the forward direction. Nevertheless, the curve does go through the origin. This indicates that the system is not capacitive and does not store energy, which would be an unwanted side effect. By applying a negative voltage is the resulting shape of the curve quite similar to the one for the positive voltage. The current decreases quite steadily till the voltage is increased further than -0,3 V. Afterwards the current increases linearly up to the maximum voltage of -1 V and reaches a value of -0,14 µA. Again the current does not follow the same path while the voltage is decreased back to zero, but is slightly shifted to the prior

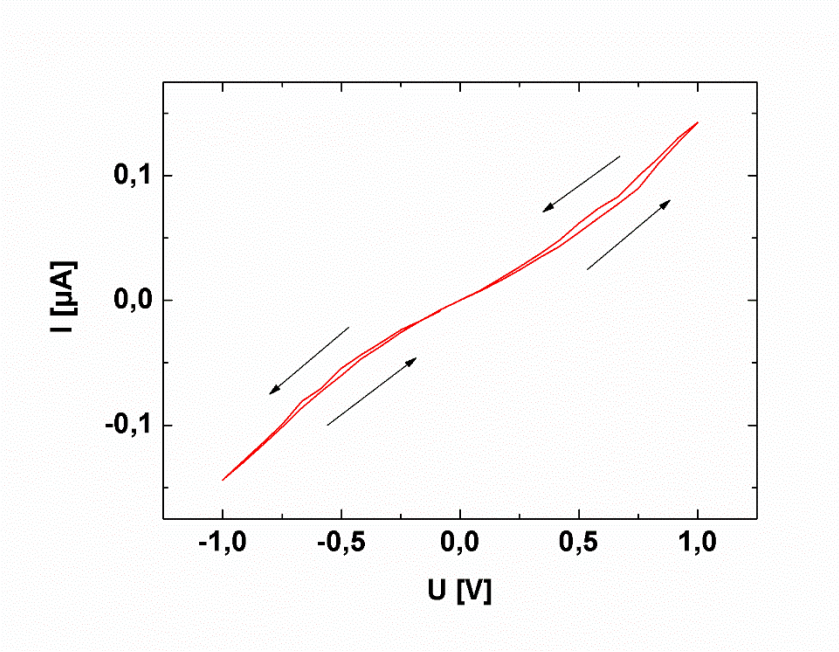

Figure 44: Virgin curve for the hysteresis measurement of S13 with a maximum voltage of 1 V.

increase in the negative direction and ends again in the origin. The most dominant behavior shown in the graph is nearly ohmic, but shows a slightly curved shaped. This sample shows so far no memristive behavior, since for a memristive device the slope of the hysteresis must differ in the way the current changes with the increase and decrease of the voltage. There must be a so called high resistive state and a low resistive state. For the displayed measurement in Figure 44 the resistivity changes in the same manner in both directions. While the voltage is increased increases the current as well and vice versa. Due to this fact the device can be stated as non memristive at this point. The measured conductivity might be mainly the result of the connected CNTs among themselves and partly increased by the added Ag clusters.

By performing a pulse measurement, here the voltage is kept constant on a level of +1 V for 10 s, and a subsequent hysteresis measurement of sample S13 the result in Figure 45 is obtained. The short duration is chosen to investigate stepwise how the system reacts to certain treatments without overshooting right from the beginning, which would lead to a destruction of the system. The measured maxima of the current are marginally smaller than the prior measured ones for the virgin curve, being 0,15 µA and -0,16 µA respectively. This difference cannot be really attributed to any changes in the sample itself caused by the voltage

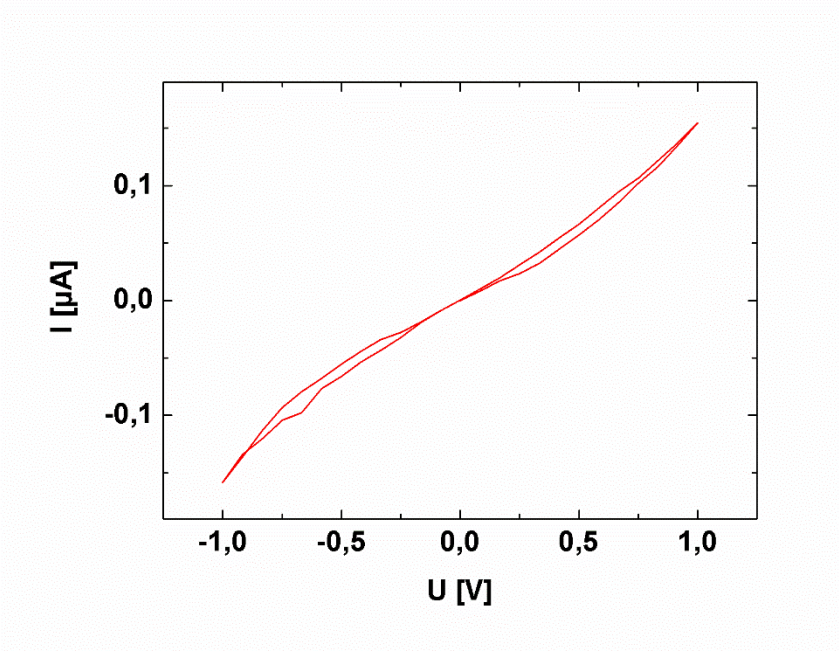

Figure 45: Hysteresis measurement of S13 with a maximum voltages of 1 V after a pulse of +1 V was applied for 10s.

pulse and might be the result of measurement error. The curve appears to have a more streched stretched shape than the virgin (untreated sample) curve. In addition the loops in the negative as well as in the positive direction are more pronounced and indicate that the applied pulse leads to a movement of the Ag clusters and therefore a change in the system itself. The directions of the loops do not change and stay the same as for the virgin measurement.

The result shown in Figure 46 is achieved after the second pulse and the third hysteresis measurement are conducted. The measured maxima for the current are 0,22 µA and -0,22 µA. The most noticeable change by comparing this and the prior pulse is that both loops started to shrink and become very narrow (compare Figure 45 and Figure 46). Therefore, the characteristics of this curve become way more ohmic. The change in the maxima for the measured current is larger than the measurement error and can be addressed, as well as the change in the slope, to the movement of the silver particles. Despite these changes the sample is still far off from being memristive.

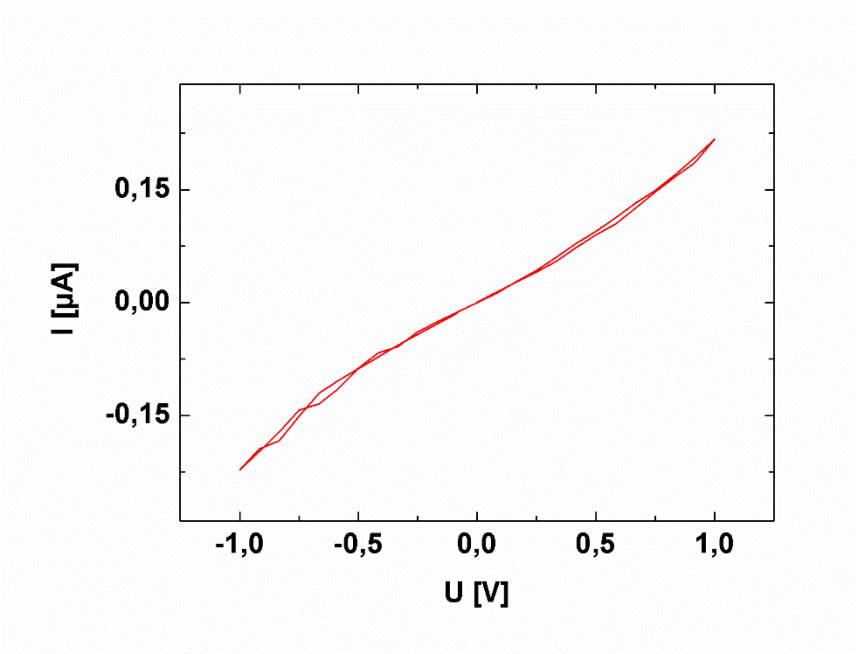

Figure 46: Hysteresis measurement of S13 with a maximum voltages of 1 V after two prior applied voltage pulses.

Applying further pulses with varying polarity and increased pulse length do not lead to drastic change in neither current maxima nor shape of the curve. For this reason only the last pulse, which was applied to sample S13, is shown in Figure 47. It can be seen that the outcome of the electrical treatment is a quasi-straight line with close to no visible loops. By comparing the

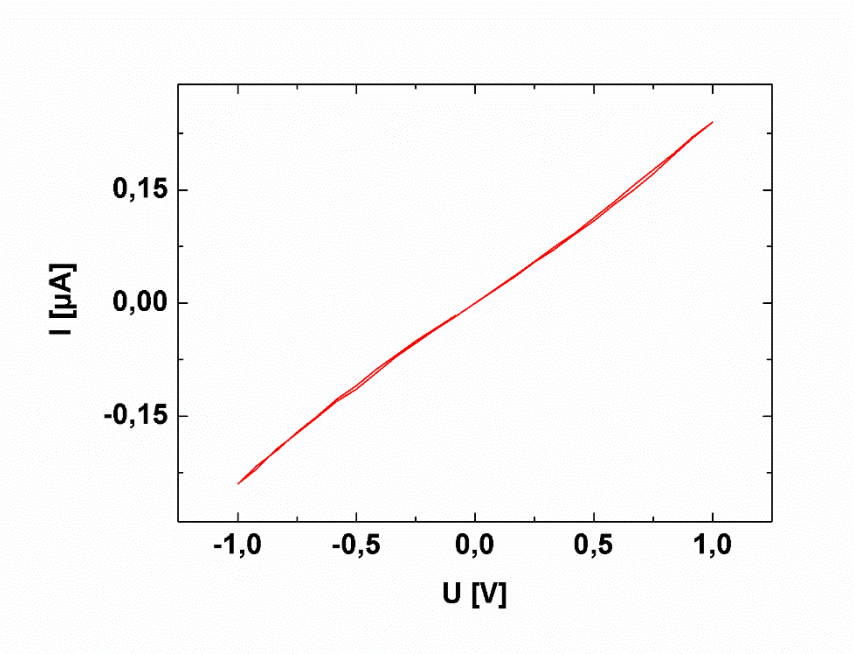

Figure 47: Hysteresis measurement of S13 with a maximum voltages of 1 V after applying prior several voltages of +1/-1 V for several seconds.

current maxima it can be seen that the result for the virgin curve (maxima of +/-0,14 µA) is lower than for the last measurement result (maxima of +0,24 µA and -0,22 µA respectively). Since the maxima nearly doubled it can be stated that this is not a measurement error, but rather caused by the movement of the clusters. The increase in the measured current can be explained by the fact that the clusters started to form conductive paths between the CNTs or strengthened already existing connections, improving their conductivity. Similar effect were already discussed earlier by F. Xin (*96*), showing that the addition of Ag increases the conductivity of carbon nanotubes.

4.5.1.2 Discussion and evaluation of sample S14

By performing the same deposition method and increasing the sputter time by 25 s under the same conditions, sample S14 is generated. In Figure 48 a SEM image of one of the outer areas of the chip for this sample is shown. It can be seen that the increased sputter time results in of course higher density of clusters, but as well in larger particles. While the cluster size for S13 ranges between 10 and 20 nm is the size after longer deposition 20 nm larger (overall 40 nm). Additionally the increased amount of silver does result not only in round, but as well tube shaped structures. Therefore, it can be stated that the via cluster sputtering deposited clusters

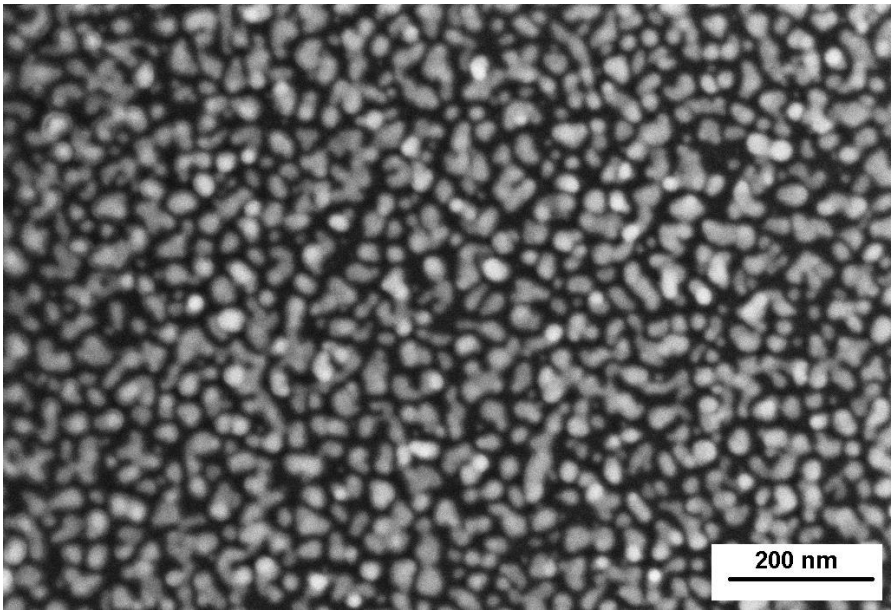

Figure 48: SEM image of S14 after 230 s of magnetron sputtering.

got enough energy after their arrival left to move for a limited time over the surface, resulting in growing, in this case tube like, structures. This process is called surface diffusion and is limited by the energy of the arriving particles and the surface particle interaction.

By applying and recording of different voltage pulses for the sample S14 changes in current during the pulses are noticeable. The recorded time versus current characteristics for an applied voltage of +1 V can be seen in Figure 49. The pulses are executed immediately after another with the black being the first pulse, red the second and the blue the last one. As mentioned the applied pulse heights is +1 V with a pulse length of roughly 6 mins. The resulting current is in the milliamp regime. When the first pulse is applied to the sample a large change in the measured current is noticeable, jumping from 0,42 to 0,47 mA immediately after applying the voltage. For the next 50 s the current increases linearly, while after this the current drops again right away down to the starting value. Afterwards it increases again in a parabolic shape up to a value of 0,54 mA. From here on the current fluctuates around a slightly lower value for roughly the next 120 s. Just to jump suddenly up by 200 µA. It stays there for the rest of the pulse, besides once dropping by 100 µA and increasing afterwards shortly after.

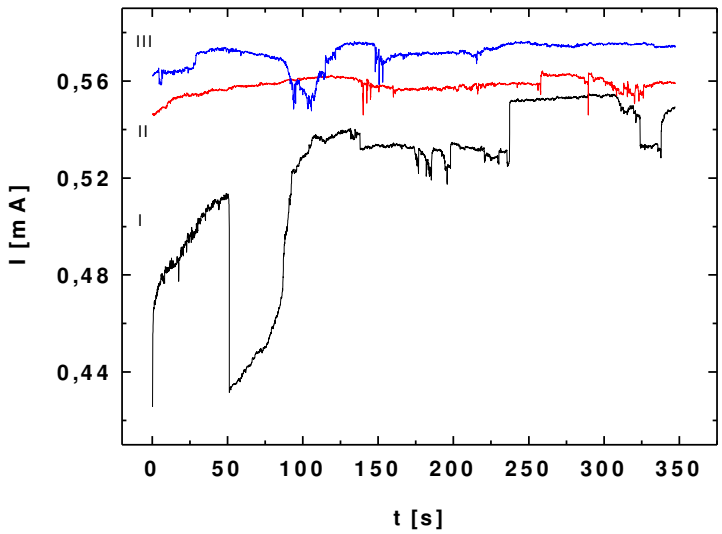

Figure 49: Time versus current of a 10 µm gap (1.4) of S14 for an applied voltage of +1 V.

The second pulse does not show any drastic changes in the measured current. Over the course of the second measurement (red line) time of 6 mins the current increases slowly, showing

only some minor bumps. During the last measured pulse the current does increase further by overall 200 µA compared to the maximum value of the prior executed pulse. The measurement shows a slow increase, but shows a small drop after 90 s and an increase again shortly after. The changes of the measured current during the second and third pulses are not that strongly pronounced as for the first cycle. This fact indicates that the first applied pulse has the biggest influence on the produced and investigated system. The smaller bumps which are visible in the recorded time versus current graphs cannot be fully attributed to the system itself and might be the result of measurement errors. The other major changes in the measured current, as they occur mostly for the first pulse, are the result of the movement of silver clusters in the present CNT network. In Figure 50a a sketch of a virgin sample is shown. It shows an area of a not completely connected CNT network. The network is decorated with Ag clusters applied by sputter deposition. The clusters are distributed randomly over the

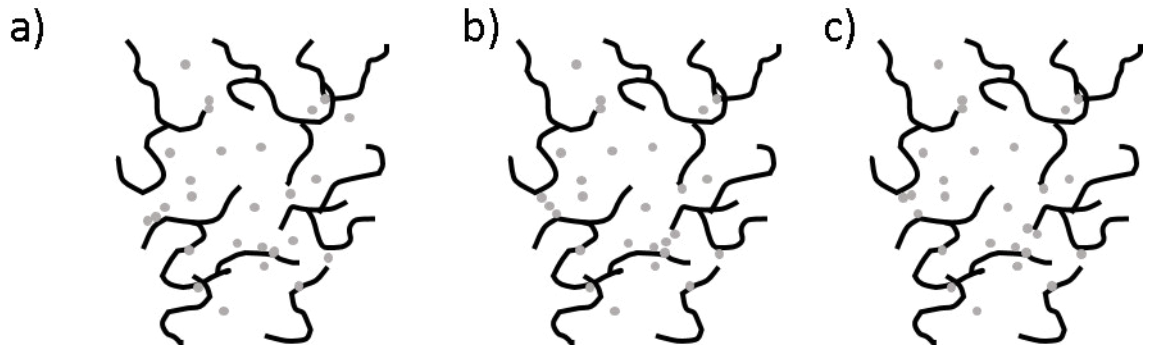

Figure 50: Sketch of a decorated CNT network a) pre and b) post applying a voltage pulse and c) after an additional one.

surface, some are lying on the nanotubes or in larger or smaller gaps in the network, as it is present for the discussed sample. As mentioned before some of the clusters are affected by the induced electrical field due to the applied voltage. This electrical field is in areas with a gap size between the nanotubes of just around 200 nm strong enough to make them move. One possible result, after an electrical pulse is applied, is shown in Figure 50b. It is shown that not all of the clusters are influenced by the electrical field. The ones which are already attached to the CNTs do not move, neither do these in gaps which are too big to build up an electrical field strong enough to make them move. The results are conductive paths between areas of the networks which were not connected before. Newly connected areas of the

network can now contribute to the overall resistance of the network. This conductivity is either the result of the formation of direct conductive paths of silver particles or the distance between the clusters becomes small enough to enable electron hopping. This formation of cluster paths and the existence of hopping events results in an increase of the current flowing through the sample and therefore a reduction of its resistivity. This explains the sudden rise of the measurement curve for the pulse at the beginning of the experiment for example, since this process can occur rapidly. By applying the voltage for even a longer time it is possible to move the clusters even further, and its result is shown in Figure 50c). Here the clusters are moved so far that the prior conductive paths ruptured. This rupturing results on the other hand in a sudden decrease of the conductivity which happened during the applied pulse after roughly 50 s (see Figure 49 first measurement). Here the measured current almost immediately drops down to the starting value. Since the sketch in Figure 50 is only representative for a small area in the samples network it is possible to explain the ups and downs in the measurement curves. Areas which were not included in the network at the start of the measurement are included in the network due to the cluster movement, resulting in a decrease of the resistance, or separated again, resulting in an increase of it.

By applying several pulses with a heights of +1 V to another 10 µm gaps of sample S14 the curves shown in Figure 51 can be obtained. It can be seen that the measured current increases again over the course of the carried out pulse experiments. At the beginning of the first pulse the measured current is at 0,1 µA and increases in two drastic jumps at the 70 s and 250 s mark up to roughly 0,1 mA. The second run shows again in the beginning of the measurement and after 200 s respectively a sudden increase in current and raises almost by 0,2 mA, compared to its starting value. The third run starts with a drop of 50 µA and stays at the same current level of roughly 0,25 mA. Noticeable is that the measured current fluctuates right after the initial drop and only stabilizes after 20 s leading to a maximum drop of 0,15 mA. The current increases slowly and steady as well by applying a +1 V pulse for the fourth time, while there is still a noticeable jump around 150 s in the measurement results shown. The ups and downs in the displayed graphs can again be explained similar to the way they were in the prior presented experiment with the formation and rupturing of conductive silver paths.

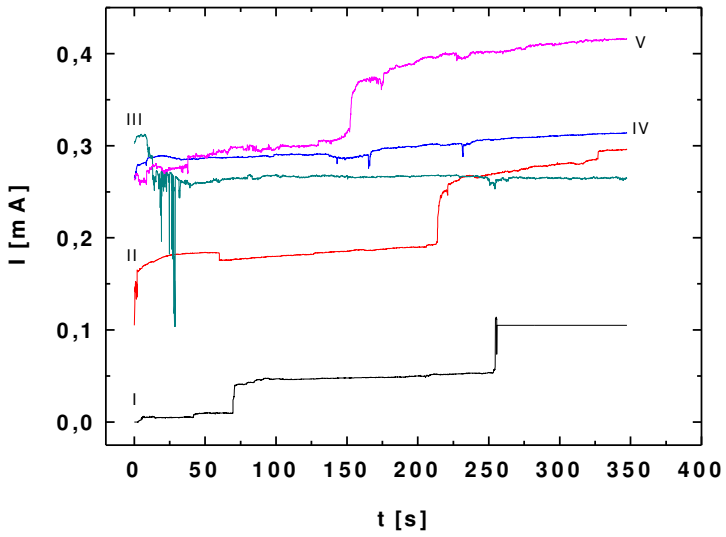

Figure 51: Time versus current of a 10 µm gap (1.4) of S14 for an applied voltage of 1 V. For each recorded pulse was the voltage applied for roughly 6 mins.

In Figure 52 the resulting hysteresis measurements are shown which are carried out after each pulse. It can be seen that the ups and downs at the end of the current values of each measurement for the scans are mirrored by the results of the respective hysteresis. The measured maximum current increases after each pulse. The most noticeable difference is seen in the virgin measurement represented in Figure 52a. Here a larger broadening of the hysteresis curve especially in the first half of the measurement is shown. The shape of the curve is the same as of the ones presented before. Independent of whether a positive or negative voltage is applied the resistance of the system increases first and drops as soon as the voltage decreases again, showing no difference in the direction nor is a differentiation into high and low resistive state indicated. Due to the fact that the positive hysteresis loop is bigger than the negative one a negative voltage is applied for the subsequent scan. Its result is shown in Figure b. Here the measured maximum current increases as indicated before by the monitored scans in Figure 51 in comparison to the virgin hysteresis. The main differences between these two hysteresis measurements is that the prior visible hysteresis loop vanishes nearly completely for the measurement after the first scan. The only recognizable loop is left in the negative voltage regime. For the other three scans no difference in hape is noticeable.

Their measured maximum current increases slowly, while their shape was almost completely linear, showing only ohmic behavior (see Figure 52c-e).

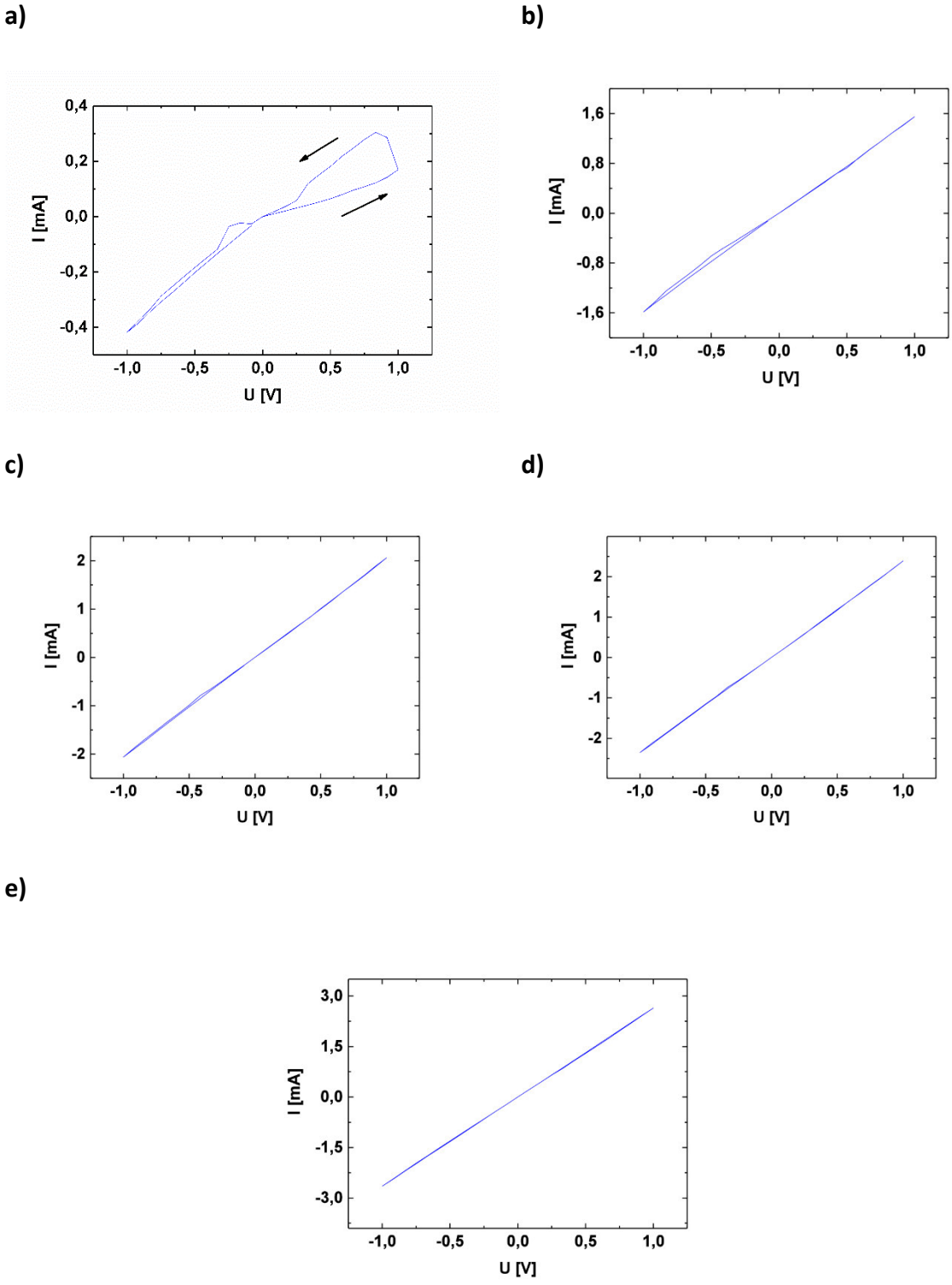

Figure 52: Hysteresis measurement of S14(1.4) with a maximum voltage of 1 V after a) no scan b) one scan, c) two scans, d) three scans, e) four scans with a voltage of -1 V for 360 s.

As well as the change in current the change in the shape of the curve can be explained by the movement of the clusters and with it associated formation of connection paths consisting of silver. While the amount of newly formed strong interconnections is larger than the ones which are disrupted, since the resistivity goes down the more additional pulses are applied.

Measurement results for the third gap of the sample S 14 are shown in Figure 53. The way the current reacts to a change in the applied voltage for the first hysteresis looks quite similar to the one reported for the other gap (see Figure 53a). The positive loop of the virgin hysteresis is again broader than the one of the negative regime. This size difference dictates, under the assumption that the biggest changes should occur by applying a voltage in the direction of the smallest loop, that the next applied pulse is a negative one. For this reason a pulse of -1 V is applied before the hysteresis measurement is carried out. The result of the second measurement is shown in Figure 53b and it can be seen that the prior bigger positive loop becomes a straight line, while the negative loop becomes more pronounced. By applying an additional -1 V pulse the measured current maximum increases further while the former curve becomes a straight line (see Figure 53c). A further -1 V pulse results as well in a straight line (Figure 53d), while a subsequently carried out applied +1 V pulse result in no mentionable changes for the system.

For this series of pulses an increase of the current can be noticed again, as for the previous measurement series. The favored change in the hysteresis curve (the broadening of the negative loop) happens to some extent, while the positive loop decreases. The movement of the clusters in the negative applied voltage direction seem to favor the amplification of the prior small loop in the same direction, but lead to a shrinkage of the other positive loop. A further pulse of -1 V leads to the formation of a completely straight ohmic line. At this point it is to be expected that an additional pulse will rather broaden up the negative loop, since a negative voltage was applied, but the result remains to be a straight line (see Figure 53d). The further use of a positive pulse with the same height and length results in no changes of the hysteresis (see Figure 53e). It seems that the system does not react to any outer changes anymore as soon as a certain point is exceeded. This non-reactive behavior can be explained with the formation of conductive filaments (*97*) and the fact that clusters which move too

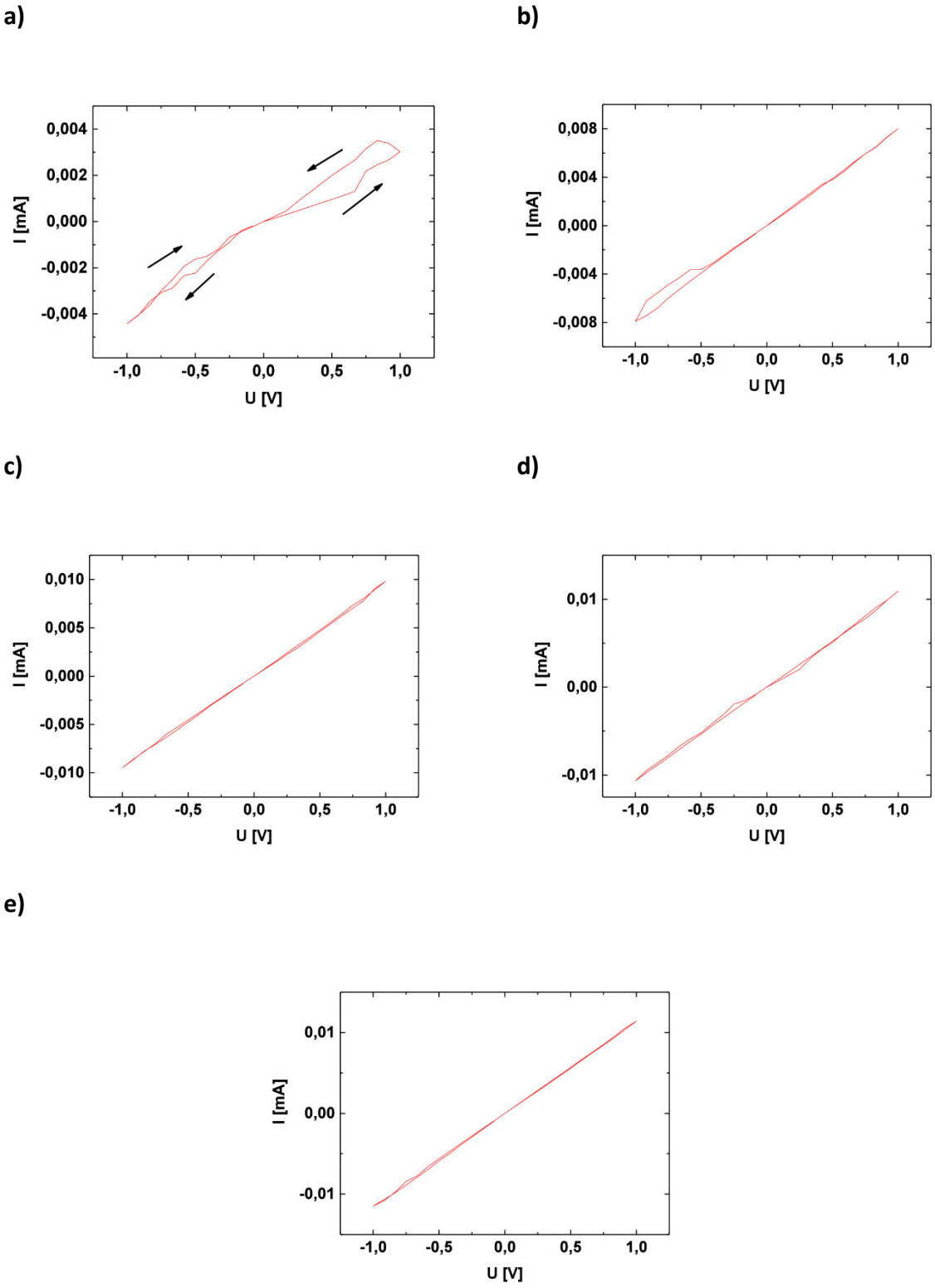

Figure 53: Hysteresis measurement of S14(1.3) with a maximum voltage of 1 V after a) no scan b) one pulse, c) two -1 V pulses, d) three -1 V pulses, e) three -1 V pulses and an additional +1 V pulse.

far are trapped at the CNTs. The reasoning behind this behavior is that as long as a cluster lays in a gap it can be influenced by an applied electrical field. While if a cluster comes too close to

a CNT it is suddenly on the same potential as the CNT itself, making the cluster immobile since it cannot be affected by the electrical field anymore. This trapping causes the cluster ultimately to remain fixed, since it cannot be moved by the electrical field anymore.

To investigate the stability of the formed conductive paths a series of additional pulses and hysteresis measurements are conducted for the same gap after six days, to investigate possible relaxation phenomena. In Figure 54 the results of this experimental series can be found. It can be seen that even though the clusters seem to be deadlocked by being stuck at the CNTs, as a result of the prior conducted experiments, that some kind of relaxation and linked to it back drift has occurred. This is the case since the newly measured hysteresis curve differ a lot from the last hysteresis measurement series (compare Figure 54a and Figure 53e).

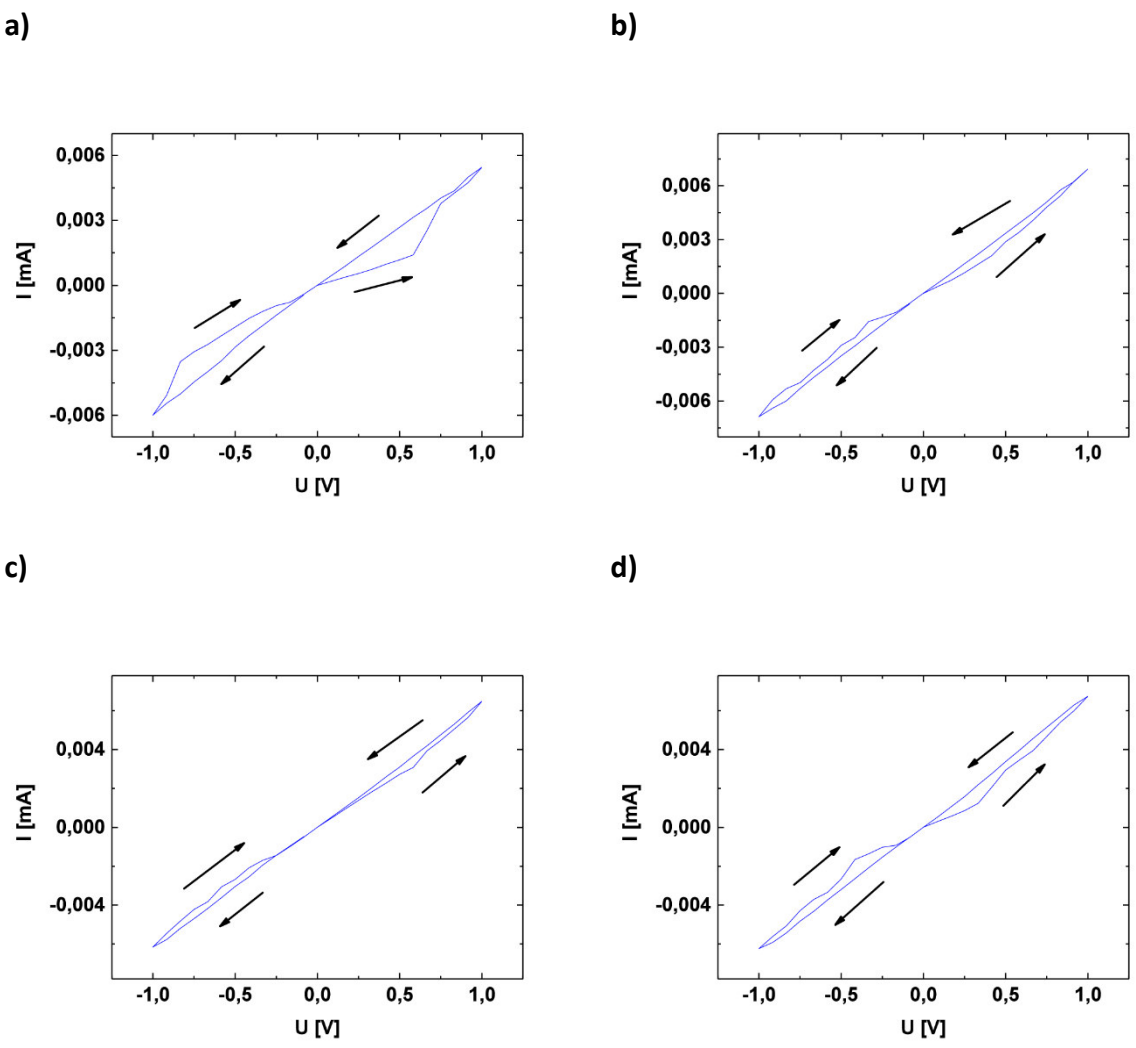

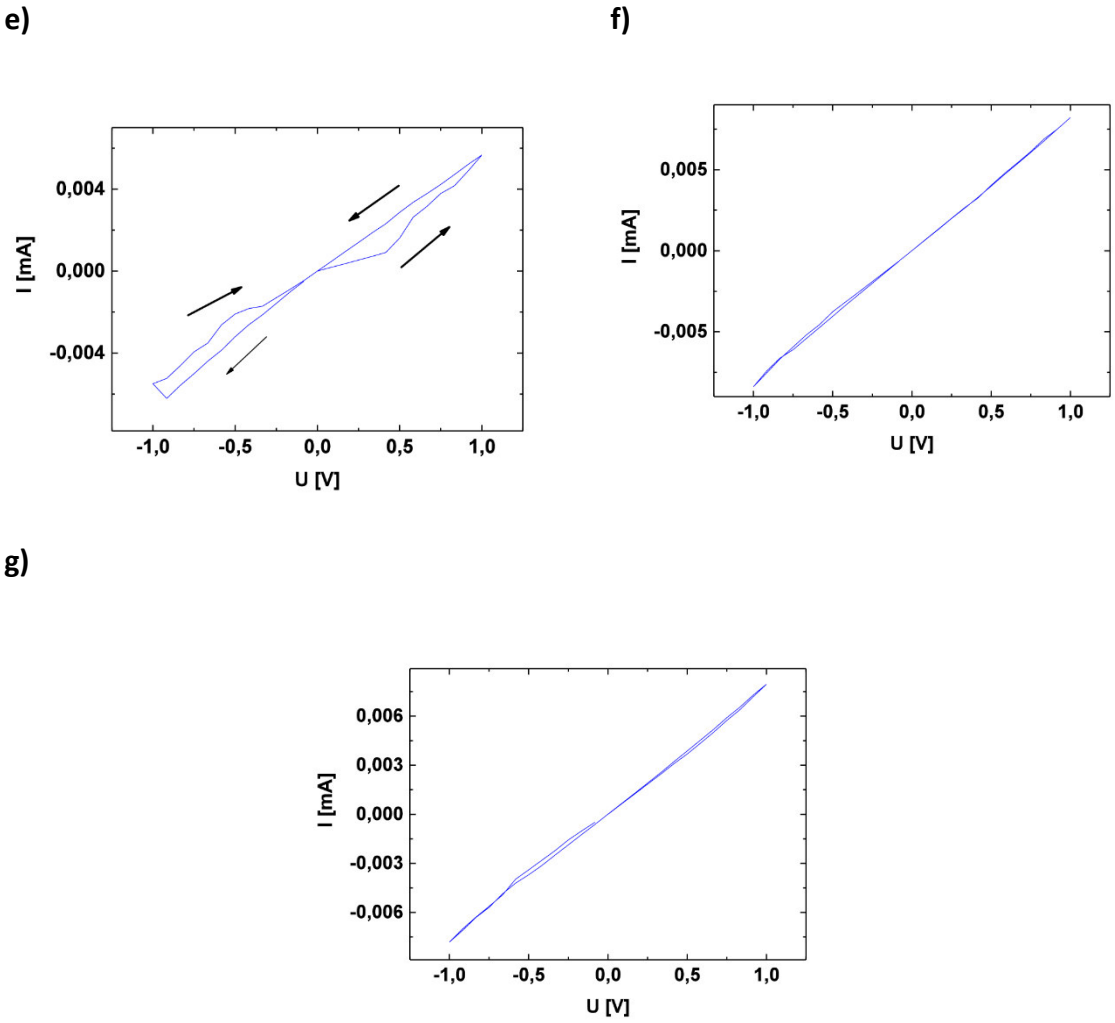

Figure 54: Hysteresis measurement of S14 (1.3) with a maximum voltage of 1 V after 6d of rest after a) no additional pulse b) one -1 V pulse, c) two -1 V pulses, d) two -1 V pulse, e) three -1 V and one +1 V pulse f) four -1 V and one +1 V pulse g) four -1 V and two +1 V pulse.

Its shape is more comparable to the result of the virgin measurement for this sample (see Figure 53a). Furthermore the current is lower after the rest proving the theory of the relaxation by particle movement to be true. Especially prominent is that the shape for both parts of the hysteresis loops are reformed again. To check for the stability of these loops a pulse of -1 V is applied. In Figure 54b the result after the first pulse is shown and it can be seen that the current increases slightly while this time both loops become smaller. The application of a further pulse leads to a narrowing of the curve and in addition the measured maximum current decreases. After this -1 V pulse a positive pulse of the same length is applied which results in a slight broadening of the hysteresis curve again in both directions. A subsequent negative pulse leads to a further broadening and can be seen in Figure 54e. To investigate if

the curve could be broadened even further an extra -1 V pulse is applied resulting in Figure 54f. The outcome is again a straight line showing nearly no broadening anymore at all. While the measured current increases again. Figure 54g shows the last result of this measurement series in which a +1 V pulse is applied. It shows a straight ohmic line with a slightly higher current than the prior described hysteresis curve.

The second part of the survey of the gap 1.3 of S14 indicates that relaxation and drift phenomena take place in the sample if it rests long enough, which is indicated by the noticeable change in the curve characteristics. In addition it can be noted that the last series of pulses and hysteresis measurements shows that it is possible to change the appearance of the hysteresis curves according to the applied voltages. While a voltage in one direction leads to a decrease of the size of the loops of the hysteresis it is possible to widen them up again by applying a voltage pulse in the opposite direction. This process cannot be repeated any number of times since from a specific point on it is not possible anymore to change the form of the curve by switching the direction of the applied pulse. The changes in the measured current are easily explainable by the relaxation of the clusters. Due to their movement it is possible that already existing connections degrade leading to a lesser number of electrical junctions inside of the CNT network and for this reason to an increase of its resistance. This rupturing has most likely happened as well between the measurements depicted in the Figure 54b+c (indicated by the drop of the current maxima). While the ascertainable increase of the current after applying a positive pulse for the first time is most likely caused by an additional shift of the clusters in the field. In this process it is possible to activate other regions in the network, which were isolated before. Therefore, the additional pulses lead to a strengthening of these freshly formed connections, leading to a further decrease in the resistivity, which happens at the cost of the shape of the curve.

4.5.2 Manipulation of the movability of the silver clusters

By taking the results of the last section into account it can be stated that it is possible to influence the clusters by applying an electrical field changing the shape and the maxima currents of the resulting hysteresis curves for the presented design. While there is a drawback

in it, since this reformation process is limited to a certain number of cycles since the clusters can move too far and become stuck at the carbon nanotubes making them immobile. Therefore, this behavior needs to be tuned, since a memristive sensor (which is the aim of this work) needs to be switchable many hundred thousand times. To fulfill this criteria the cluster movement has to be slowed down. To achieve this two different ways are tried in the course of this work. In a first approach the samples produced are treated with NaOH, in order to lower the amount of Ag^+ ions, which move much easier in the electrical field than the clusters (*27*). The second idea is to pin the silver clusters on certain positions to make them less mobile and decreasing the risk of moving them too close to the CNTs.

4.5.2.1 NaOH treatment of the silver clusters

The NaOH treatment was carried out as described in the experimental section. The results obtained for the hysteresis measurements shown in Figure 55 are carried out with a sample produced in the same manner as S13. Figure 55a shows the result of the hysteresis curve of the sample after its NaOH treatment. The curve has a maximum current of close to 2,0 nA and it can be seen that it is slightly widened so that it does not go through the origin, which means that this sample shows some capacitive behavior. Besides this its shape is quite uniform, while it is noticeable that the direction of increase and decrease follow the opposing direction similar to the prior presented samples, which is indicated by the arrows. By applying several alternating pulses the shape of the curve changes to the one shown in Figure 55b, leading as well to a change of the maximum current by a factor of almost 10^5. The curve seems to be pinched in the middle, while a closer look into the measurement data reveals that there is still a deviation from the origin in the nA regime. The direction of the current remains unchanged and is the same as for the virgin curve. The application of additional pulses leads with an intermediate state to the same result as it was present for the virgin measurement and are not presented here. The initial change from the first measurement to the one in Figure 55b might indicate that some movement of the silver cluster is induced by the electrical field, which results in a major strengthening of already present connections in the network. Since such drastic increase was not observed prior for a CNT + Ag system to change from a capacitive

a) b)

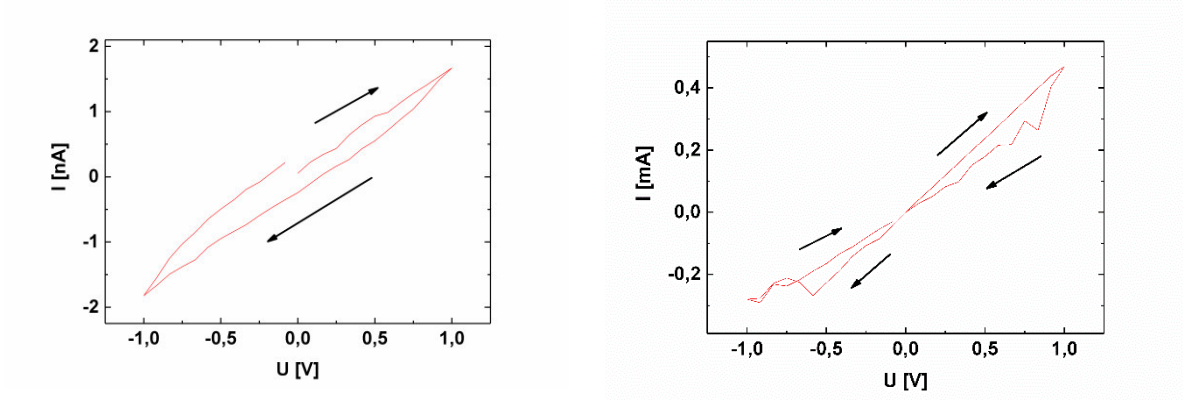

Figure 55: Hysteresis measurement results for S15 with a maximum voltage of 1 V, after NaOH treatment a) no pulse, b) after applying alternating pulses with a height of 1 V.

behavior to a non-capacitive one some SEM measurements were carried out (see Figure 56).In contrast to the prior presented samples no CNTs are visible in both images. In addition the number of silver clusters appears to be way too low for a sputter time of 230 s. Furthermore, some structures grew across the gap which is covered with small (see Figure 56a) and larger crystalline structures (see Figure 56b). The SEM images lead to the cnmclusion that the

a) b)

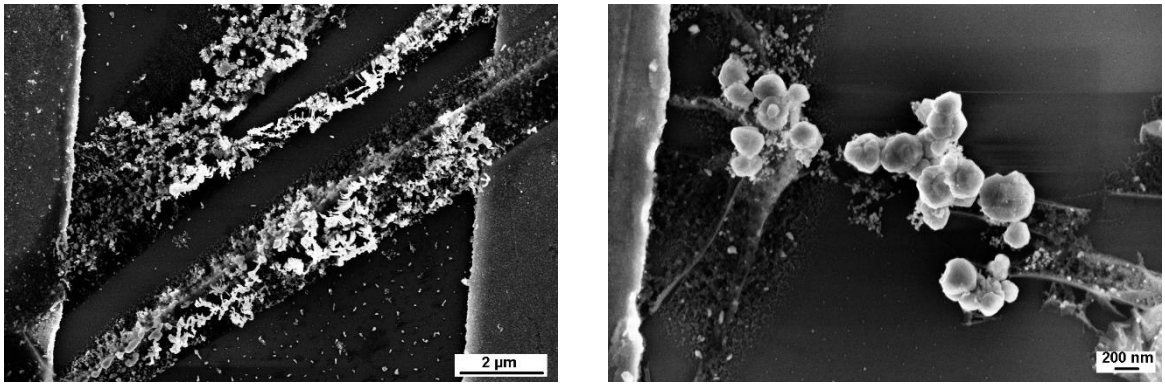

Figure 56: SEM images of S15 after NaOH treatment showing the growth of several crystal structures in and over the gaps.

measured conductivity is not caused by the CNTs and the silver clusters, but rather being the result of the bridging structures. These structures can be the result of the CNTs (as carbon source) reacting with the silver clusters and the NaOH and maybe other present

contaminations. Therefore, the larger crystals in Figure 56b can be the result of an additional chemical reaction which is induced and boosted by local joule heating due to the applied voltage pulses, which leads to a further growth of the crystal structures. Since the appearance of the sample changed drastically can this explain the structural difference as well as the investigated changes in the hysteresis curves.

To verify the hypothesis of the generation of the crystals further EDX and XPS measurements on the obtained structures are needed. However since the IV and SEM results show that the NaOH treatment results in a major conversion of the sample components is this inappropriate for further experiments.

4.5.2.2 Simulation and Validation of the introduction of Au clusters

4.5.2.2.1 Evaluation of the Au cluster Approach via Monte Carlo simulation

To realize the second idea it was decided to add gold clusters to the existing system, to work as pinpoints for the Ag clusters and to slow these down during their movement, reducing the possibility that they become fixed to the CNTs. Gold is a seemingly good candidate for this since its mobility in an electrical field is rather limited in contrast to the silver clusters making these clusters more stationary. For example they are not prone to the formation of metal cations. Additionally it was reported earlier that the presence of gold eases the ionization of silver ions from electrodes (*98*), so in this case the used clusters. A further benefit of the gold is as well that these two noble metals have an unlimited miscibility leading to a possible incorporation of the silver into the gold matrix and for this reason can lead to a slowing down of the silver clusters.

In Figure 57 an illustration is depicted to show the difference the addition of gold to the system can have. In the first image the original and untreated system is shown. By applying a voltage and creating an electrical field the clusters move according to the field, if the gap between the nanotubes is small enough as it is shown in the second image. This arrangement has the downside that the clusters move either too far or to quick depending on the applied field. Here they become stuck and therefore immobile since they are on the same potential as the CNT. To overcome this the addition of Au clusters (depicted in Figure 57c) might solve this

problem. Here the silver clusters move as well but are held by the gold clusters, hindering them from moving too close to the CNTs, keeping them mobile and allowing the back motion of them, respectively.

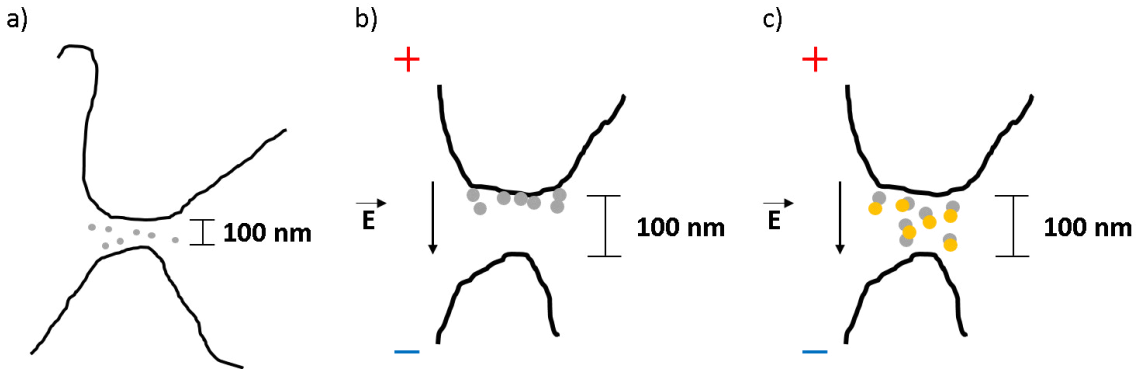

Figure 57: Influence of the addition of Au particles to the CNT/Ag system with a) being the origin without additions nor the application of an electrical field, b) after applying an electrical field without the addition of Au cluster and c) when Au clusters are added to the system.

To validate this hypothesis, of the gold clusters working as pinpoints and only the silver clusters being the mobile species ,a simplified Monte Carlo simulation was run. As mentioned this simulation was run to do a brief check if the presented theory holds or not. For the simulation an area of 50x50 nm was simulated. All of the used parameters can be found in Table 1.

The area is assumed to be borderless so that influences over the corners of the system can take place. This means that, for example, particles growing out of the left side of the simulated area will continue to grow on the right side and vice versa. As for the present samples a substrate surface consisting of silicon dioxide and as its surrounding matrix air is assumed. Whereas the air is not taken into account to have that much influence on the system itself and is more treated as the surrounding matrix. A random number of silver and gold clusters is added to the surface taking into account that a too large number would mostly result in conductive film. The approximated size of the clusters is set to 10 nm, while the Ag clusters are slightly smaller. The interaction of the clusters is simplified so that a temporary absorption of Ag clusters into Au clusters does not appear. Two different voltage pulses are applied with a voltage heights of +/-5 V. It was intentionally decided to use a higher voltage than the one

used in the previous experiments, since this simple simulation should only prove whether the designed hypothesis holds or not. Each of the voltage pulses Is applied for 15 s, starting

Table 1: List of parameters used for the simulation of the gold + silver system.

Lattice distance = hopping length of an ion per iteration	0,5 nm
Conductivity of Ag/Au	$6{,}3 \cdot 10^{7} \frac{S}{m}$
Conductivity of the surrounding material	$8{,}0 \cdot 10^{-2} \frac{S}{m}$
Reduction of silver at a) electrode b) step c) hole d) Ag/Au	 0,60 eV 0,58 eV 0,58 eV 0,67 eV
Oxidation of Ag	0,80 eV
Hopping of Ag	0,60 eV
Surface diffusion at all surfaces	0,58 eV

with a pulse of +5 V. The starting point for this simulation directly after applying the voltage can be seen in the first image of Figure 58. Here the gold clusters are represented as the yellow circles while the silver is depicted as the red ones. On the y-axis and at the x-axis the dimensions of the simulated area are given in nm. The right side of the y-axis shows the intensity of the applied electrical field in $\frac{V}{m}$. Therefore, areas colored in blue show a field close to zero or very low, while red or white indicate very high field strengths. As mentioned is the amount and position of the clusters defined randomly, in this case three of each species. The clusters are mostly arranged in the top left of the system. Consequently the highest field strength ($3 \cdot 10^{8} \frac{V}{m}$ or higher) present is close to the clusters especially in regimes where the distance between gold and silver is very low. The reason for this is that the electrical field is

defined as the ratio of volts per meter. Accordingly, if the distance between two conductive parts, i.e. the noble metals used, becomes smaller leads this to an increase in the flowing voltage due to the fact that the lowered distance increases the hopping probability between these particles and therefore the amount of measured voltage. In these areas an intensification of the field strength due to the shape of the gold clusters (*99*) occurs. The rest of the simulated area shows non or very low ($0{,}5 \cdot 10^8 \frac{V}{m}$ or lower) field strengths. The second image shows a moment shortly after the +1 V is applied. It can be seen that the strong electrical field strength between the clusters leads to the initiation of the growth of one of the

a)

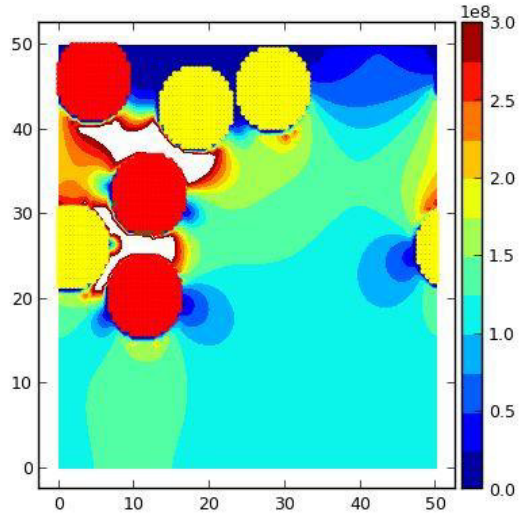

b)

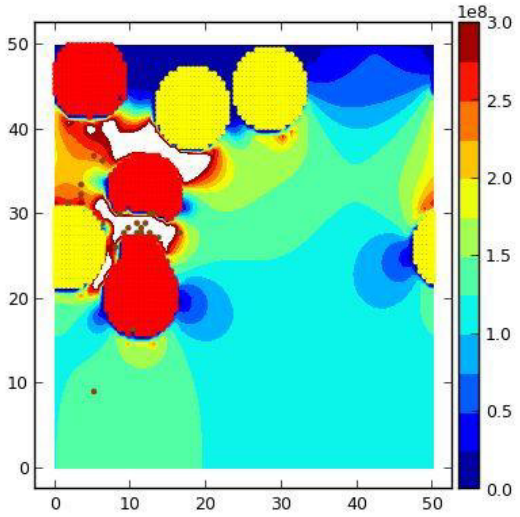

c)

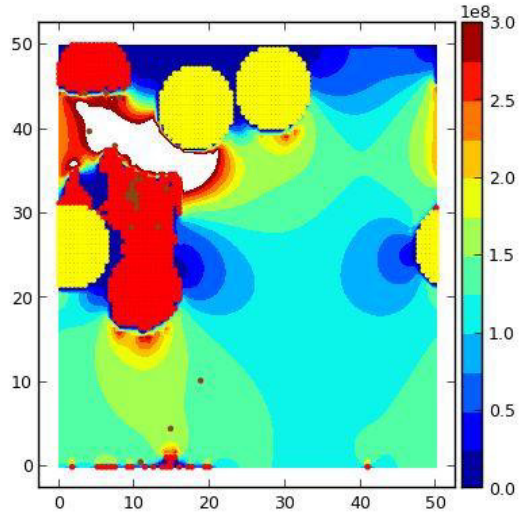

d)

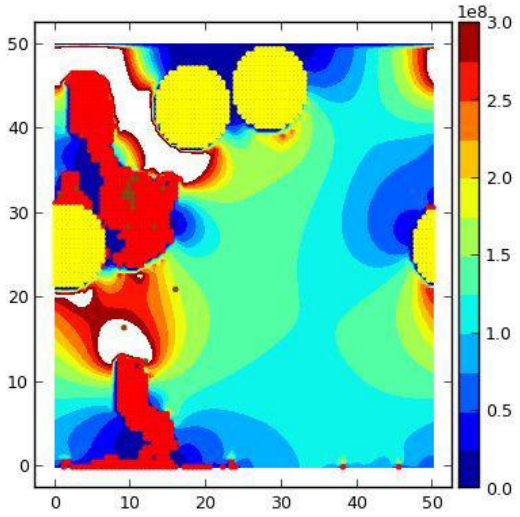

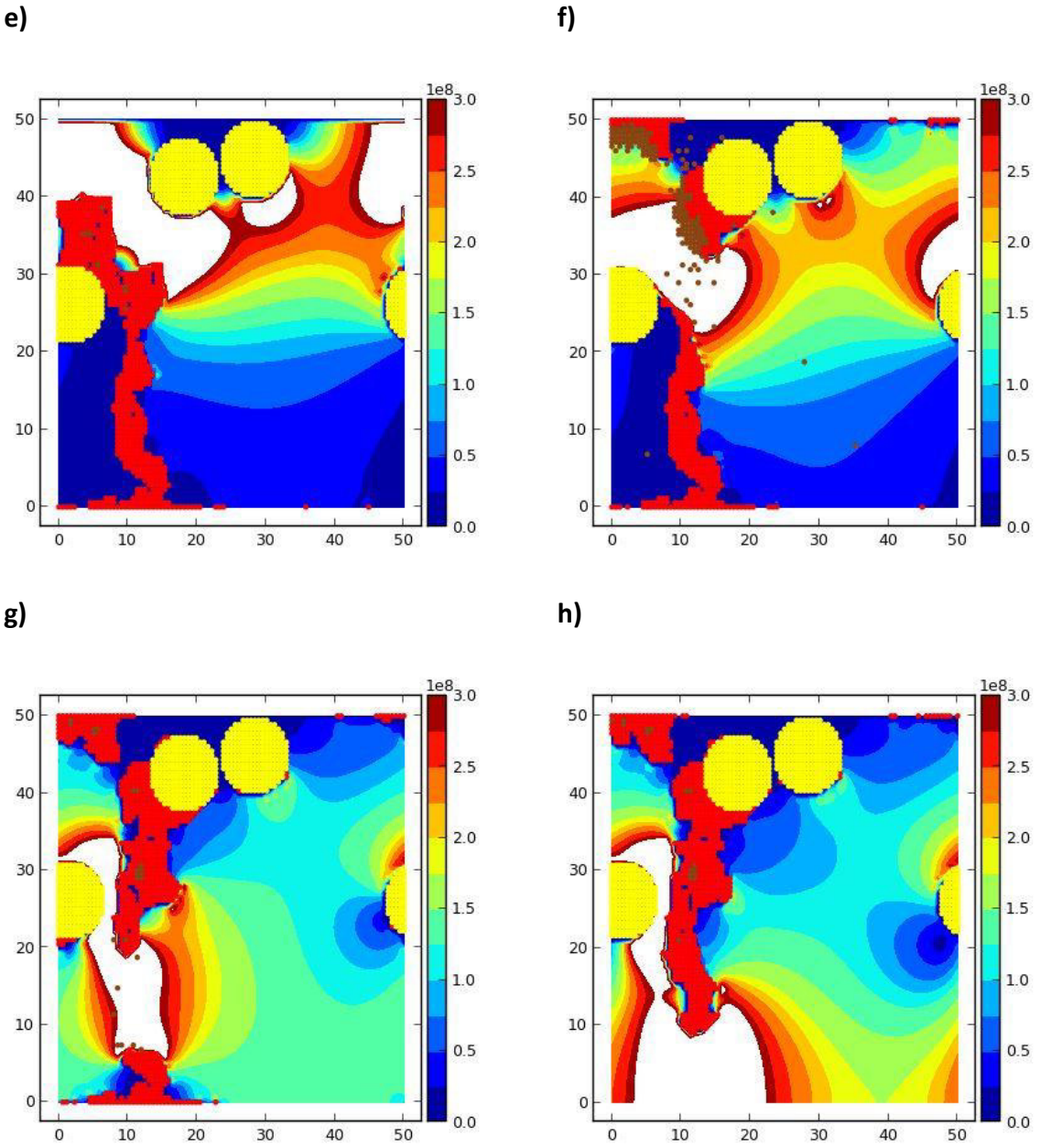

Figure 58: Simulation results for the investigated Au/Ag cluster system (simulated are 50x50 nm))at different time stamps and under different applied voltages. a) directly after applying +5 V, b) shortly after applying +5 V, c) after few seconds, d) 10 s into simulation, e) 15 s into simulation, f) few moments after switching polarity, g) 20 s into simulation, h) end of the simulation ℕŜI·ŧÎI·úλ2Y2Ŧ ŭKŜ ăK2ǿY a 2yŭŜ /I·Nŧ2 ăλY·ʊzfI·úλ2Y·ōè {℗ 5ℕ℩Y I·yŸ.

silver clusters. This happens due to the movement of silver particles and the with it linked decomposition process of another cluster (*97, 100*). This process of particle deformation and decomposition is benefitted as well by the formation of the large potential gradients across the partly non-conductive gaps (*101*). In the course of this growing process these changes widen the area of higher electrical field strength (around $1{,}5 \cdot 10^8 \frac{V}{m}$) between the lowest silver cluster and the bottom of the simulated area. The third image shows how the system looks a

few seconds into the simulation. It can be seen that the in the beginning separated two silver clusters merge due to the applied field to one larger one. In this process the electrical field strength starts to grow as well between the former upper silver cluster, one of the gold clusters and the silver cluster, leading to a field strength much larger than $3 \cdot 10^8 \frac{V}{m}$. This on the other hand leads to the decomposition of the silver particle next to the others by field induced diffusion. In the third simulated image it can be clearly seen that the other silver particle shrinks to nearly half of its size while the silver particles which drift away join the now much larger, deformed silver cluster. Not all particles which move away from the last cluster start to merge together with the other one, some start as well to accumulate on top of the gold particle next to it. Due to the very low electrical field between this small particle island and the grown silver cluster no directed diffusion and therefore no merging of these happens at this point. In addition the electrical field increases below this grown cluster as well in its intensity. This is caused by the fact that the growth of this agglomerate leads to an increase in its electrical field and its reach (*101*). This causes, on the other hand parts of the cluster to move to the bottom of the simulated area. This effect is even catalyzed by the fact that the cluster loses its circular shape, resulting in more and more needle shaped arrangements. The electrical field is at these formed tips higher than for roundish particles and is used, for example, in the transmission electron microscopy to extract an electron beam from the source tip via cold emission (*64*). This increase causes already some particles to diffuse to the bottom half of the simulated area. In Figure 58d the simulation status is shown after roughly 10 s. It can be seen that all clusters merged together in a larger one induced by the diffusion processes caused by the electrical field. The field between the top part of the agglomeration and the gold cluster in the top area shows one of the highest field strengths causing the upper silver cluster to completely merge with the larger silver agglomerate beside the small silver island on top of the gold cluster. The steadily increasing electrical field under the agglomerate and the steadily growing number of silver particles on the bottom half catalyze each other leading to the formation of another agglomerate at the bottom half of the simulated area at the cost of the other one. Due to the alignment of the electrical field is its tip pointing into the direction of the other agglomerate which leads to a decrease in their distance to each other and therefore an increase of the electrical field. Furthermore, the field is also very small at the bottom part of the newly growing agglomerate which promotes the prior described growth direction even more. The fifth image in Figure 58 shows a timestamp 15 s into the simulation

and for this reason right before the switch of the voltage from plus to minus occurs. It can be seen that the silver clusters and the silver island on top of the gold cluster merged into one elongated agglomeration reaching to the bottom of the simulated area. This results overall in a decrease of the electrical field around the grown filament and as well the gold cluster, which was in contact with it. While the electrical field between the silver and the gold clusters on the other hand increases further than $3{\cdot}10^8 \frac{V}{m}$. Due to the inversion of the voltage switching from plus to minus 5 V a movement of the clusters occurs again. Figure 58f shows the simulation shortly after switching the polarity of the applied voltage. The switching leads to a change in the orientation of the electrical field which leads to a quick initial rupture of the prior formed filament. The result of this is that smaller silver particles start to drift to the top side of the area and form agglomerates at the top side and at a neighboring gold cluster, which makes this cluster work similar to a pinpoint for the back drifting silver particles, hindering them from moving too far and therefore keeping them mobile. During this process the intensity of the electrical field changes around the remaining filament. This increase is caused by the thinning and later on rupturing of the connection between the filament and the gold cluster to which it is attached. After 20 s into the simulation (see Figure 58g) the distribution of the electrical field strength has shifted drastically. The remaining areas having a low intensity are the ones consisting of the gold clusters being in contact with the newly growing filament from one of the other gold clusters. Especially between the forming filaments the remnants at the bottom and the one gold cluster does it come to regions of higher field strengths. These high field strengths amplify even more the degradation of the old filament and a complete removal of it. The last image shows the outcome of the simulation after 30 s. It can be clearly seen that all of the silver particles are removed from the bottom half of the simulated area and form one filament growing down from one of the gold clusters. Additionally to mention is that the agglomeration of the silver particles on the filament is already finished 2,5 s before the simulation ends. This indicates that this process is a rather fast one. Similar to the end of the first half of the simulation (see Figure 58e) the field strength is around the silver agglomeration and especially around the gold cluster it is in contact with at the lowest. Therefore a movement of silver particles does not happen here anymore. On the other hand an increase of the field strength is present between the filament and a neighboring gold cluster and at the tip of the filament. This indicates that if there would be

even larger amounts of silver it would mostly move and agglomerate at the filament as well due to the high field strengths present.

The presented simulation shows that it is possible to not only move the silver particles in the sample by applying an electrical field, but also to make use of the gold clusters as pinpoints. By utilizing the gold clusters it comes to an increase in the electrical field strength between them and the silver which leads simplified to a guidance of the silver since it follows where the electrical field is the strongest.

As mentioned earlier this simulation is not a perfect representation of the real system, since it does not take the influence of the ambient air, neighboring CNT/cluster systems or the absorption and desorption of silver into the gold into account. Therefore it needs to be understood as a proof of principle of the prior stated theory, which could be successfully done.

4.5.2.2.2 Addition of gold clusters via sputter deposition

The incorporation of Au clusters into the system via sputter deposition is one of the approaches carried out in the course of this thesis. This was done by using a self-build Au/Ag target. The target consisted of a basic silver target with the addition of two gold strings. In Figure 59 such a target is depicted. The advantage of such a target is that it is possible to deposit the cluster simultaneously and at varying gold and silver ratios. This possible variation was earlier presented by Vahl et al. (*102*). By using such a target it is possible to change the composition by regulating the pressure. This happens since the decrease in pressure results in a broadening of the sputtering profile which leads to a higher amount of silver in the resulting clusters. To increase the investigated range of the composition even further a used target is chosen which shows a decrease in the amount of gold at the same pressure. For this reason the pressure is kept constant during this series so that the amount of gold decreases evenly over the course of the experiments. After running a successful experiment the sample is later on investigated by utilizing the EDX of the SEM or the TEM to determine the correct cluster composition.

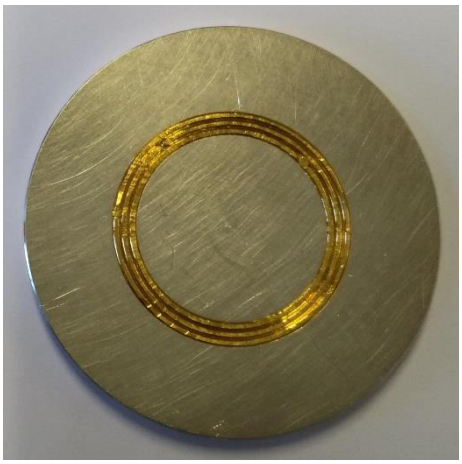

Figure 59: Self-build AuAg target for cluster deposition (consisting of a Ag target with three added Au rings).

Prior to their application an investigation of the AgAu clusters is carried out via TEM. The resulting bright field image can be seen in Figure 60. The sample was prepared under a processing pressure of $6{,}0 \cdot 10^{-3}$ mbar and a power of 40 W. As a substrate a standard TEM grid was used. It can be seen that the deposition time is long enough to let the clusters percolate

a) b)

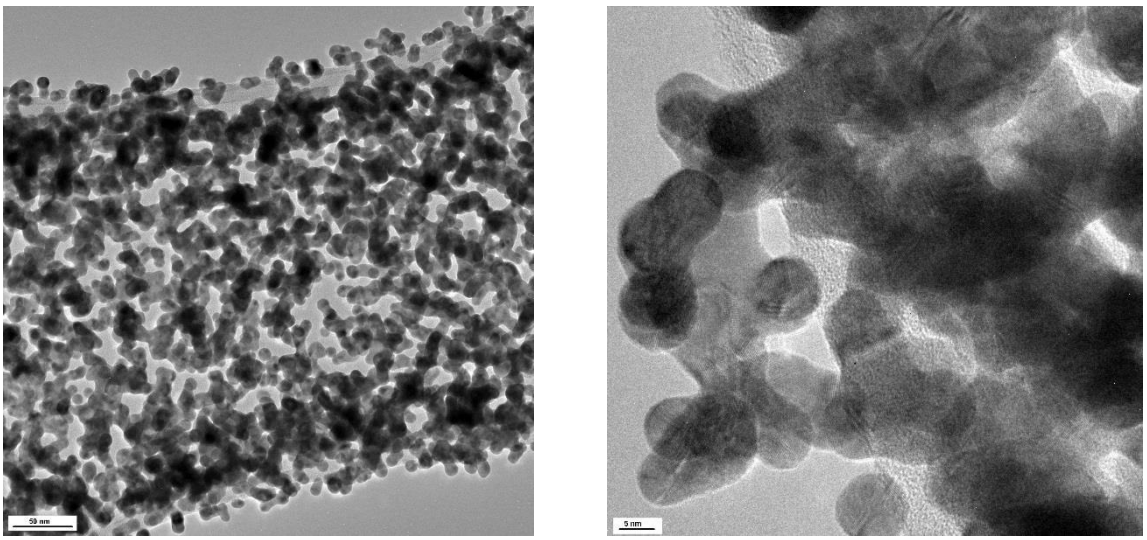

Figure 60: TEM results (bright field image) for sputtered AgAu clusters on a TEM grid (a) overview, b) close-up).

so that they start to form a film across the substrate (see Figure 60a). With a more magnified view (see Figure 60b) one wis able to determine the approximate size of the clusters being around 10 nm. In addition it is possible to see under this magnification that the clusters started

to merge together due to their high concentration which leads to a deviation of their originally roundish shape.

All samples presented in this series were prepared using a 1:64000 dispersion and have been applied by dipping small droplets onto the pre-heated sample surface six times, as it was described earlier in the experimental section. The first experiment presented here is carried out at a processing pressure of $6{,}0 \cdot 10^{-3}$ mbar. The prepared sample is sputtered under an argon pressure of 0,8 $\frac{mbar \cdot l}{s}$ and a power of 40 W for 112 s as indicted in Figure 61, which shows the logarithmic resistivity versus time. The prior described sputter setup V2 is used to monitor the deposition. It needs to be mentioned that the measurement starts with a small offset of approximately 10 s which is caused by the fact that the measurement begins right

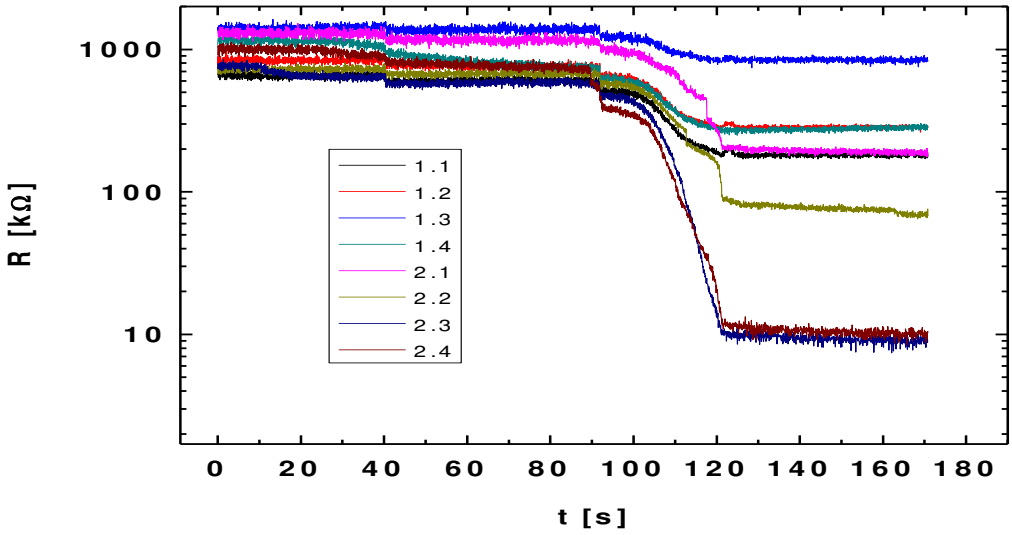

Figure 61: In-situ sputter measurement for S16 (deposition of Ag clusters).

away, while the shutter of the cluster source is removed after 10 s in order to guarantee a clean and homogenous sputter result over the whole course of the deposition process. It can be seen that in the first 90 s of the experiment nothing really noticeable happens. All measured channels show the same maxima resistance of 1000 kΩ. After this point the resistivity of all the channels starts to drop slowly, while the resistivity of two of the channels 2.3 (6 µm) and 2.4 (8 µm) falls more drastically reaching 10 kΩ after roughly 120 s sputter time. Here the in-

situ measurement setup stops the sputtering process on its own since this value is the chosen stop criterion. The other channels show a quite similar behavior compared to each other resulting in a resistivity between 200 and 300 kΩ. The only outstanding channels are channel 1.3 and 2.2 which end at 800 and 80 kΩ respectively. The sudden drastic changes in the measured resistivity indicate that the system is quite close to the percolation threshold. The major differences between the individual channels might be caused by a relatively inhomogeneous sputter process induced by an off-center position of the mounted sample or inhomogeneity in the self-made sputter target. Another reason can be that the CNT deposition and the resulting network is not evenly distributed over the whole sample.

The SEM image shown in Figure 62 shows sample S16 at the 1.4 gap after the sputter process. It can be seen that the CNTs as well as the clusters are evenly distributed over the gap. The investigational electrical measurements are carried out in the same order as reported earlier with the difference that the applied pulses are increased step by step starting with a pulse

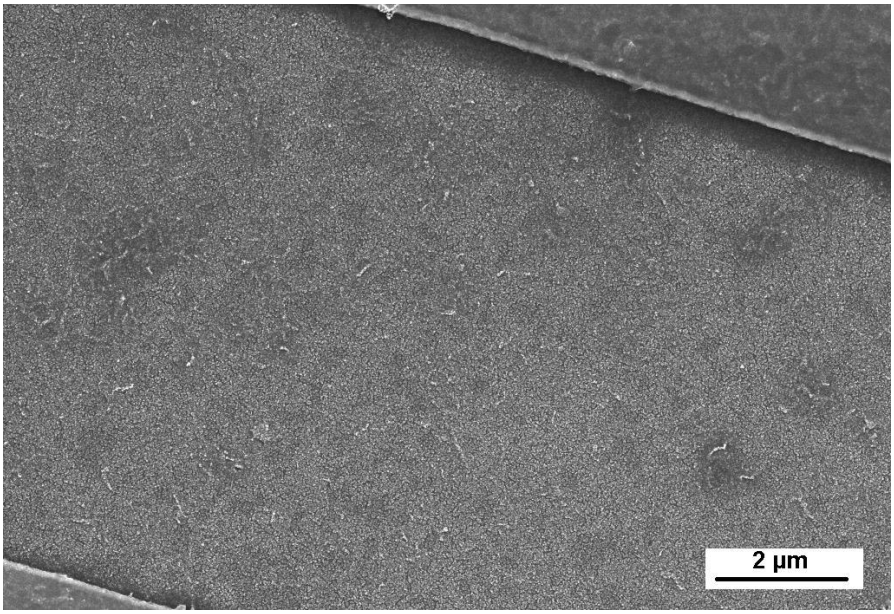

Figure 62: SEM image of S16 with applied CNTs and after AgAu cluster deposition.

0,5 V and going up to 5 V and are applied for 30 s. The results of the first and the last pulse in this series are shown in Figure 63. It is quite noticeable that for both of the displayed pulses no sudden ups and downs in the measured current occur as was seen in the earlier pulse experiments. Both measurements started with an abrupt rise of the current in the first second

but converted to a slower and steady increase afterwards. The measured current values differ by a factor of 10, but since the pulse heights differs by the same factor the current is overall in the same range. The steady increase indicates that the application of an electrical field only leads to a strengthening of already existing connections for this sample.

a) **b)**

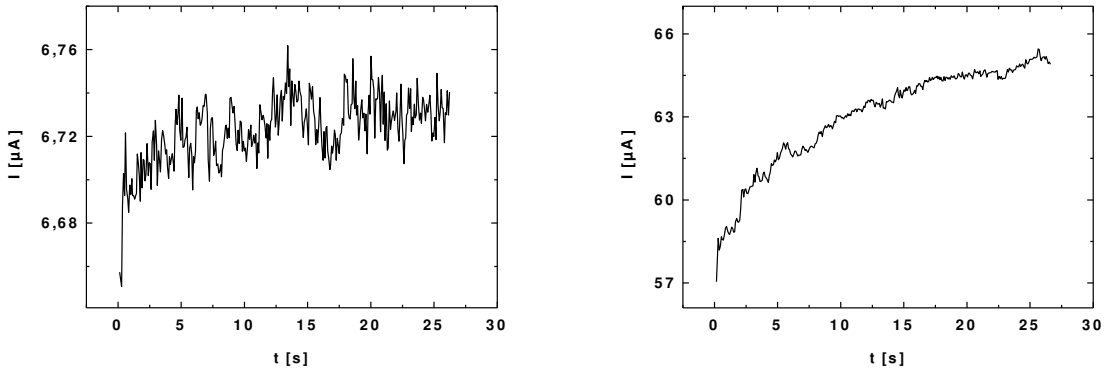

Figure 63: Pulse results for S16 (1.4) after a) one pulse (+0,5 V) with a length of 30 s and b) one pulse (+5 V) with a length of roughly 30 s.

The conclusion that the usage of an electrical field for these kinds of samples only results in a strengthening of the existing connections in the system and not a rearrangement of clusters, and therefore formation of new conjunctions in the network, is mirrored by the hysteresis results depicted in Figure 64 as well, which shows the measurement results for another 10 µm gap. Here the results before the first pulse, after the first one is applied and after the last one are shown. All of the measurements show that the current increases linearly with the voltage. For the virgin curve and after the first pulse the results are quite similar and only differ slightly in the maximum current with the virgin curve having a somewhat lower one. To check if this system can be somehow influenced by applied voltages the pulse height as well as the hysteresis length are increased. The outcome is that the shape of the curve is not altered at all. Even after a 5 V pulse is applied the outcome of the hysteresis is ohmic behavior with a slightly higher maximum current. The current is only slightly higher since the length of the hysteresis is increased as well for the last measurement. It seems that for the high amount of clusters in the system no major cluster movement occurs, which might be caused by their high density. The only noticeable effect of the electrical field is that it results in a strengthening of

already existing internal connections. This happens by slight deformation of clusters which are located next to the conductive path. It is a slow and steady process which is indicated by the

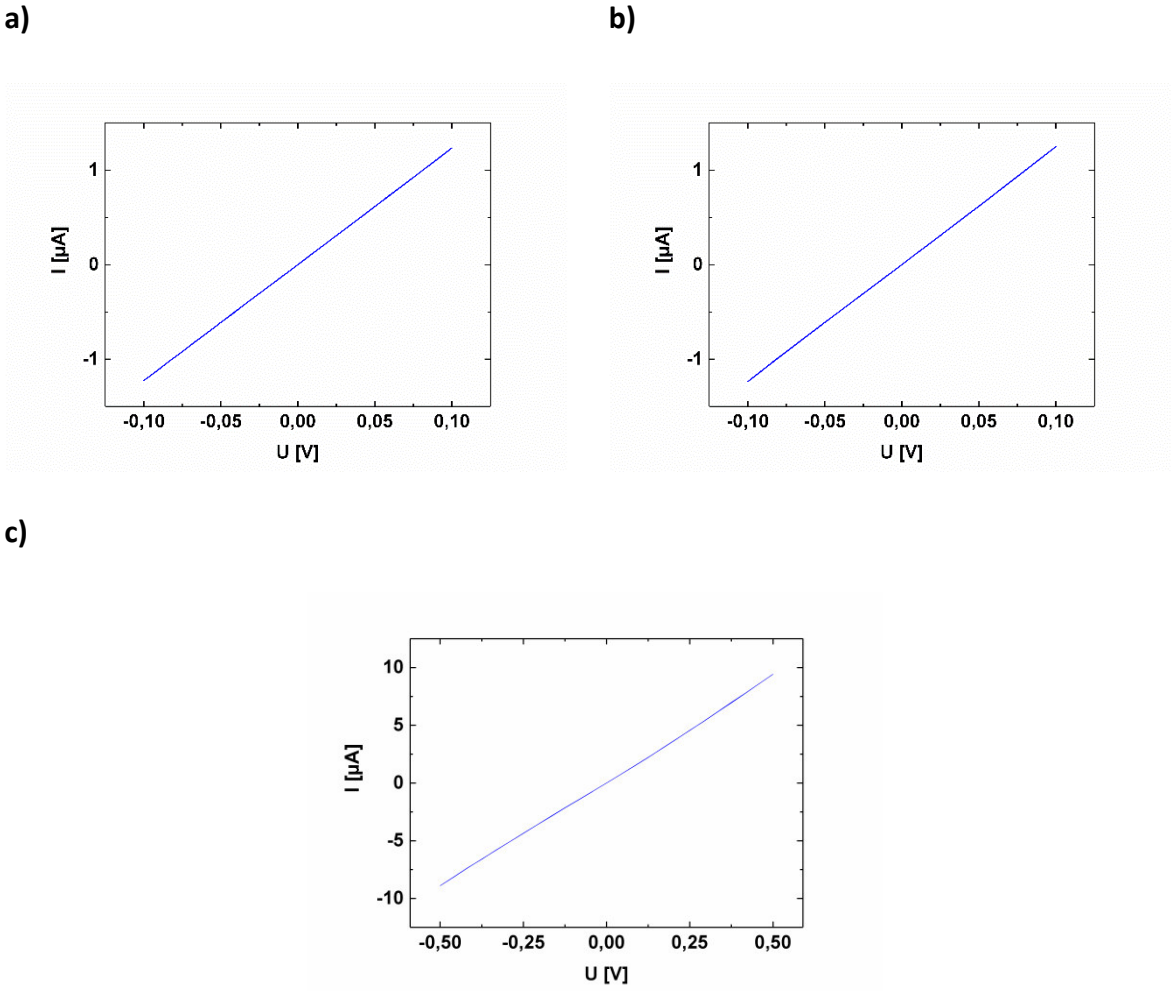

Figure 64: Results for the hysteresis measurements for S16 1.4 a) virgin curve (maximum voltage 0,1 V), b) after a +0,5 V pulse was applied (maximum voltage 0,1 V), c) after a +5 V pulse was applied (maximum voltage 0,5 V).

steady increase of the measured current during the applied pulses. The overall movement of the particles is limited by the interaction of the particles themselves with the electrical field, shown already in the simulation earlier. As long as there is some spacing between the cluster and the conductive path a deformation of the cluster in the direction of the electrical field occurs. But the field vanishes between cluster and path as soon as they are connected and therefore stops the further deformation of the cluster. On the backside of the cluster it will come now to an increase of the electrical field leading to an attraction and connection of the next neighboring cluster. This process continues as long as there are particles close enough to become attracted by the electrical field leading to a further strengthening of the conductivity

path and therefore increase in the conductivity of the system. It is also possible to find this described behavior partly in the previously presented simulation.

Since the sample only reacts in an ohmic way is the amount of deposited clusters and their composition adjusted, since it is assumed that their amount is too high, causing the described behavior.

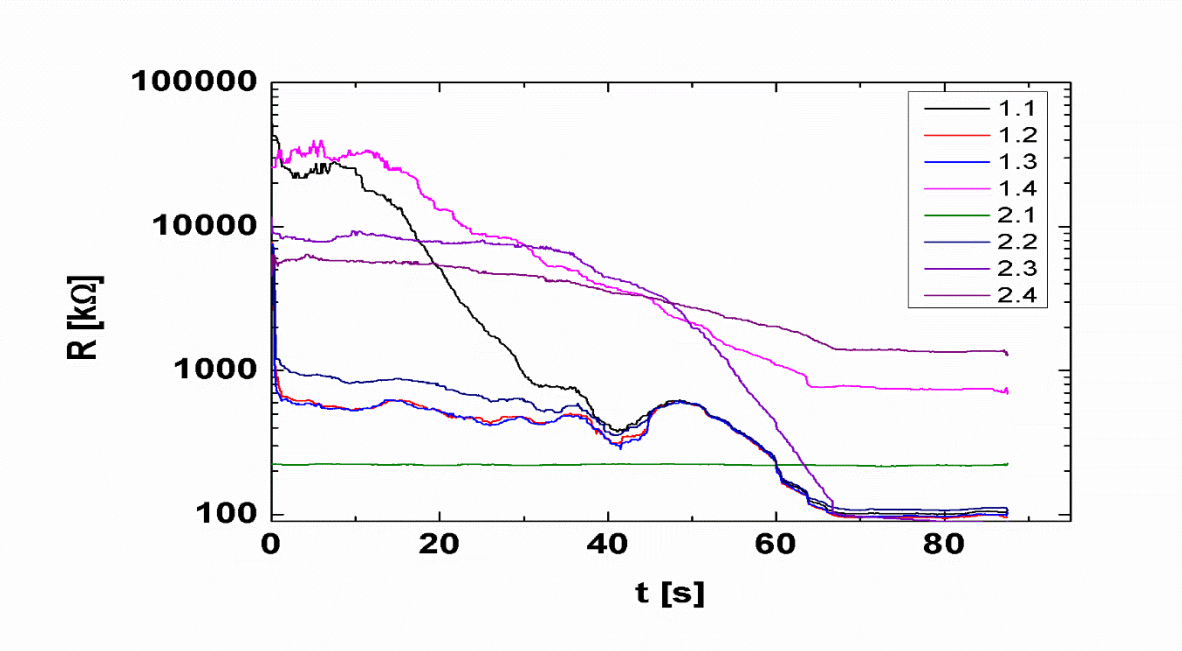

Figure 65: In-situ sputter measurements for S17 (deposition of AgAu clusters).

Figure 65 displays the in-situ sputter measurement results for sample S17. For this experiment the argon pressure is set to 0,8 $\frac{mbar \cdot l}{s}$ and a power of 40 W is used. The resulting pressure in the chamber is $5{,}6 \cdot 10^{-3}$ mbar and the sputtering takes 56 s. The sputtering is stopped when the prior set threshold voltage is undershot. The straight line from gap 2.2 (dark blue) can be ignored since it is later found that the sample was not properly connected for this gap. The blue (1.3) and purple (1.4) curves are the only ones which do not fall under the threshold voltage, for which reason they are investigated further. Both start at a resistivity of around 10^5 and 10^4 kΩ respectively, while the purple one starts at a higher resistivity and drops quite rapidly after 17 s and ends at a lower resistance value than the blue one around 10^3 kΩ. In Figure 66 a SEM image of S17 is shown after sputter deposition. The SEM image shows the 1.3 gap of S17 and it can be seen that the CNTs as well as the clusters are distributed quite evenly. The additional image in Figure 66 shows a magnification of the area marked in the picture

showing that the clusters already started to form agglomerations despite the lower sputter time while these agglomerates are still quite evenly spaced. The fact that there is still a decent amount of space (in some cases even more than 30 nm) between the clusters indicates that it might be possible to achieve some cluster movement in the sample itself leading to non-ohmic behavior, similarly demonstrated for the previously examined sample.

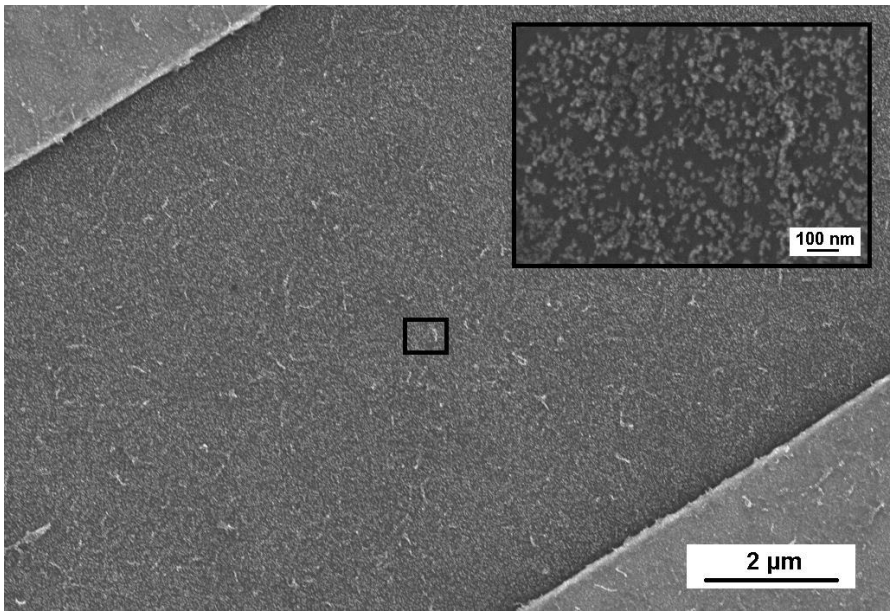

Figure 66: SEM image of S17 decorated with CNTs after AgAu cluster deposition.

For the electrical investigation are pulses of -3 V and in a last step a +3 V pulse applied, for a timeframe of 60 s and 120 s for the last pulse, respectively. The results for the pulse measurements are shown in Figure 67. Figure 67a shows the result for the first pulse. Since a negative voltage is applied the resulting current is negative as well. In the further discussion will be referred to the absolute value of current. It can be seen that in the first seconds of the run a large spike in the current occurs leading to an increase of the current from 2,4 to 3,6 µA. Afterwards the current drops slightly by 0,25 µA and falls down to the prior level after 10 s. From here on the current mostly increases slightly and reaches 4,0 µA showing only smaller decreases over the course of the experiment. Due to a small perceptible change, which will be discussed later, in the upper hysteresis curve after the first negative pulse the next applied pulse is a negative one as well. Its outcome is shown in Figure 67b. It can be seen that there is a spike in the measured current, lowering its value from 3,9 to 3,6 µA. This spike is the most noticeable measurement result for this pulse since in the course of the next 30 s the current

a)

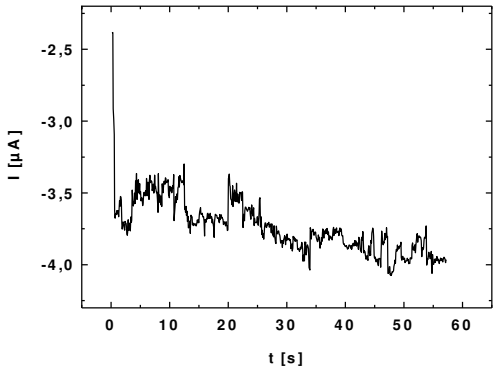

b)

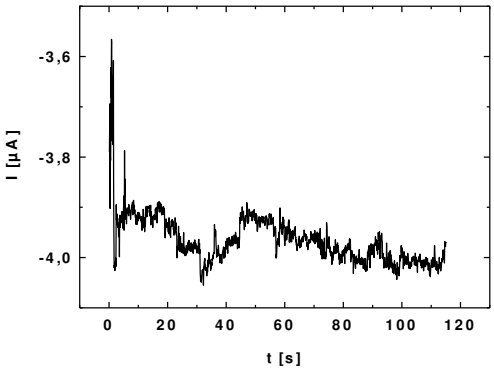

c)

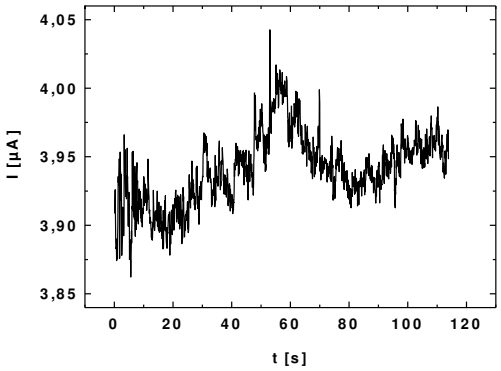

Figure 67: Pulse results for S17 (1.3) for a) one pulse (-3 V) with a length of 60 s and b) one additional pulse (-3 V) with a length of roughly 120 s c) and a further pulse (+3 V) with approximately a length of 120 s.

increases slowly by 0,1 µA, drops over the next 20 s by the same amount and increases again back to 4,0 µA. Since there are no major changes in the pulse measurements for this sample a final pulse with a voltage of +3 V is applied for roughly 120 s, which result is displayed in Figure 67c. The measured current level for the positive pulse is similar to the negative ones applied previously. The current does not increase by much and shows a small jump after 40 s, but the overall change is slightly more than 0,05 µA.

The little to no changes for the pulse measurements are mirrored as well by the hysteresis measurements carried out after each pulse, which are displayed in Figure 68. All hysteresis

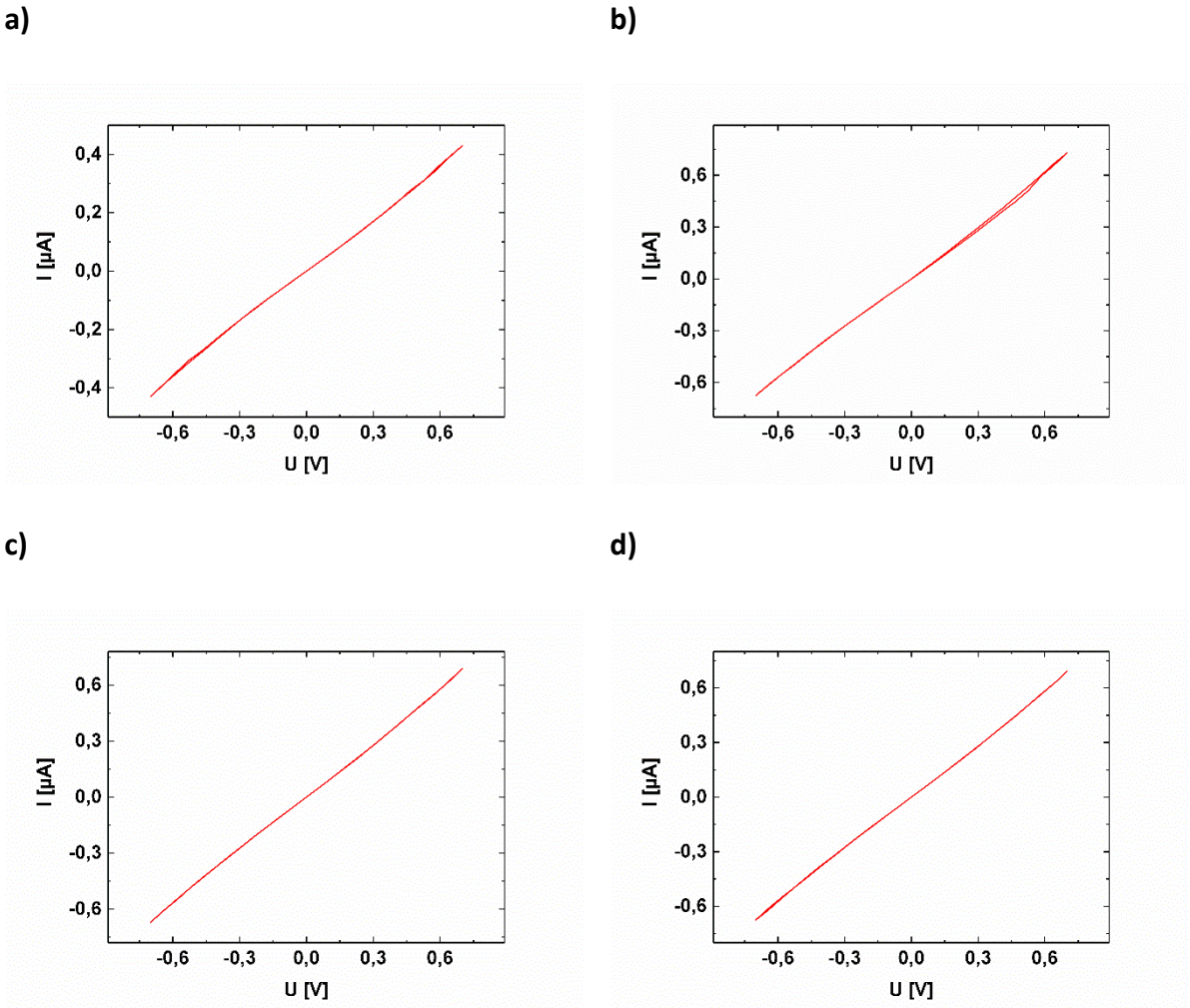

Figure 68: Results for the hysteresis measurements for S17 1.3 a) virgin sample, b) after a -3 V pulse, c) a second -3 V pulse d) after a +3 V pulse (with a maximum voltage of 0,6 V).

measurements are carried out by applying a maximum voltage of +/-0,7 V, to match the voltage of the in-situ measurements. There is no big change in the outcome of the studied sample as mentioned before. The shape of the curve for all four hysteresis measurements is a nearly straight ohmic line, similar to the discussed results of S16. Again an increase in the maximum current can be noted by comparing the virgin curve (Figure 68a) with the others showing a change in current from 0,4 to 0,6 µA. The only deviation from the linear shape of the curve is visible after the first negative pulse is applied, since a very narrow broadening of the curve happens for the positive part of the loop.

By combining the results of the pulse and hysteresis measurements it is not possible to note significant changes in the system due to the electrical field. The spikes which occur in the second and especially first pulse measurement and the changes which occur in the first 20 s of the first pulse also indicate that it results in a shift of the position for some of the silver

particles. This change of position is confirmed as well by the increase of the maximum current change from the virgin measurement to the ones after the pulses.

To conclude the AuAg sputter experiments it can be stated that their outcome is, despite lowering the sputter time, a system that only reacts to an applied voltage in an ohmic way with only slight movements of silver cluster detectable. Since this experimental outcome differs from the prior presented simulation another approach is tested to incorporate gold clusters into the system.

4.5.2.2.3 By adding Au particles from Au glucose solution

The new approach involves the usage of a gold nanoparticle dispersion that is discussed in the experimental section (see 3.4.2).

Even though several methods are tested for the application of the dispersed gold nanoparticles is the outcome of the experiments carried out similar to the ones presented in the prior section. For this reason only one of the methods and its results will be discussed further. The method discussed here is the application of the dispersion by drop coating on an 85 °C hot plate. The distribution for such a sample looks as depicted in Figure 69. As mentioned

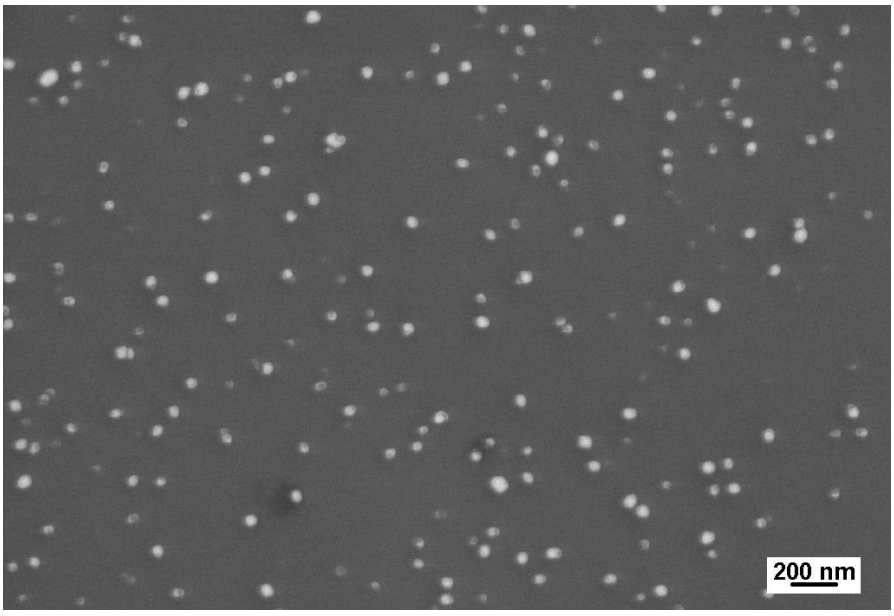

Figure 69: SEM image of a sample coated with Au cluster utilizing an Au dispersion stabilized with glucose and applying it via drop coating on an 85 °C hot plate.

in the experimental section of this thesis is the sample plasma etched after the dispersion is applied to remove the glucose coating of the particles. In Figure 69 it can be seen that the particles have the same size and are not completely evenly distributed. Despite using plasma etching there are still some dark spots, which are probably contamination present on the sample. The CNT decoration is carried out after the plasma etching, to ensure that the nanotubes are not harmed. The deposition is carried out using a 1:120000 dispersion and applying it on a 115 °C warm hotplate. Again the silver clusters are applied via sputter deposition with a sputter time of 91 s. The hysteresis curves for sample S 18 after application of different pulses are shown in Figure 70. It can be seen that for the virgin measurement the result is a straight ohmic line on both sides with a maximum of the measured current of almost 0,3 mA. The applied pulses are applied for a period of 30 s and with a pulse height of +/-1 V.

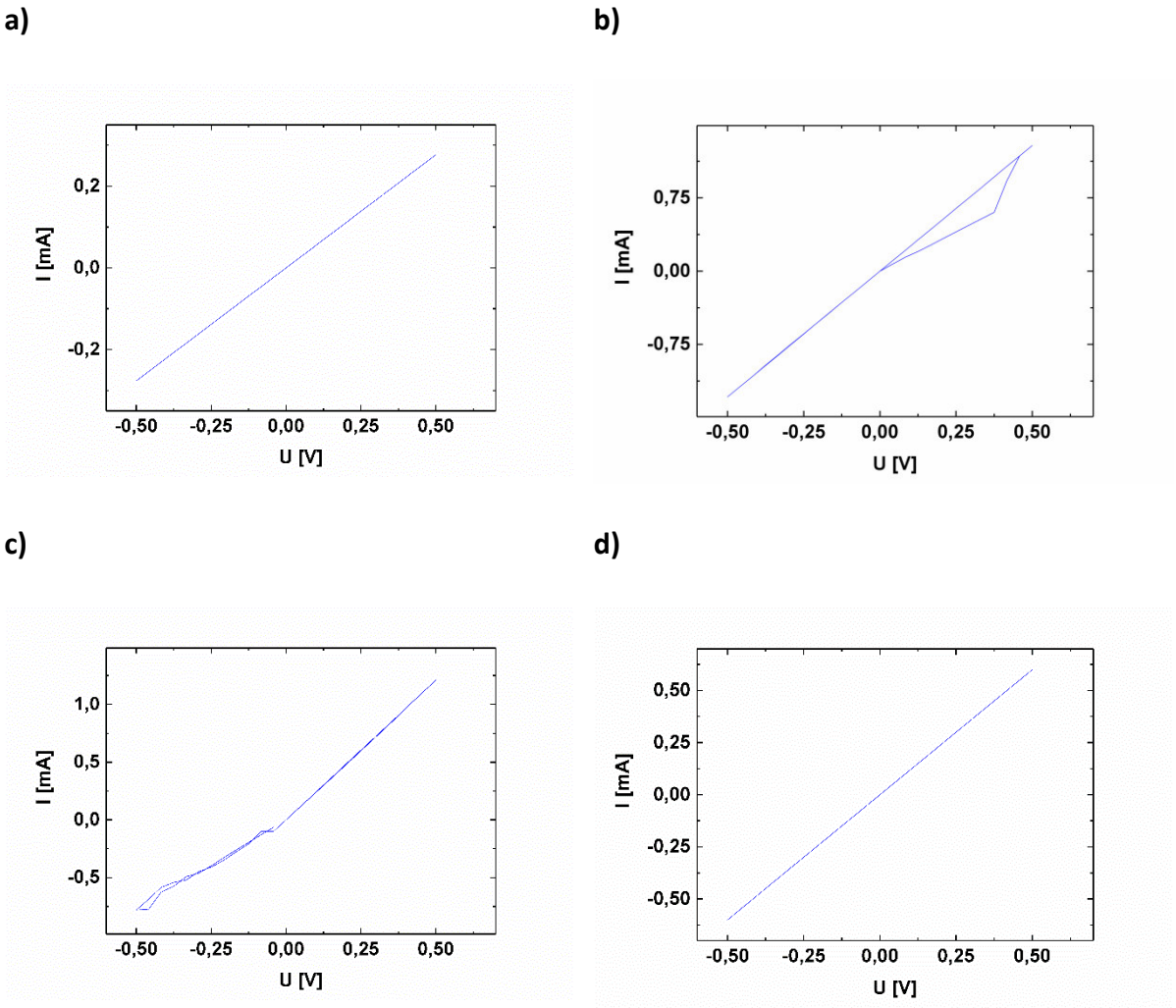

Figure 70: Hysteresis measurement results for S18 after applying a) no pulse, b) a positive pulse, c) a negative pulse, d) an additional negative pulse (maximum hysteresis voltage 0,5 V, applied pulse height +/- 0,5 V).

The first applied pulse is a positive one resulting in a widening of the positive hysteresis loop and a change in the maximum current to 1,3 mA (see Figure 70b). The widening and change of the shape indicate that it is also possible for the gold dispersion system to move the clusters by applying an electrical field, even though there is some small contamination still present after the plasma etcher is used, as indicated by the SEM image. To see if it is possible to open up the loop further, especially for the negative quadrant, a further negative pulse is applied. Its result is shown in Figure 70c) and it reveals that the additional pulse had a major effect on the system in contrast to the measurement results for the AgAu cluster samples. The maximum current achieved for the positive pulse was again around 1,3 mA and the shape of the curve became a straight line. On the other hand the effect on the negative quadrant was that the curve tilted slightly, the forward and backward direction did not overlap completely anymore and the maximum current value achieved decreased to 0,75 mA. The field induced movement of the silver particles led to a more asymmetric arrangement leading to the presented result. The usage of an additional negative pulse resulted in a complete ohmic line again with a maximum current of 0,6 mA. Further pulses did not lead to any other changes in the behavior in the resulting hysteresis, always showing the same characteristics.

Apparently the initial separation of the different cluster types (gold and silver) by separate deposition has a positive effect on the influence of the electrical field on the samples behavior. The result improved since it is possible to move the cluster from an ohmic to a slightly asymmetric hysteresis behavior. A reasoning why the approach of using the gold dispersion does not lead to a memristive sample can be that the number of gold clusters might have been too low in the respective gaps or it is caused by the remainings after the plasma treatment. It is possible that the Au clusters hinder the Ag clusters from forming too strong connections with the carbon nanotubes in first place, but are unable to support this effect long enough as the sample is further stressed by the usage of additional pulses.

4.5.2.2.4 By adding Au particles from Au solution stabilized by micelles

A second way of incorporating Au clusters into the system from dispersion is carried out by using the previously described technique from Kadem et al. (*67*). Two different approaches are tried to apply the gold particles. The samples are either spin or dip coated using varying

speeds. The rotation speeds vary from 1000 to 3000 rpm while the dip coating speeds are ranging from 8 to 25 $\frac{mm}{min}$, respectively. Not all of the speeds used will be presented here since not all show interesting, from the ohmic behavior differing, results.

In Figure 71 the SEM image of a result with the gold cluster decorated sample prepared via the Kadem et al. technique using spin coating is shown. It can be seen that the size of the gold clusters is very equal and they are much more evenly distributed than the ones applied by using the hot plate.

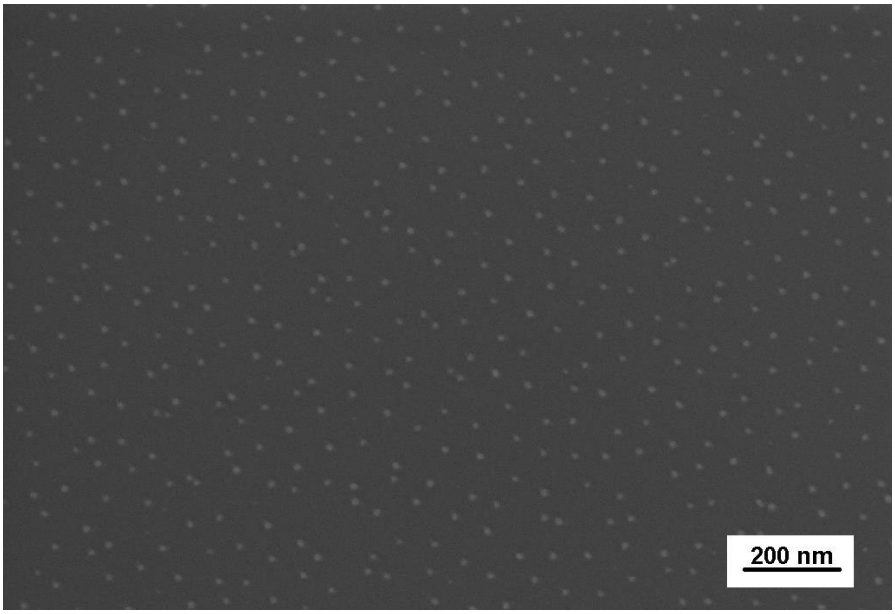

Figure 71: SEM image of a spin coated sample following the deposition technique reported by Kadem et al.

The results presented in the following show one of the used speeds since most of the other experiments did not result in noticeable differences (mostly ohmic) and therefore are not of further interest. The here presented and investigated sample is S19 for which are rotation speed for the deposition of the gold clusters is set to 1000 rpm while the CNTs are applied by using a hot plate at 115 °C and a dispersion with the ratio 1:80000, while the silver clusters are deposited for 215 s under a sputter pressure of 0,4 $\frac{mbar \cdot l}{s}$. For this sample the usual pulse and hysteresis measurements are carried out to investigate it further. The results are shown in Figure 72 and show the outcome of a hysteresis curve after five applied voltage pulses and after ten pulses. Both resulting hysteresis curves show similar behavior, having a maximum

around 0,6 µA and a very linear shape. For this sample it is not possible to alter its behavior despite the usage of different pulses. This gives a strong hint that the usage of a homogenous arrangement of gold clusters does not lead to a memristive sample, since it is possible for the random arrangements alter the shape of the hysteresis curve. The main difference here between the samples S18 and S19 is that the cluster arrangement of S18 is more irregular (see Figure 69 and Figure 71). It appears to be crucial for the fabrication of a sample having asymmetric contacts that the applied gold clusters are arranged already in an irregular structure as well. For this reason a further series of experiments are carried out following the approach of Kadem et al., but without applying the clusters via spin coating.

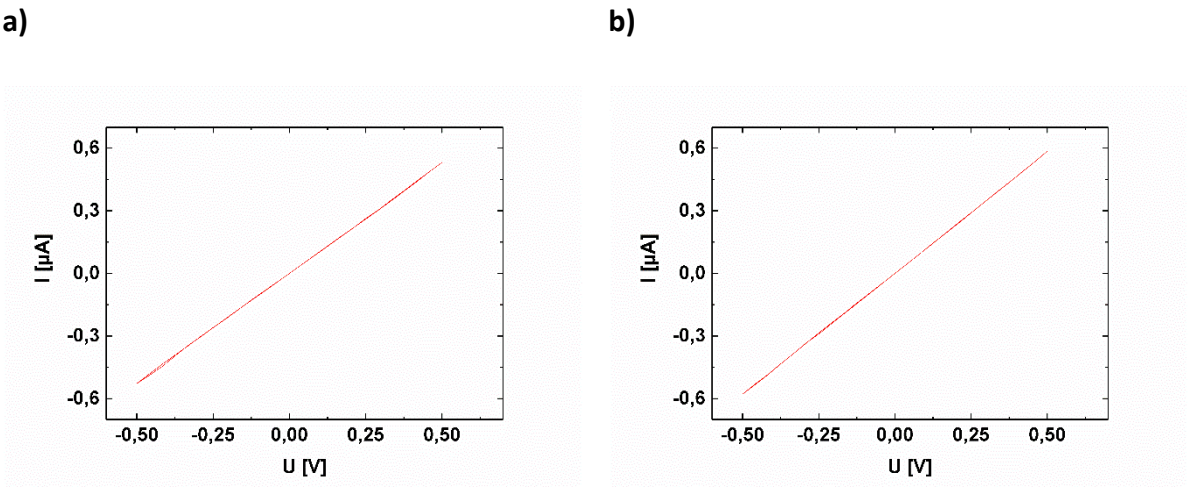

Figure 72: Hysteresis curve of S19 after applying a) five voltage pulsse, b) ten voltage pulses (maximum voltage 0,5 V).

For the other approach a technique called dip coating is utilized and as mentioned before different dipping speeds for the sample preparation are tried. The most interesting results are obtained for the dip coated samples which are prepared with a speed of 25 $\frac{mm}{min}$ and can be seen in Figure 73. It is shown that the gold clusters are not distributed evenly over the sample surface. There are some single clusters present, but most of them started to form agglomerations with a length between 30 to 140 nm. Still the shape of the clusters formed is elongated and not round.

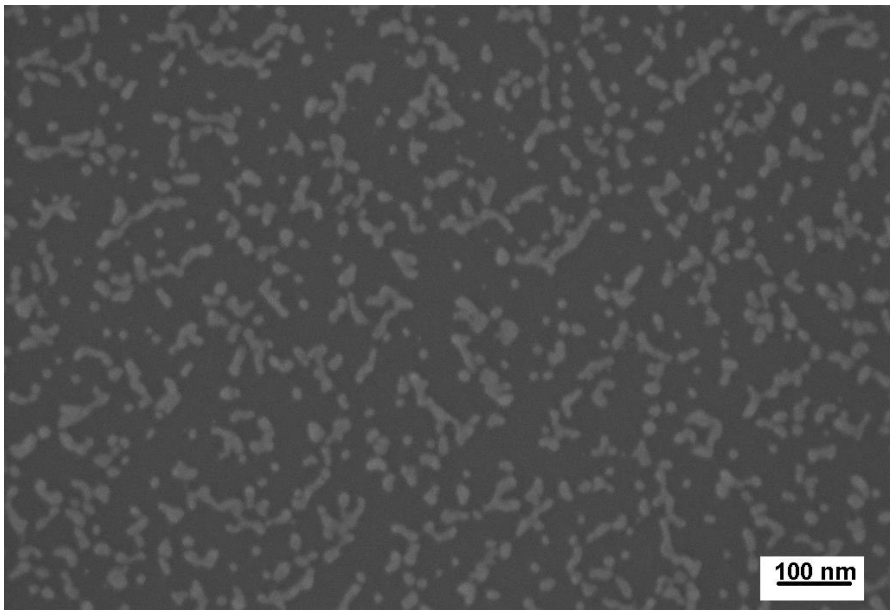

Figure 73: SEM image of a dip coated sample prepared with a speed of 25 $\frac{mm}{min}$ followting the approach of Kadem et al.

The samples prepared via dip coating are afterwards decorated with CNTs, which are added using the same technique as for S19 and a dispersion in the concentration 1:80000. While the Ag cluster are added for 215 s via sputter deposition at an argon pressure of 0,4 $\frac{mbar \cdot l}{s}$. In Figure 74 the result for S20 can be seen, which shows a sparse nanotube network across the gap. In addition are the CNTs decorated with the silver clusters while the density of the previously added gold clusters and the silver is not high enough to cover the whole area, nor

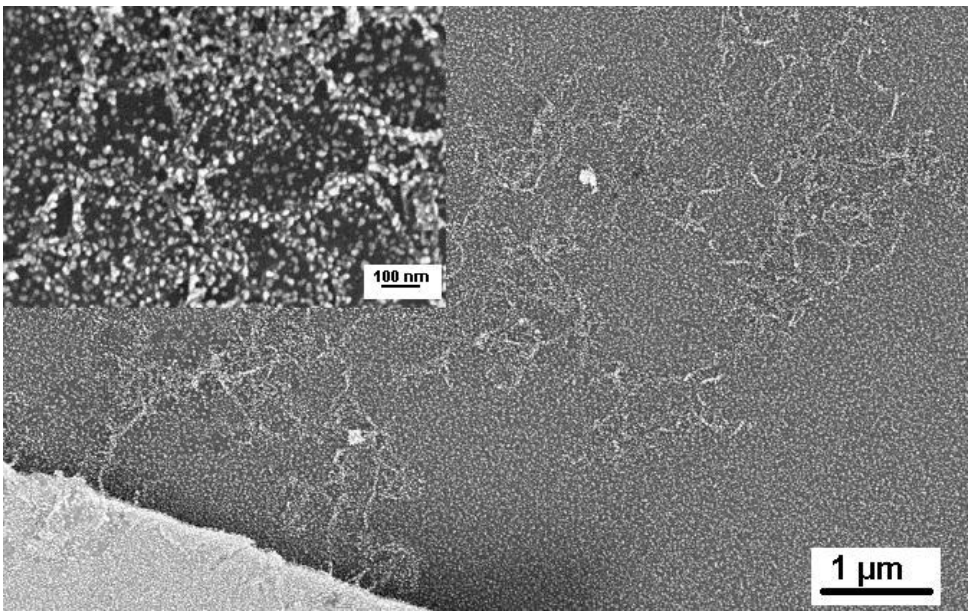

Figure 74: SEM image of S20 after Au cluster and CNT deposition and sputtering of Ag clusters.

is their spacing too large. The virgin scan for this sample reveals some major differences between the upper and the lower loop. In Figure 75 the curve is shown. It can be seen that the current jumps up close to the maximum applied voltage up to 6,9 µA and decreases after lowering the voltage not following the prior path until a voltage of 0,15 V is reached, resulting in a sudden drop of the current. The curve goes through its origin and describes a straight line for the negative regime with a maximum current of -0,12 µA. The shape of the positive loop can be attributed to CNTs which are not attached completely to the sample surface, which might be caused by the introduced gold clusters. The behavior of the hysteresis curve while the voltage decreases indicates again that a spontaneous event took place since the change in current is very abrupt. It is possible that this spontaneous process is caused by the movement of one or many nanotubes. The behavior shown looks quite similar to that of a spring which is stressed. A spring has a specific restoring force, which has to be overcome to be elongated. This process is very quick as soon as a force large enough is applied. The elongated spring will snap back as soon as the force which is holding it is not big enough anymore, resulting in a sudden movement. This analogy to the behavior of a spring can be found in the present measurement which makes it very likely that these sudden changes in current are caused by a stressed and afterwards relaxed CNT, since it is the only possible part of the system that can react in such a manner. Furthermore this mirrors the behavior presented in the paper from Hansen et al. (*19*). Another explanation could be the movement of silver clusters, although this is quite doubtful, since for example the applied voltage is quite low where the back-switching occurs.

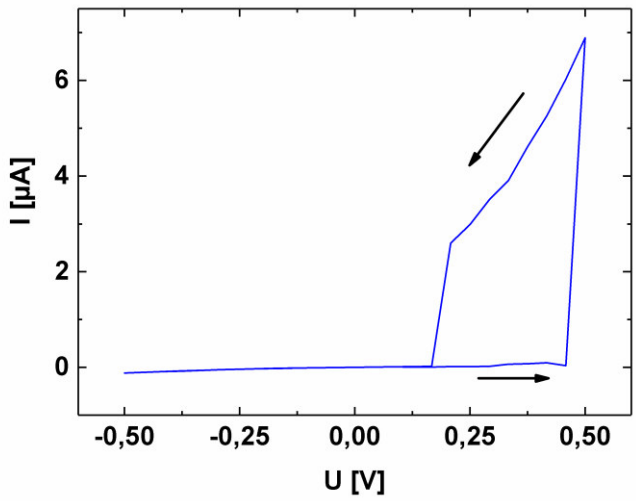

Figure 75: Hysteresis curve of the virgin sample S20 (maximum voltage 0,5 V)

After applying a voltage of -1 V for 10 s and performing a hysteresis the curve in Figure 76 is achieved. The result is similar to the one obtained for other samples presented earlier after the first pulse. Figure 76 shows a linear ohmic behavior with maximum current of 12 µA. It seems that the applied electrical field only leads to an alignment of the silver clusters, resulting in the present hysteresis curve.

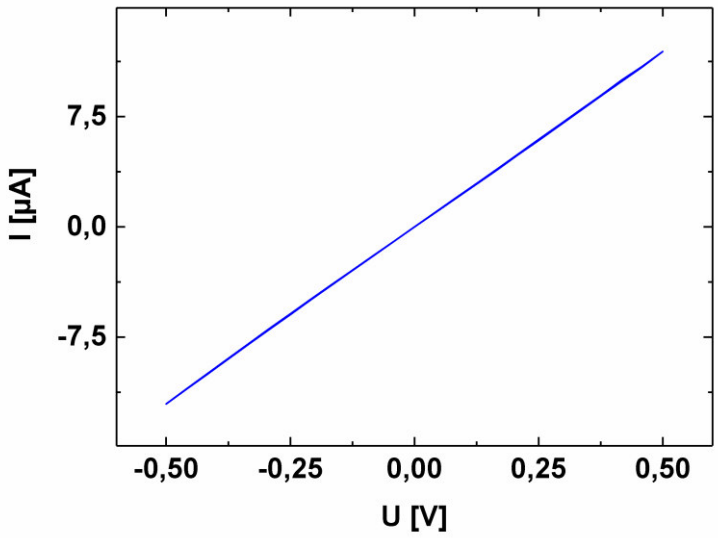

Figure 76: Hysteresis curve of S20 after applying the first voltage pulse (maximum voltage 0,5 V).

The usage of an additional positive voltage pulse leads to the hysteresis curve shown in Figure 77. It can be seen that the measured current is very low in the beginning and rises after just 1 s close to 25 µA. For the remaining time the current stays on this level showing two smaller and a major drop after 3, 5 and 6 s. The small current drops and especially the big one indicate the movement of the clusters. While the small ones might represent a brief disruption of side arms of the network indicates the large drop after 6 s that there must be an interruption of the main path in this specific network by the cluster movement. Its interruption leads to a sudden current drop close to zero. Apparently the gap generated between the separated silver particles is not too big, resulting in a large electrical field and a sudden closure of the gap. This closure is marked by the fact that the current goes up to the prior level again afterwards. The hysteresis curve measured afterwards is shown in the same figure. The measured hysteresis curve (see Figure 77b) differs from the one in Figure 76 not only by its shape but as well by the

reduced maxima for the measured current. While the current of the previous hysteresis curve is in the 10^{-5} A regime does it drop down after the second pulse to the $10^{-6/7}$A regime. By comparing these maximum values with each other it can be concluded that some parts of the network are disconnected and are not reconnected during the pulse, resulting in a drop of the measured current. For the positive quadrant the back and forward direction is quite linear, but not overlapping, while the negative one shows an abrupt increase and subsequent decrease in the current directly after the negative voltage is applied and before the maximum negative voltage is reached.

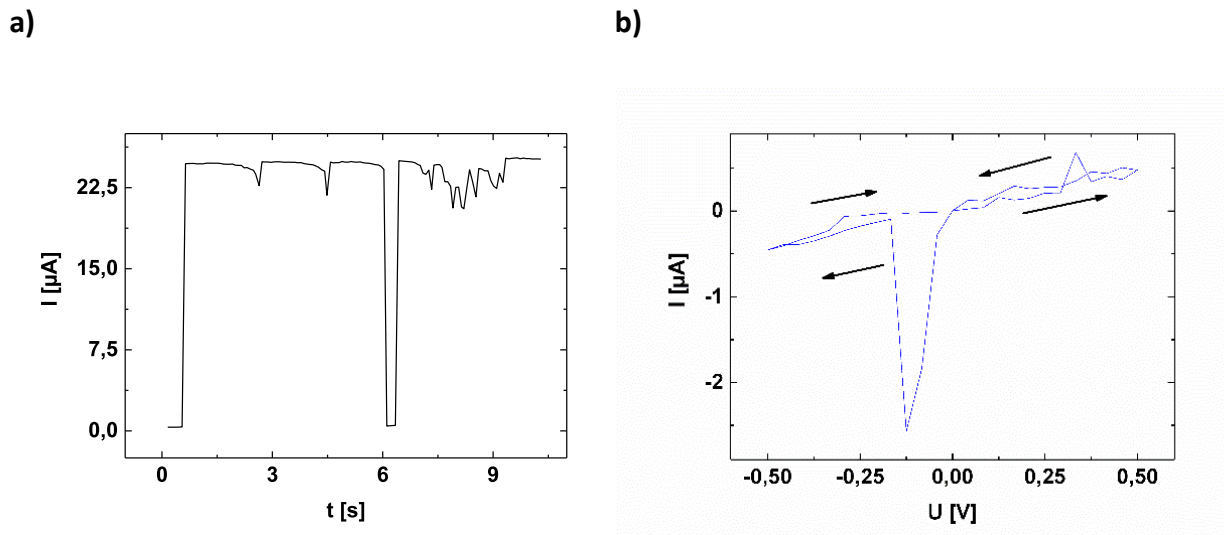

Figure 77: Measurement results for S 20, a) pulse measurement and b) hysteresis curve of S20 after applying the second voltage pulse (maximum voltage 0,5 V).

A further positive pulse results again in an ohmic behavior with the maximum current being in the 10^{-5} A regime. It seems that the prior (by cluster movement) disconnected areas need a longer pulse than 30 s to form some connections again.

Figure 79 shows the results for applying the sixth voltage pulse. The pulses applied between the results in Figure 79 and Figure 78 are alternating pulses showing no big influence on the sample. The shown current versus time graph for the pulse shows that the current fluctuates between 23,5 and 25,0 µA. The current increases over the course of the experiment slowly, showing two large drops down by 0,6 and by 1,5 µA, while the last one occurs more suddenly. These small drops and changes in the network system result again in a change in the hysteresis

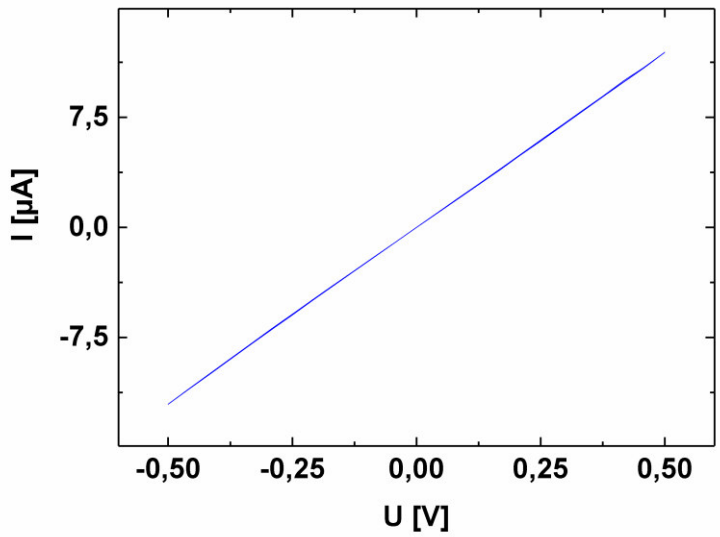

Figure 78: Hysteresis curve of S20 after applying the third voltage pulse (maximum voltage 0,5 V).

curve. The resulting curve does go through the origin but shows some broadening of the loop at the tip of the positive and across the negative quadrants, indicating that the drops in current from the pulse showing first influences on the hysteresis curve.

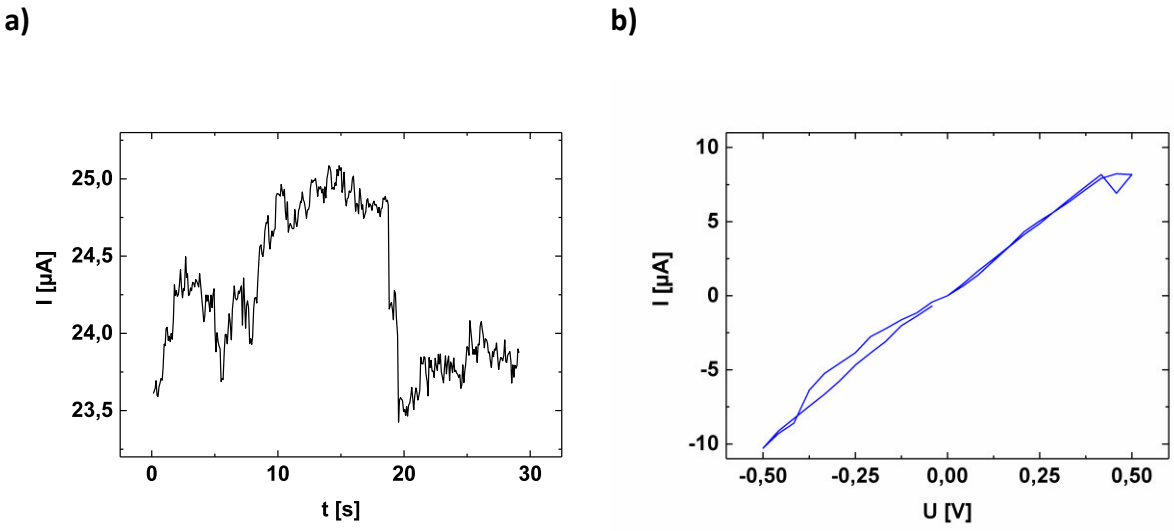

Figure 79: Measurement results for S 20 after applying five prior pulses, a) pulse measurement and b) hysteresis curve of S20 after applying the fifth voltage pulse (maximum voltage 0,5 V).

By applying a further +1 V and performing a subsequent hysteresis measurement are the results in Figure 80 obtained. The resulting current versus time curve shows again an increase in the current having sudden spikes after 7, 17 and 22 s resulting in an increase of around

4 µA. The most noticeable change in the curve appears after16,5 s. At this time a drop down to roughly zero ampere occurs. However, after this drop does the current increase back to its previous value and rises for 1 s even quicker than before. The reasoning behind this spike can be that a main path in the network is disrupted leading to a sudden drop in the conductivity but is immediately closed again due to the surrounding silver particles and the heavily increased electrical field. Again this change in the network can be found as well in the afterwards measured hysteresis. The resulting curve is displayed in Figure 80b showing a clearly asymmetric shape. The positive side of the hysteresis loop is broadly opened and shows a sudden snap back, similar to previously reported ones, on the way back to the origin. It is possible that this can be attributed again to the movement of slightly moveable CNT ends. Nevertheless the observable effect in this measurement is much lower than for the previous observed ones since the change in current is in the nA and not µA range. After a negative voltage is applied starts the curve to increase steadily indicating that an asymmetry in the system is present and therefore memristive switching might be possible. However, the current drops afterwards, again resulting in a linear behavior for the rest of the measurement. Since the system shows major switching, from the asymmetric curve in the virgin measurement to a linear one after applying several pulses and resulting again in an asymmetrical shape, are additional pulses applied to switch the sample further into other states.

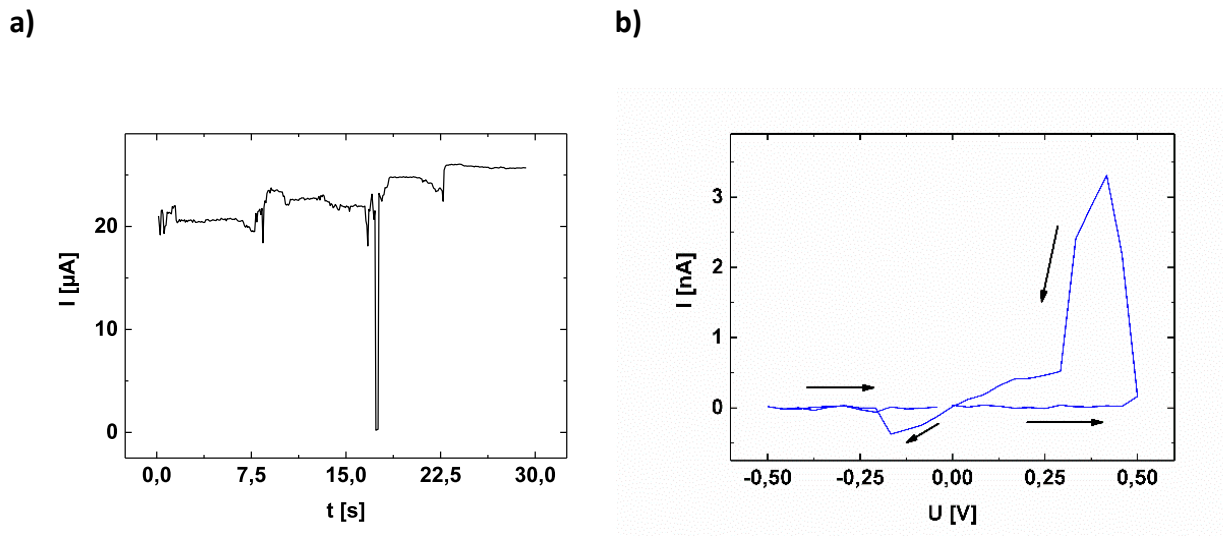

Figure 80: Measurement results for S 20 after applying six prior pulses, a) pulse measurement and b) hysteresis curve of S20 after applying the sixth voltage pulse (maximum voltage 0,5 V).

Since the broadest loop in Figure 80b is the positive one is the next applied pulse a negative one, since here a change should be the most pronounced. This pulse results again in a linear hysteresis curve (see Figure 81b) and a rise in the current back to the µA level. The prior generated current versus time curve from the negative pulse (see Figure 81a) shows that the current is very low in the beginning of the measurement and increases drastically close to 25 µA in roughly 2 s. This means that the connection in between the network, which is destroyed resulting in a hysteresis curve in the nA regime, is renewed or a connection with a similar conductivity is connected to the system since the current increases back to the µA level.

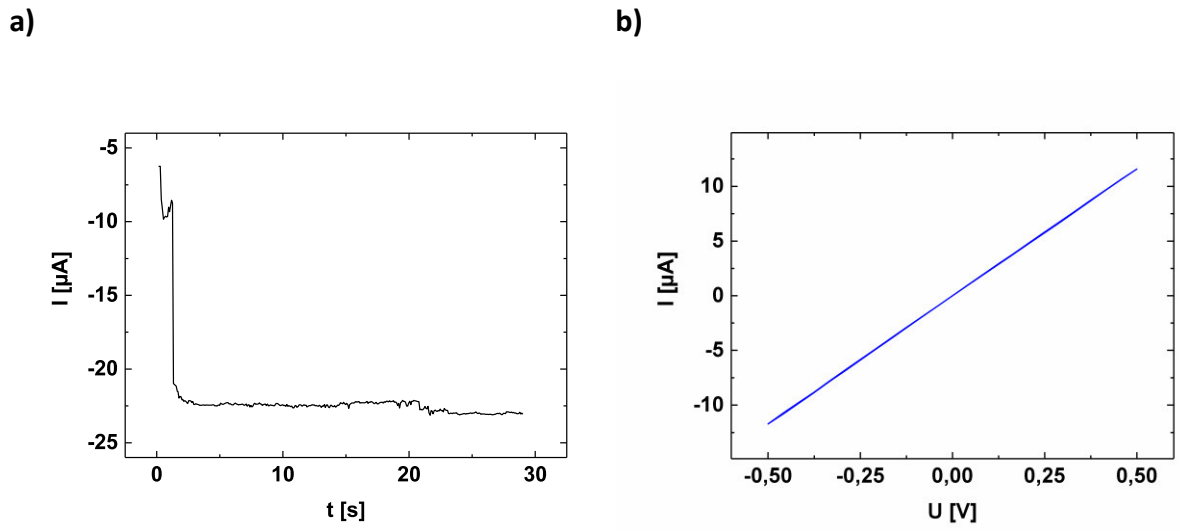

Figure 81: Measurement results for S 20 after applying seven prior pulses, a) pulse measurement and b) hysteresis curve of S20 after applying the seventh voltage pulse (maximum voltage 0,5 V).

Since the negative voltage pulse results in an ohmic behavior of the hysteresis curve are the next applied positive ones. The first one shows no big effect on the sample while the second one (see Figure 82b) leads again to an asymmetric result of the hysteresis curve. The current slowly increases for the hysteresis measurement and results in a major spike similar to the one of the original virgin curve. After reaching the maximum voltage applied does the current follow a different path on its way back, resulting in a good visible loop. The result for the negative quadrant is an ohmic line. The pulse measurement which leads to this hysteresis curve indicates as well that a significant change happens in the sample. Similar to all other measurements which lead to a drastic change in the hysteresis shape, does the pulse

measurement in Figure 82a show a major change in its conductivity, this time at the end of the measurement. The rest of the measurement behaves quite uncharacteristically since the measured current decreases instead of increasing over the course of the pulse. It goes down from 22 to around 15 µA with small steps until it drops down below 7 and increases right away again over a value of 26 µA. It appears that the use of different pulse directions results in a slow and steady decrease of the number of bridging connections formed by silver clusters, since the conductivity decreases with the time. This decrease hits a limit at the end of the measurement resulting in again in a rise. This is caused by formation of new connection paths in the other direction. It is unclear if these connections are formed at former connection paths or if only the formation of new connection paths results in the detected current increase.

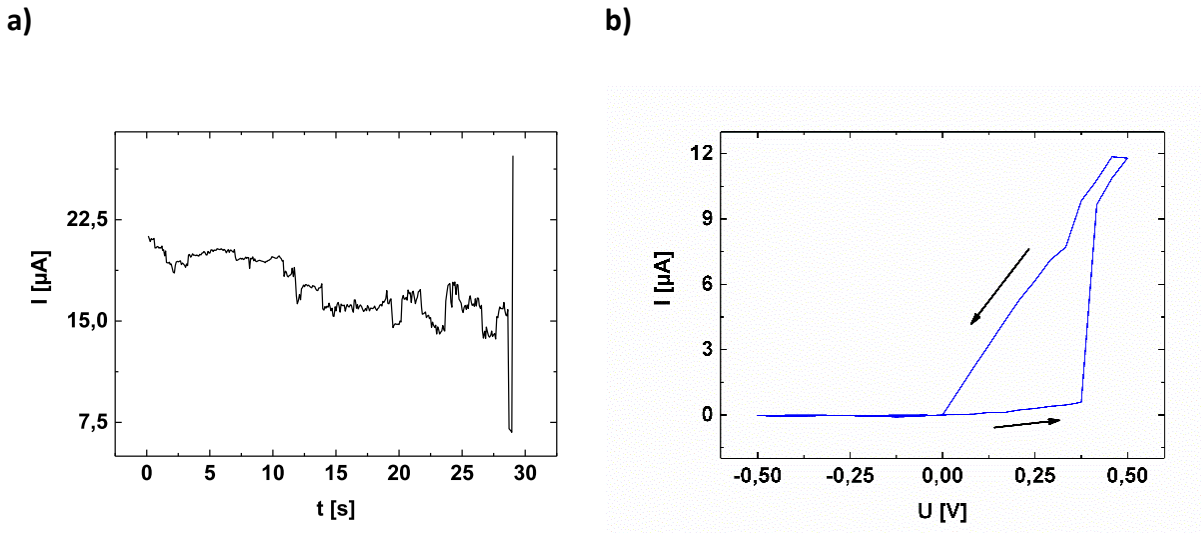

Figure 82: Measurement results for S 20 after applying nine prior pulses, a) pulse measurement and b) hysteresis curve of S20 after applying the ninth voltage pulse (maximum voltage 0,5 V).

Due to the detected spike and the large broadening of the curve is the voltage pulse applied next a negative one in order to widen up the negative quadrant again, whereas it needs two additional negative pulses to get the result shown in Figure 83. A sudden increase of the current can be seen after the first second of the experiment resulting in a change from nearly 0 to 23 µA. The remaining time in which the pulse is applied does the current stay on this level. The outcome of the hysteresis measurement is the one with the most pronounced differences for all of the reported ones so far. The current increases not only close to the end as it does for the virgin measurement and decreases afterwards, following a different slope, but also a change in the direction movement occurs when a negative voltage is applied. This indicates

that the sample possesses an asymmetric structure and therefore as well an asymmetric hysteresis behavior. The current only increases in the negative direction until a value of -0,2 V is reached. From here on it decreases until the set maximum voltage is applied. After this point it decreases and becomes more linear, but follows another path than before. In this state of the sample many of the small gaps between the nanotubes show an asymmetric distribution of the silver clusters, where the amount of clusters is higher at one side of the gap resulting in a difference in the outcome of the applied voltage direction. The differentiation of the system into a low-resistive and a high-resistive state are fundamentals for the classification of a memristive system for many others as well (*30, 103*).

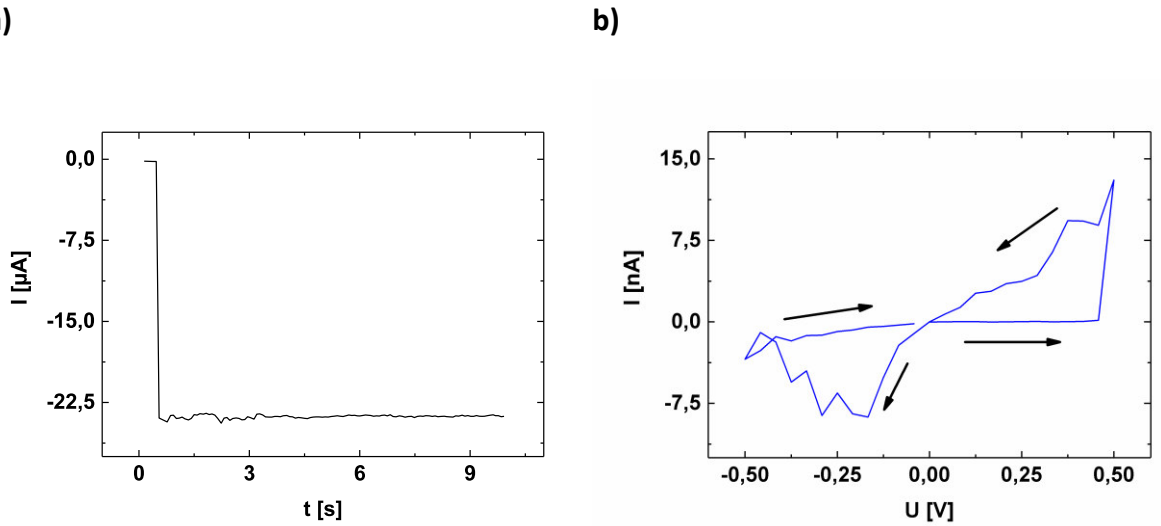

Figure 83: Measurement results for S 20 after applying twelve prior pulses, a) pulse measurement and b) hysteresis curve of S20 after applying the twelves voltage pulse (maximum voltage 0,5 V).

The application of an additional positive pulse leads to the results shown in Figure 84. From the pulse measurement it can be concluded that the applied voltage leads again to a drastic change in the system, leading to a jump in the current 1 s into the measurement from roughly 0 to 23 µA. This sudden increase in current remains to be the only one for this pulse measurement since it keeps fluctuating around the 23 µA mark. The outcome of the hysteresis measurement also shows a major change, which is recorded in the pulse measurement. The loop in the positive quadrant vanishes and becomes an ohmic line not differing in its forward or backward direction. The direction of the negative quadrant changes as well. In the prior conducted measurement the current increases quite quickly, leading to a reduction of the resistance, but after the positive pulse is applied does it hardly increase and only changes its

behavior after overcoming a threshold voltage. When the voltage is lowered again follows the current a different path back, while the shape of the negative loop changes stays the maximum current in the same regime.

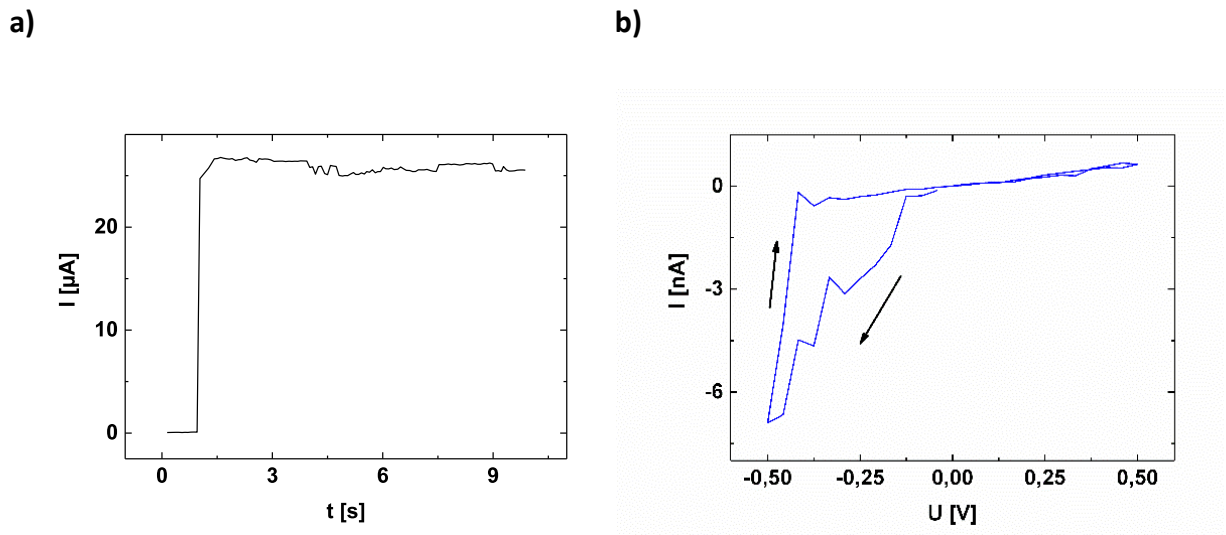

Figure 84: Measurement results for S 20 after applying thirteen prior pulses, a) pulse measurement and b) hysteresis curve of S20 after applying the thirteens voltage pulse (maximum voltage 0,5 V).

The application of an additional pulse leads to a further increase of the current close to 29 µA (see Figure 85a). The hysteresis measurement (see Figure 85b) shows that an even more drastic change takes place in the sample when the additional pulse is applied. Its result is a

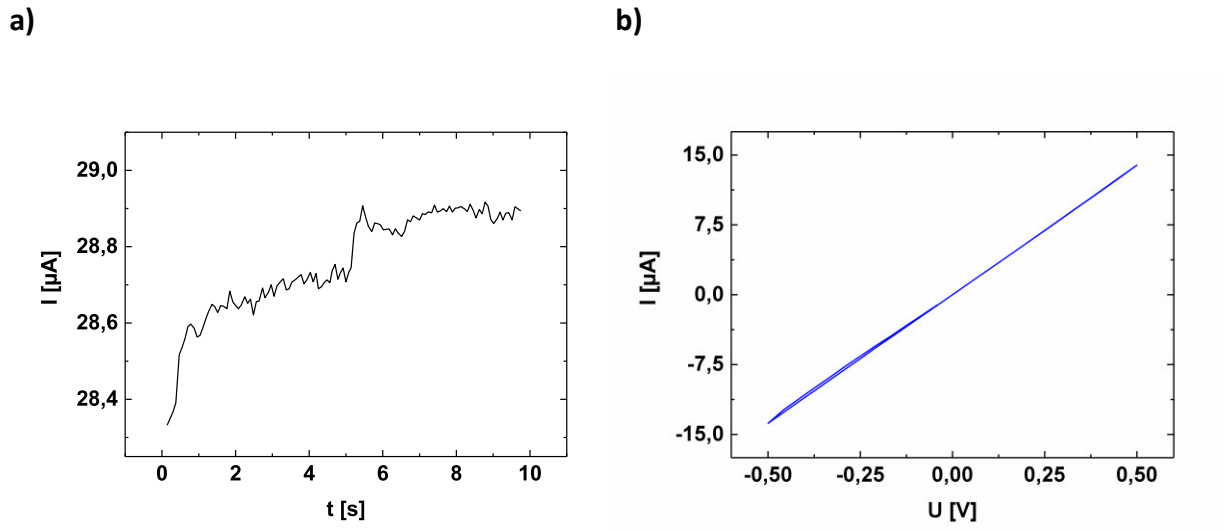

Figure 85: Measurement results for S 20 after applying fourteen prior pulses, a) pulse measurement and b) hysteresis curve of S20 after applying the fourteens voltage pulse (maximum voltage 0,5 V).

straight ohmic line with a maximum current of 15,0 µA. Additional pulses show no noticeable effect anymore on the sample, meaning that it stays in this ohmic state even after applying several additional pulses. The sample was left in a resting state for a few days and additional measurements were carried out resulting in the same behavior akin to the last presented curve here. With the usage of additional pulses and letting the sample rest it is attempted to switch the sample back into a memristive or non-linear state. But since it is not possible anymore to switch the sample it can be assumed that too many direct connections between the gaps are formed in the process or that the clusters moved again too far, respectively. Similar to it shown with the help of the simulation a direct connection leads to a sudden decrease of the electrical field meaning that the force which is the most probable drive behind the movement of the silver clusters being not present anymore.

In Figure 86 the results for a further experiment of the memristive system CNT + Ag + Au clusters is shown. The here shown sample S21 is produced with a slightly lower dispersion concentration (1:120000), while the Au clusters and CNTs are applied with the same methods as used for S20 are the silver clusters deposited for 115 s. By carrying out the same measurement routine as for S20 the results shown in Figure 86 are obtained. The result of the virgin measurement (see Figure 86a) shows that the initial shape of the curve for this sample is a linear one with a maximum current around 0,1 mA. By applying a positive voltage pulse it is possible to already change this linear shape (see Figure 86b). The direction of the current is indicated by the arrows, showing first a slow increase and a sudden jump in the end whereas it takes another path back leading to a widened hysteresis loop in the positive quadrant. The behavior in the negative regime on the other hand shows a more or less linear shape with some smaller irregularities. The maximum current is slightly higher in the positive quadrant and five to six times higher than in the initial measurement. These facts show that the field has a major influence on the way the Ag clusters are arranged in the system as well for this composition. In some areas this rearrangement of the clusters results in a strengthening of the existing connection path, which leads to the improvement of the conductivity, while in other areas does this rearrangement lead to a widening and an asymmetrical behavior of the curve. Further pulses resulted in a slimming and re-broadening of the positive loop. After six positive pulses are successively applied vanishes the loop in the positive quadrant completely

while in the negative quadrant a new loop is formed (see Figure 86c). The resulting curve is again asymmetric, but shows only one loop. It can be mentioned as well that the current maxima increases further over the course of the applied pulses and is in the end 20 times higher than for the virgin curve. The altering of the size of the loop, such as it is mentioned before for the positive quadrant, is possible as well for the negative quadrant by applying additional pulses. However in contrast to S20 it is not possible to switch sample S21 into a memristive state as shown in Figure 83 where the hysteresis curve shows two loops. Since it is still possible to switch the size of the loop and altering its position being in the positive or negative quadrant such as it was possible for S20 as well, but failing in achieving the memristive behavior, it can be assumed that this is caused

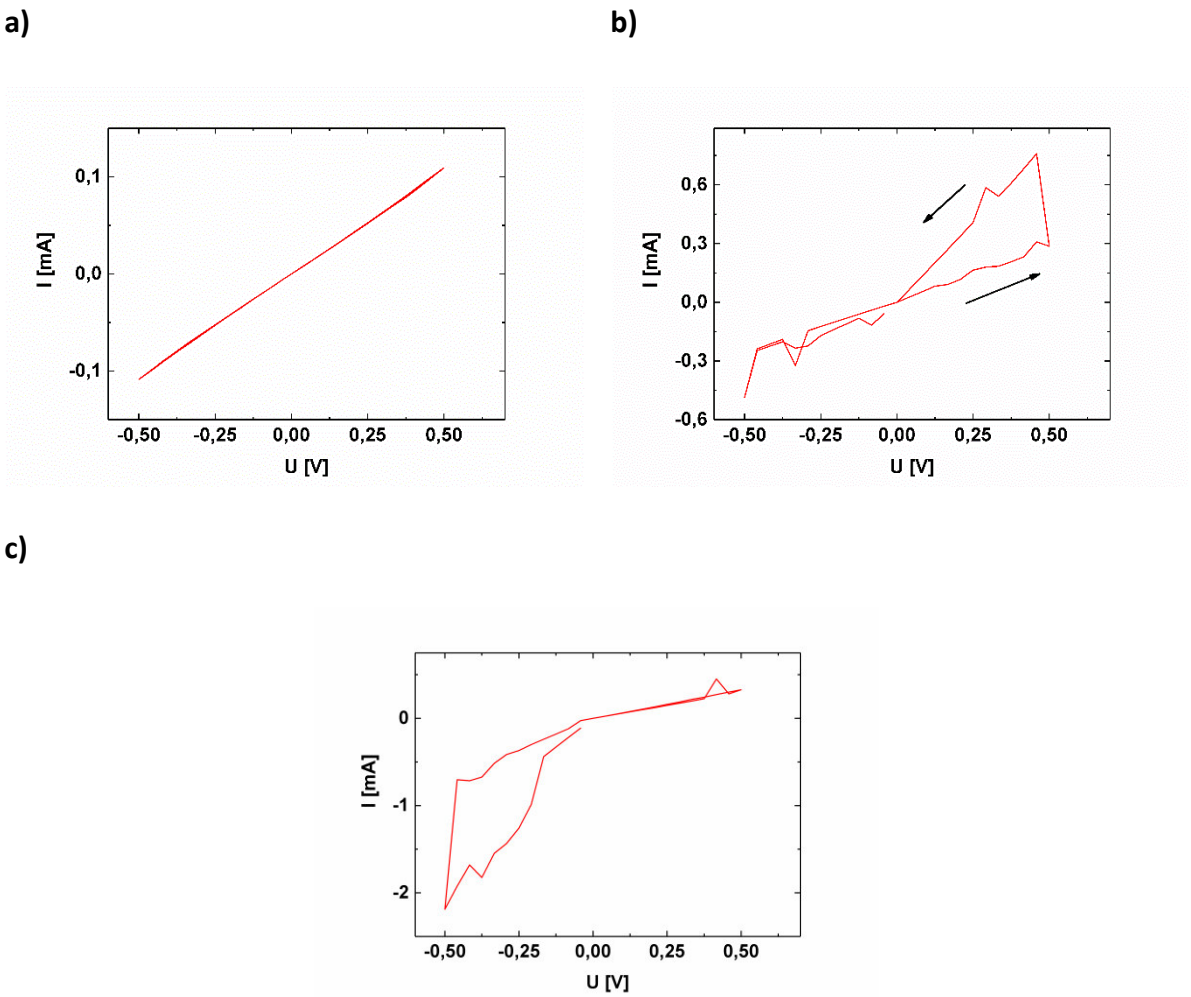

Figure 86: Hysteresis measurement results for S21 a) showing the virgin curve, b) after one pulse, c) after several pulses (all with maximum voltage of 0,5 V).

by the lower number of CNTs. Therefore, a lower number of nanotubes leads to a network with a lower number of connection possibilities. It can be assumed that for the presented system in S21 the amount of gaps in the sparse CNT network is too low for which reason not enough intermediate states are obtainable – which occur due to the movement of the silver particles by the applied field – for the system to reach a memristive state.

The conducted and here presented experiments show that it is possible to get a horizontal designed memristive device by adding carbon nanotubes between two gold electrodes, which have a spacing of 10 µm, and decorating it with Ag clusters as mobile species and Au clusters as further tuning. This switching behavior was first proofed to work by performing a Monte Carlo simulation, while the carried out experiments mirrored perfectly the behavior. Furthermore, the carried out experiments show that the memristive behavior for this new approach is can be sconsidered as a bipolar one which is indicated by the different behavior of the system depending on the direction of the applied voltage (*104*). While the switching properties of the system are still limited do different results obtained by slight variations of the system (amount of CNTs or clusters) indicate that there is still a lot of room for improvement of the switchability, showing the high potential of the demonstrated system.

5 Summary and Outlook

In this work two highly promising approaches for the fabrication of a horizontal memristive device were presented. The first and novel one utilizes self-grown iron oxide needles capable of gas sensing, being outstanding in their response time, with conclusive memristive behavior bearing the potential for both properties to be combined into a memsensor. The second and entirely new approach, on the basis of a simple microchip in combination with mobile and immobile noble metal clusters on a complex network of CNTs, showed already good and promising memristive hysteresis during the course of this thesis, building a good base for further researches.

The fabrication of the iron oxide devices is straight forward, since the modus operandi was inspired by prior works (*73, 74, 105*). The approach is based on the growth of iron needles from iron particles placed on silicon wafers with subsequent temperature treatment. The resulting needles have a maximum length of several µm and were transferred in between gold contacts via a complex FIB process. Experiments suggested sensing capabilities for NH_3, H_2, ethanol and acetone while showing the highest sensitivity for acetone. Furthermore, reaction times (8 s as gas response and 7 s as recovery time) are exceptionally quick compared to other metal oxide based publications (*70, 71*). Additionally, prolonged heat treatment of 24 h at 250 °C of the iron oxide results in needles showing memristive behavior, which can be attributed to the same mechanism as for titanium oxide memristors, i.e. the movement of oxygen vacancies (*10*) due to the porous surface of the needles (*76*).

Initial sample fabrication for the nanotube based approach was carried out by testing different kinds of CNT dispersions, with CarboBYK-9810 being the most promising candidate due to its easy handling and low amount of additives and impurities in contrast to other dispersions. Preliminary experiments show that the formation of an even sparse nanotube network is not achievable by simply drop coating and drying of the CNT dispersion. Several different deposition techniques were surveyed as well as the influence of further additions such as isopropanol to let the dispersion dry quicker due to its high vapor pressure. In addition the

droplet size was varied as well by the application of a perfume atomizer for spray deposition to achieve smaller droplets and therefore a reduced evaporation time. The outcome of these experiments are not sufficiently satisfying since they lead to stronger agglomeration behavior and coffee stain formations, as well as circular agglomerations of the deposited carbon nanotubes. The usage of different surface coatings of thin layers of AZO (Al doped ZnO), ZnO or Al_2O_3 does not lead to an improvement of these obstacles either. More promising results are achieved by increasing the substrate temperature up to 115 °C and modifying the surface by adding a monolayer of silane. Both result in a rise of the hydrophobicity of the samples surface, benefitting the application of nanotubes. By swiping a droplet of the CNT dispersion across the sample surface it is possible to get a more evenly distributed network for the outer gaps, but not the inner ones of the used chip structure. The lack of homogeneity is attributed to a direct deposition of the CNTs at the interface to the hot chips surface and a further resulting depletion zone of CNTs at the bottom side of the droplet al. (*86*)(*87*). Additional sweeping of the droplet over the surface results therefore in a lower deposition of CNTs since most of them are already deposited during the droplets first contact. Furthermore, it is possible to improve the homogeneity of all gaps across the whole sample by performing a dipping the dispersion on the hot sample surface for two seconds repeatedly instead of swiping it. The result is an evenly spread and sparse nanotube network over all gaps.

Additional experiments to improve the sparseness of the network were carried out by exposing it to different acids (HNO_3, $H2SO_4$) and by applying various voltage pulses of up to 150 V. Whereas the usage of acids occasionally results in the formation of unwanted crystal-like structures, result the high voltage pulses in a breakdown of the insulating layer rather than of the carbon nanotubes for voltages higher than 100 V.

The most reproducible approach with respect to the network is for this reason the application of the dispersion by dipping a droplet several times on a silanated and pre-tempered surface, making it the deposition method of choice.

The addition of silver clusters to the system from dispersion result in insufficient conductivity, while the results for the cluster sputter deposition show very promising results. It was possible to measure the change of the sample's resistivity in situ with a self-built setup during the sputtering process. This enables the determination of appropriate sputtering times without

the need of individually checking each sample after the respective deposition times. The measured sputter curves give good insight into the changes on the surface of the samples. The resulting sputter curves served as basis for following experiments. Over the course of this thesis the setup was further enhanced, i.e. by speeding up the measurement routine or allowing to measure with variable voltages, leading to an improvement of the measurements and making them more individually adjusted to each of the unique samples. This individuality is achieved by setting threshold resistances for each gap. As soon as enough gaps show a lower resistivity (due to cluster percolation) stops the measurement automatically, allowing the sample indirectly to determine the sputter time and therefore the amount of the deposited clusters.

The first samples examined show a high mobility of the particles, indicated by the fact that the current changes in the pulse measurements very abrupt. It can for this reason be concluded that the mobility of the silver particles over the chip surface is too high rather than too low, resulting in them moving too far and letting them get in contact with the CNTs. However, this leads to an immobilization of the silver clusters since they end up being on the same potential as the CNTs. To slow them down influence of base treatments were tested, but these lead to unwanted side reactions such as crystal formations.

Subsequent analysis reveal the need of an immobile sentinel for the silver clusters. It is noted that they drift too fast in the applied electrical field, which is indicated by the conducted electrical measurements. To overcome the immobilization of the clusters it was decided to add gold particles to the system. Gold possesses the advantage of being more resistant to the formation of ions than silver and being completely miscible with it making it an ideal sentinel for the mobile silver particles. Monte Carlo simulations prove that the addition of gold to the system leads to a more reliable memristive system and prevents the silver clusters from becoming immobile. This is achieved by the slowing down of the mobile clusters, hindering them from getting pinned to the CNTs. The addition of gold was accomplished initially by applying it via sputter deposition as AgAu alloy clusters. While in latter approaches the clusters were deposited either out of glucose stabilized dispersion or by using a deposition technique which employ micelles to arrange and stabilize the clusters.

For the sputter deposition of the alloy clusters a self-build target (consisting of silver with three incorporated gold wires) was used. However, experiments conducted with these clusters in this thesis mostly result in a purely ohmic behavior with little to no cluster movement. This behavior is mostly caused by an improper Ag/Au ratio, wrong size or density of the clusters. Even though various compositions and densities of clusters have been tested during the course of this thesis.

The application of gold clusters from dispersion leads to an improvement of the electrical behavior of the system. Still, the process is mainly dominated by ohmic behavior in the beginning. Nonetheless further results show that it is possible to alter the hysteresis curve to be slightly asymmetric by applying different electrical pulses with this approach. A reason why the approach of using the gold dispersion does not lead to a memristive sample might be that the number of gold clusters could have been too low in the respective gaps. It is possible that the Au clusters hindered the Ag clusters from forming too strong connections with the carbon nanotubes in first place, but are unable to promote this effect long enough as the sample is further stressed by the usage of additional pulses.

Using the approach by Kadem et al. to apply the gold clusters onto the sample by employing a micelle approach in order to fabricate ordered arrays of Au particles (*67*) leads to a working memristive device generally proving the high potential of this system. However, different results are achieved for this method, depending on the way the clusters are applied. Samples with a regular arrangement of clusters result again in ohmic voltage response, while samples with an irregular distribution of non-monodisperse gold clusters show the tendency to have an asymmetric I-V curve. Therefore it can be stated that not only an asymmetric contact is important to get a memristive device (*19*), but as well that it is crucial for the added sentinels (the gold clusters) to alter in their shape and distribution to result in a memristive behavior.

The successful fabrication of a first working memristive device shows the potential of the approach and leaves still much room for further improvements, for example the enhancement and determination of the optimal required conditions to fabricate a memristive device with improved repetition rate is part of future investigations. In addition, it should be possible to alter the mobility of the integrated silver not only by the addition of the gold clusters, as it is already shown in the course of this thesis, but also by changing the surface layer of the

substrate. Furthermore, this can also be achieved by applying a voltage to the backside of the sample itself, which results in a retardation of the movement of the silver depending on its strength. The investigation of other coatings and the usage of applied backside voltages or the combination of both provide an outstanding basis for additional studies.

In addition to the possible improvements mentioned, further fundamental investigations of memristive switching samples, i.e. by in situ TEM, are required. In particular, the information gained can lead to a better and deeper understanding of the release and transport of silver ions.

Following the experimental series of this thesis, additional experiments have been conducted in the scope of the project this thesis was carried out. These experiments focus again on the manipulation of the deposited carbon nanotube network. This time, the aim of the experiments is the removal of the surfactant, due to the assumption that this protects the CNTs from fusing at higher voltages. Therefore, resulting networks are treated with a mixture of diluted HCl and HNO_3 and only diluted HCl to remove the coating and subsequently investigated by applying voltages of 2 V.
Different concentrations and resting times were tested for these samples. Some selected results are presented in Figure 87. The results presented indicate that neither of the conducted acid experiments result in the formation of crystal like structures, which was one of the main problems in this thesis for the acid treatments. Moreover, the conducted acid treatments result in damaging of the gold contacts rather than helping to manipulate the network. Figure 87a shows the outcome of an acid treatment of 3M HCl overnight, followed by concentrated HNO_3 overnight and a voltage pulse of +2 V. The sample was carefully rinsed after each acid treatment in order to remove residuals. It can be seen, that the network stays intact even after application of the voltage, while the gold contact is removed. Only the edge of the contact remains while nearly 700 nm of the gold are etched away. At this point it was uncertain whether this is caused by the applied voltage pulse or the acid treatment. The experiment conducted with only HCl (shown in Figure 87b+c) reveal that not only the additional HNO_3 and pulse treatment results in the removal of the gold contact. The sample shown here was only exposed to 3M HCl overnight and shows also partial removal of the gold contact, already. The

a)

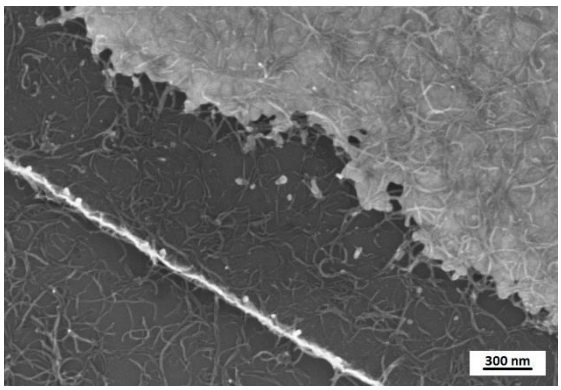

b)

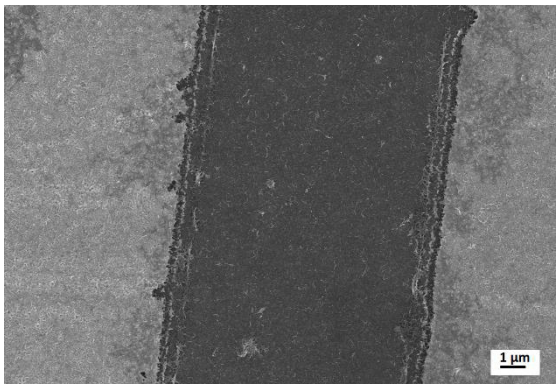

c)

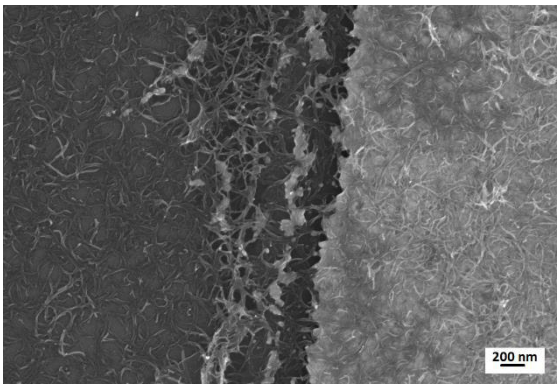

Figure 87: SEM results for acid treated samples a) after the sample was treated with 3M HCl overnight, with HNO3 for the same time and after a voltage pulse of 2 V was applied, b+c) after the sample was only treated with 3M HCl.

result of this treatment can be seen best in in the magnified view of Figure 87c and shows that the etching of the gold contact partly occurs here as well. However, it is not as distinctive as for the experiments with the additional HNO_3 and voltage treatments.

From these experiments and from the ones reported before it can be concluded, that any sort of acid treatment is not recommended for the manipulation of the nanotube network. The reason is that the gold contacts from the chip do not withstand any treatments like this. A further possibility to increase the stability of the gold contacts could be achieved by increasing their thickness since the gold cannot be attacked by the acids so easily anymore, due to a lowered volume to surface ratio. However, the thickness cannot be increased unlimitedly. For the reason that this would result in unwanted shadowing effects due to the increased edge height for the CNT and especially cluster deposition, since this process is not completely spotty.

In addition it can be concluded from the nanotube treatments reported in this thesis that it should be refrained from the further usage of surfactant coated CNTs. For the simple reason that in order to get an even more rigged network all voltage treated samples do not result in a fusing of the nanotubes, even though the binding energy of the carbon bonds they consist of is exceeded by a multiple. Due to the mentioned shielding effects it is advised use uncoated SWCNTs and MWCNTs since these bear the potential to become fused if a voltage is applied due to no present protective layer coatings.
It should be furthermore possible to increase the reproducibility and density of the generated CNT networks even further by trying additional surface coatings which show a self-assembling tendency of the nanotubes as it is reported by Choi et al. (*106*) and Kim et al. (*107*) for amine coated samples. Nevertheless, these amine coatings should be investigated with regard to their ability to retard the movement of the Ag clusters, since these might lead to a negative influence of the system. Furthermore, it has to be kept in mind that the nanotube arrangement should not follow a too repetitive pattern since the distribution of the gold clusters already indicated the need of a more random spreading to get a memrsitive response from the system.

Both of the devices analzyed in the scope of this thesis show promising results. The iron oxide based sensor shows compelling gas sensing capabilities, especially for acetone which detection rate is 5,2 times higher than for the second highest (ethanol with 24). In addition it displays substantial memristive switching repeatable over many sweeps, after being exposed to elevated temperatures long enough, showing that the properties can be simply altered by this treatment. Therefore the conducted measurements show convincingly that this device can - at least after further investigations - be enhanced to be later used as memristive sensor, like it is already shown for other nano needle based devices (*78*). Despite their large potential, these kind of devices hold the drawback of requiring challenging and time-consuming FIB fabrication for transporting and mounting of the needles. Furthermore, it is mandatory to repeat this step many times, to mount several needles to a single device to ensure sensing capabilities. In contrast, the CNT based device relies on facile fabrication steps which do not require time consuming complex tools, but instead can be scaled arbitrarily. Additionally the chosen design allows the fabrication of multiple devices at once in one single gap. This means that the design does not depend on a single needle, like it is the case for devices which are operating with nano needles, but instead bears the potential to bypass non-functional

sections of the network by a working one. The conducted experiments show that the setup of a CNT network decorated with silver particles as mobile species and gold as anchor points is capable of memristive switching. However, it is important to tune the repeatability for the switching behavior of this promising approach further in regards to build a more persistent memristive device. The sensing characteristic can then either be achieved by functionalization (*5*) or combination with additional metal oxides (*70, 71*), since these show sensoric properties in various approaches already. A combination of these two features would lead to the fabrication of a memsensor and therefore to an improvement of the level of safety, for example in the region of chemical storage.

In addition to this it is a good approach to increase the efficiency of a sensor by increasing its detection area. This has already been done partly for the nanotube system presented here, since the design is a horizontal one. Previously reported horizontal sensing systems are based on the usage of single (*78, 79*) or multiple (in this case 4) (*42*) nanowires (similar to the second presented device). A big advantage of the carbon based system shown here is that it consists of a high number of individual memristive systems. Accordingly, its detection rate exceeds the sensor systems reported thus far. In addition, the demonstrated approach contains an array of interconnected memristive devices on a very small area. Normally, this kind of interconnectivity needs a lot of additional components to connect several memristive devices, which increases the size of the unit. This high level of complexity can be realized here within just a single device.

Furthermore, it is possible to increase the complexity and detection capability of the nanotube with AgAu cluster system even further by going from a 2D to a 3D approach. This further tuning can be realized, for example, by infiltrating a CNT dispersion, which contains silver and gold cluster already into a cylindrical and highly porous system like it was done by Hansen et al. (*19*). Such systems bear the potential to result in a memristive switching sensor device with a 3D architecture and for this reason higher complexity than for present memristive systems reported thus far. However, a possible realization of such devices was not part of this thesis and is therefore element of further scientifically researches.

From the presented results and followed discussion can be concluded that the examined novel (iron oxide) and new (CNT and noble clusters) approaches show already promising memristive

and sensing behavior – with outstanding response times – and first memristive switching properties, respectively. Whereby the metal oxide device marks (to the knowledge of the author) the first memsensor based on iron oxide needles. Furthermore the carried out discussion reveals auspicious ways of tuning for both devices not only showing that they can expand the so far existing detection range for memsensors, but also be employed in areas like solvent cabinets to ensure a way higher level of security.

Acknowledgements

First of all I would like to thank Prof. Rainer Adelung for giving me the opportunity to be part of his group, to write this thesis and his support. I would like to thank as well the whole FuN group for the time we spent together and all the assistance I received from you guys. Especially I would like to express my gratitude to Dr. Jürgen Carstensen for always helping and discussing my experimental results with me and being a helpful guidance. Same goes for Dr. Sören Kaps who not only always had an open ear and good advices for me, but as well for building up the in situ measurement setups used in this thesis from scratch.

I would like to thank the members of the groups of Prof. Kienle, Prof. Quandt, Prof. Kohlstedt and Prof. Selhuber-Unkel (additionally for helping me with the fabrication of some samples) for always helping and supporting me when I needed smaller or bigger assistance.

Especially I would like to thank Prof. Faupel and his group and in particular Alexander Vahl for assisting me with my experiments and giving me the possibility to use their measurement setups and sputter chamber.

Thank you as well to all member of FOR2093 and as well Dr. Oleg Lupan for the collaboration.

A special thanks goes as well to my HiWi, bachelor and master students: Jonas Drewes, Lea Jessen and Heather Cavers for helping me during my experimental phase, the writing process and all the fun we had in the lab.

I would like to thank as well Sven (Dirk) Dirkmann not only for performing the Monte Carlo simulations for this thesis, but for being always helpful and for becoming a friend of mine.

Big thank you goes as well to my old flatmates from our big six person office with which I spent most of my days and with whom I found very close friends. Furthermore I would like to thank all my friends in and outside of our faculty for their scientifically and especially personal support during the years. You guys really helped me a lot during tough times.

Last but not least I would like to express my greatest gratitude to my cousin, sister, mother and father for always being there in my life, for supporting me in every condition of it and giving me the opportunity to study and to write this thesis in the end.

This thesis is dedicated to all the folks who helped and supported me during all my life without all these friends and colleagues it would not have been possible to finish this work.

Thank you.

Eidesstattliche Erklärung

Hiermit erkläre ich:

Diese Dissertation mit dem Titel "**Development of horizontal memristive devices and their potential application as memsensors**" habe ich noch nie, weder ganz noch teilweise im Rahmen eines anderen Promotionsverfahrens vorgelegt oder veröffentlicht. Ich habe mich bislang noch keiner mündlichen Prüfung im Rahmen eines Promotionsverfahrens unterzogen. Die vorliegende Arbeit habe ich ohne unzulässige Hilfe Dritter und ohne Benutzung anderer als der angegebenen Hilfsmittel angefertigt; die aus fremden Quellen direkt oder indirekt übernommenen Gedanken sind als solche kenntlich gemacht. Die Arbeit ist unter Einhaltung der Regeln guter wissenschaftlicher Praxis der Deutschen Forschungsgemeinschaft entstanden. Insbesondere habe ich nicht die Hilfe eines Promotionsberaters in Anspruch genommen. Dritte haben von mir weder unmittelbar noch mittelbar geldwerte Leistungen für Arbeiten erhalten, die im Zusammenhang mit dem Inhalt der vorgelegten Dissertation stehen.

ORT, DATUM UNTERSCHRIFT

Parts of this here presented work were previously published in the following publications:

Publications

1. S. Hansen, F. Schütt, J. Carstensen, V. Kaidas, R. Adelung, On the mechanisms for resistive switching at local point contacts for 3D Si-nano-architectures, submitted in ACS Nano (Forthcoming, 2017).
2. O. Lupan, V. Postica, N. Wolff, O. Polonskyi, V. Duppel, V. Kaidas, E. Lazari, N. Ababii, F. Faupel, L. Kienle, and R. Adelung, Localized Synthesis of Iron Oxide Nanowires and Fabrication of High Performance Nanosensors Based on a Single Fe2 O3 Nanowire, *Small (Weinheim an der Bergstrasse, Germany)* (2017), doi:10.1002/smll.201602868.

(further publications)

3. J. Gröttrup , I. Paulowicz, A. Schuchardt, V. Kaidas, S. Kaps, O. Lupan, R. Adelung, Y. K. Mishra, Three-dimensional flexible ceramics based on interconnected network of highly porous pure and metal alloyed ZnO tetrapods, *Ceramics International*. **42**, 8664–8676 (2016), doi:10.1016/j.ceramint.2016.02.099.
4. O. Lupan, V. Cretu, V. Postica, N. Ababii, O. Polonskyi, V. Kaidas, F. Schütt, Y. K. Mishra, E. Monaico, I. Tiginyanu, V. Sontea, T. Strunskua, F. Faupel, R. Adelung, Enhanced ethanol vapour sensing performances of copper oxide nanocrystals with mixed phases, *Sensors and Actuators B: Chemical*. **224**, 434–448 (2016), doi:10.1016/j.snb.2015.10.042.
5. O. Lupan, V. Cretub, V. Postica, O. Polonskyi, N. Ababii, F. Schütt, V. Kaidas, F. Faupel, R. Adelung, Non-planar nanoscale p – p heterojunctions formation in Zn x Cu 1−x O y nanocrystals by mixed phases for enhanced sensors, *Sensors and Actuators B: Chemical*. **230**, 832–843 (2016), doi:10.1016/j.snb.2016.02.089.
6. V. Postica, I. Hölken, V. Schneider, V. Kaidas, O. Polonskyi, V. Cretu, I. Tiginyanu, F. Faupel, R. Adelung, O. Lupan, Multifunctional device based on ZnO, *Materials Science in Semiconductor Processing*. **49**, 20–33 (2016), doi:10.1016/j.mssp.2016.03.024.
7. J. Gröttrup, V. Postica, D. Smazna, M. Hoppe, V. Kaidas, Y.K. Mishra, O. Lupan, R. Adelung, UV detection properties of hybrid ZnO tetrapod 3-D networks, *Vacuum*. 1-9 (2017, In Press), doi:10.1016/j.vacuum.2017.03.017.
8. V. Postica, T. Reimer, E. Lazari, N. Ababii, S. Shishiyanu, S. Railean, V. Kaidas, S. Kaps, O, Lupan, W. Benecke, R. Adelung, Sensing Properties of Ultra-Thin TiO2 Nanostructured Films Based Sensors. 3rd International Conference on Nanotechnologies and Biomedical Engineering: ICNBME-2015, September 23-26, 2015, Chisinau, Republic of Moldova. Vol. 55. Springer, 2015.
9. S. Wille, P. Zumstrull, V. Kaidas, L. K. Jessen, M, Kern, Low temperature degradation of single layers of multilayered zirconia in comparison to conventional unshaded zirconia: phase transformation and flexural strength, Journal of the Mechanical Behavior of Biomedical Materials (2017, In Press).

Curriculum Vitae

Personal

Name: Eric, Alexander, Victor, Petar Kaidas

Adress: Schauenburgerstraße 74, 24118 Kiel

Date / Place of Birth: 23/06/1987 in Lüneburg

Nationality: German

Parents: Carmen Kaidas and Horst-Peter Richter-Kaidas

University Education

10/2006–10/2010

Study of Bachelor Course of Materials Science at the Kiel University (Germany), thesis topic: "Untersuchung des Einflusses einer Co-Evaporation von Edelmetallen auf das Wachsumsverhalten von TeTraCain-HCl und Indometacin auf verschiedenen Substraten"

number of semester: 8

10/2010–05/2013

Study of Master Course of Materials Science at the Kiel University (Germany)

number of semester: 3,5

Master Thesis: "Development of Ni-based metallic glassed for high-strength applications" at Chair of Metal Physics and Technology, ETH, Switzerland (Prof. Löffler)

number of semester: 1,5

01/2014 – present

PhD. student / research scientist of Prof. Dr. Rainer Adelung (FUN) at the Kiel University, CAU, Germany, thesis topic: "Development of horizontal memristive devices and their potential application as memsensors"

List of Figures

List of Tables

References

1. U. Cvelbar, K. Ostrikov, A. Drenik, M. Mozetic, Nanowire sensor response to reactive gas environment, *Appl. Phys. Lett.* **92**, 133505 (2008), doi:10.1063/1.2905265.
2. Q. Wan *et al.,* Fabrication and ethanol sensing characteristics of ZnO nanowire gas sensors, *Appl. Phys. Lett.* **84**, 3654–3656 (2004), doi:10.1063/1.1738932.
3. F. Yang, D. K. Taggart, R. M. Penner, Joule heating a palladium nanowire sensor for accelerated response and recovery to hydrogen gas, *Small (Weinheim an der Bergstrasse, Germany)*. **6**, 1422–1429 (2010), doi:10.1002/smll.201000145.
4. O. Lupan, Single and networked CuO nanowires for highly sensitive p-type semiconductor gas sensor applications, *Phys. Status Solidi RRL*. **10**, 260–266 (2016), doi:10.1002/pssr.201510414.
5. A. Kolmakov, D. O. Klenov, Y. Lilach, S. Stemmer, M. Moskovits, Enhanced gas sensing by individual SnO2 nanowires and nanobelts functionalized with Pd catalyst particles, *Nano letters*. **5**, 667–673 (2005), doi:10.1021/nl050082v.
6. L. O. Chua, Memristor-The missing circuit element, *IEEE Trans. Circuit Theory*. **18**, 507–519 (1971), doi:10.1109/TCT.1971.1083337.
7. D. B. Strukov, G. S. Snider, D. R. Stewart, R. S. Williams, The missing memristor found, *Nature*. **453**, 80–83 (2008), doi:10.1038/nature06932.
8. T. Driscoll, Phase-transition driven memristive system, *Appl. Phys. Lett.* **95**, 43503 (2009), doi:10.1063/1.3187531.
9. S. Kaeriyama *et al.,* A nonvolatile programmable solid-electrolyte nanometer switch, *IEEE J. Solid-State Circuits*. **40**, 168–176 (2005), doi:10.1109/JSSC.2004.837244.
10. A. H. Edwards *et al.,* Reconfigurable Memristive Device Technologies, *Proc. IEEE*. **103**, 1004–1033 (2015), doi:10.1109/JPROC.2015.2441752.
11. F. Puppo, Memristor-Based Devices for Sensing, *Proceedings of the IEEE International Symposium on Circuits and Systems (ISCAS),*, 2257–2260 (2014), doi:10.1109/ISCAS.2014.6865620.
12. F. Puppo, M. Di Ventra, G. de Micheli, S. Carrara, Memristive sensors for pH measure in dry conditions, *Surface Science*. **624**, 76–79 (2014), doi:10.1016/j.susc.2014.01.016.
13. O. A. Olumodeji, Behavioural Modelling of Memristive Devices Targeted to Sensor Interfaces, *AISEM Annual Conference, 2015 XVIII*, 4 (2015), doi:10.1109/AISEM.2015.7066780.
14. Y. Massoud, A Memristor-Based Random Modulator for Compressive Sensing Systems, *Circuits and Systems (ISCAS), 2012 IEEE International Symposium*, 4 (2012), doi:10.1109/ISCAS.2012.6271793.
15. S. Vaidyanathan, C. Volos, Eds., *Advances in memristors, memristive devices and systems* (Springer, Cham, 2017).

16. J. Song, Y. Zhang, C. Xu, W. Wu, Z. L. Wang, Polar charges induced electric hysteresis of ZnO nano/microwire for fast data storage, *Nano letters*. **11**, 2829–2834 (2011), doi:10.1021/nl2011966.
17. T. Chang *et al.,* Synaptic behaviors and modeling of a metal oxide memristive device, *Appl. Phys. A*. **102**, 857–863 (2011), doi:10.1007/s00339-011-6296-1.
18. S. H. Jo *et al.,* Nanoscale memristor device as synapse in neuromorphic systems, *Nano letters*. **10**, 1297–1301 (2010), doi:10.1021/nl904092h.
19. S. Hansen, On the mechanisms for resistive switching at local point contacts for 3D Sinano-architectures, *ACS nano* (Forthcoming, 2017).
20. L. O. Chua, Memristive Devices and Systems, *Proceedings of the IEEE*. **64**, 209–223 (1976), doi:10.1109/PROC.1976.10092.
21. L. O. Chua, If it's pinched it's a memristor, *Semiconductor Science and Technology*. **29**, 104001 (2014).
22. L. O. Chua, Resistance switching memories are memristors, *Appl. Phys. A*. **102**, 765–783 (2011), doi:10.1007/s00339-011-6264-9.
23. G. Snider, *Molecular-junction-nanowire-crossbar-based neural network* (Google Patents, 2008) (available at https://www.google.ch/patents/US7359888).
24. X. Wang, Spintronic Memristor Through Spin-Torque-Induced Magnetization Motion, *IEEE Electron Device Lett.* **30**, 294–297 (2009), doi:10.1109/LED.2008.2012270.
25. H. Li, Memristive behaviors of LiNbO3 ferroelectric diodes, *Appl. Phys. Lett.* **97**, 12902 (2010), doi:10.1063/1.3462067.
26. D. J. Kim, Ferroelectric tunnel memristor, *Nano letters*. **12**, 5697–5702 (2012), doi:10.1021/nl302912t.
27. Y. Yang, Observation of conducting filament growth in nanoscale resistive memories, *Nature communications*. **3**, 732 (2012), doi:10.1038/ncomms1737.
28. J. J. Yang, Memristive devices for computing, *Nature nanotechnology*. **8**, 13–24 (2013), doi:10.1038/nnano.2012.240.
29. P. R. Mickel, Isothermal switching and detailed filament evolution in memristive systems, *Advanced materials (Deerfield Beach, Fla.)*. **26**, 4486–4490 (2014), doi:10.1002/adma.201306182.
30. Y.-C. Chen, Nonvolatile bio-memristor fabricated with egg albumen film, *Scientific reports*. **5**, 10022 (2015), doi:10.1038/srep10022.
31. E. Gale, A. Adamatzky, B. de Lacy Costello, Slime Mould Memristors, *BioNanoSci.* **5**, 1–8 (2015), doi:10.1007/s12668-014-0156-3.
32. V. Erokhin, Bio-inspired adaptive networks based on organic memristors, *Nano Communication Networks*. **1**, 108–117 (2010), doi:10.1016/j.nancom.2010.05.002.

33. Y. Lei, Memristive learning and memory functions in polyvinyl alcohol polymer memristors, *AIP Advances*. **4**, 77105 (2014), doi:10.1063/1.4887010.
34. A. Radoi, Memristor device based on carbon nanotubes decorated with gold nanoislands, *Appl. Phys. Lett.* **99**, 93102 (2011), doi:10.1063/1.3633352.
35. O. A. Ageev, Memristor effect on bundles of vertically aligned carbon nanotubes tested by scanning tunnel microscopy, *Tech. Phys.* **58**, 1831–1836 (2013), doi:10.1134/S1063784213120025.
36. M. V. Ilina, Resistive switching of vertically aligned carbon nanotube by a compressive strain, *Proc. SPIE*. **10224** (2016), doi:10.1117/12.2266762.
37. B. Zhao, Architecting a Common-Source-Line Array for Bipolar Non-Volatile Memory Devices, *Design, Automation & Test in Europe Conference & Exhibition (DATE)*, 1451–1454 (2012), doi:10.1109/DATE.2012.6176594.
38. C. Zamarreno-Ramos *et al.,* On spike-timing-dependent-plasticity, memristive devices, and building a self-learning visual cortex, *Frontiers in neuroscience*. **5**, 26 (2011), doi:10.3389/fnins.2011.00026.
39. Y. V. Pershin, M. Di Ventra, Experimental demonstration of associative memory with memristive neural networks, *Neural networks : the official journal of the International Neural Network Society*. **23**, 881–886 (2010), doi:10.1016/j.neunet.2010.05.001.
40. *IEEE International Symposium on Circuits and Systems (ISCAS), 2014*, *1 - 5 June 2014, Melbourne, Australia* (IEEE, Piscataway, NJ, 2014).
41. G. de Micheli, *Proceedings of the Conference on Design, Automation and Test in Europe* (European Design and Automation Association, 3001 Leuven, Belgium, 2010).
42. F. Puppo, M. Di Ventra, G. de Micheli, S. Carrara, Memristive sensors for pH measure in dry conditions, *Surface Science*. **624**, 76–79 (2014), doi:10.1016/j.susc.2014.01.016.
43. H. Göbel, *Einführung in die Halbleiter-Schaltungstechnik* (Springer Vieweg, ed. 5, 2014).
44. B. Wu, A. Kumar, Extreme ultraviolet lithography, *J. Vac. Sci. Technol. B*. **25**, 1743 (2007), doi:10.1116/1.2794048.
45. L. Chrisey, Covalent attachment of synthetic DNA to self-assembled monolayer films, *Nucleic Acids Research*. **24**, 3031–3039 (1996), doi:10.1093/nar/24.15.3031.
46. M. Sasou, S. Sugiyama, T. Yoshino, T. Ohtani, Molecular Flat Mica Surface Silanized with Methyltrimethoxysilane for Fixing and Straightening DNA, *Langmuir*. **19**, 9845–9849 (2003), doi:10.1021/la035054b.
47. J. H. Clark, Catalysis of liquid phase organic reactions using chemically modified mesoporous inorganic solids, *Chemical Communication*, 853–860 (1998), doi:10.1039/A709143E.
48. J. Blümel, Reactions of Ethoxysilanes with Silica: A Solid-state NMR Study, *Journal of the American Chemical Society*. **117**, 2112–2113 (1995), doi:10.1021/ja00112a033.

49. D. W. Sindorf, Solid-state NMR Studies of the Reactions of Silica Surfaces with Polyfunctional Chloromethylsilanes and Ethoxymethylsilanes, *Journal of the American Chemical Society*. **105**, 3767–3776 (1983), doi:10.1021/ja00350a003.
50. H. Haberland, M. Karrais, M. Mall, Y. Thurner, Thin films from energetic cluster impact, *Journal of Vacuum Science & Technology A: Vacuum, Surfaces, and Films*. **10**, 3266–3271 (1992), doi:10.1116/1.577853.
51. D. Smith, *Thin-Film Deposition*, *Principles and Practice* (McGraw Hill Professional, 1995).
52. G. Medeiros-Ribeiro *et al.,* Lognormal switching times for titanium dioxide bipolar memristors: origin and resolution, *Nanotechnology*. **22**, 95702 (2011), doi:10.1088/0957-4484/22/9/095702.
53. R. L. Vander Wal, G. M. Berger, T. M. Ticich, Carbon nanotube synthesis in a flame using laser ablation for in situ catalyst generation, *Applied Physics A: Materials Science & Processing*. **77**, 885–889 (2003), doi:10.1007/s00339-003-2196-3.
54. M. Kusaba, Y. Tsunawaki, Production of single-wall carbon nanotubes by a XeCl excimer laser ablation, *Thin Solid Films*. **506-507**, 255–258 (2006), doi:10.1016/j.tsf.2005.08.037.
55. C. E. Baddour, A simple thermal CVD method for carbon nanotube synthesis on stainless steel 304 without the addition of an external catalyst, *Carbon*. **47**, 313–318 (2009), doi:10.1016/j.carbon.2008.10.038.
56. S. Zhu, C.-H. Su, S. L. Lehoczky, I. Muntele, D. Ila, Carbon nanotube growth on carbon fibers, *Diamond and Related Materials*. **12**, 1825–1828 (2003), doi:10.1016/S0925-9635(03)00205-X.
57. P. R. Bandaru, Electrical Properties and Applications of Carbon Nanotube Structures, *J. Nanosci. Nanotech.* **7**, 1239–1267 (2007), doi:10.1166/jnn.2007.307.
58. J. Y. Rho, Young's modulus of trabecular and cortical bone material: ultrasonic and microtensile measurements, *Journal of Biomechanics*. **26**, 111–119 (1993), doi:10.1016/0021-9290(93)90042-D.
59. S. Subramoney, Science of fullerenes and carbon nanotubes. By M. S. Dresselhaus, G. Dresselhaus, and P. C. Eklund, XVIII, 965 pp., Academic press, San Diego, CA 1996, hardcover, ISBN 012-221820-5, *Adv. Mater.* **9**, 1193 (1997), doi:10.1002/adma.19970091518.
60. A. Thess, Crystalline Ropes of Metallic Carbon Nanotubes, *Science*. **273**, 483–487 (1996), doi:10.1126/science.273.5274.483.
61. E. Fuchs, *Particle Beam Microanalysis Fundamentals, Methods and Applications* (Wiley-VCH, ed. 1, 1990).
62. P. J. Goodhew, *Electron Microscopy and Analysis*, *Third Edition* (Crc Press, ed. 3, 2000).
63. R. Schlögl, *Particle Beam Microanalysis. Fundamentals, Methods and Applications* (WILEY-VCH Verlag GmbH, 1992).

64. D. B. Williams, *Transmission Electron Microscopy*, *A Textbook for Materials Science* (Springer, ed. 2, 2009).
65. Merck, Technical Data Sheet (AZ 5214 E Photoresist), *Merck Performance Materials GmbH*.
66. A. Slistan-Grijalva *et al.,* Assessment of growth of silver nanoparticles synthesized from an ethylene glycol–silver nitrate–polyvinylpyrrolidone solution, *Physica E: Low-dimensional Systems and Nanostructures*. **25**, 438–448 (2005), doi:10.1016/j.physe.2004.07.010.
67. L. F. Kadem, C. Lamprecht, J. Purtov, C. Selhuber-Unkel, Controlled Self-Assembly of Hexagonal Nanoparticle Patterns on Nanotopographies, *Langmuir : the ACS journal of surfaces and colloids*. **31**, 9261–9265 (2015), doi:10.1021/acs.langmuir.5b02168.
68. O. Lupan *et al.,* Localized Synthesis of Iron Oxide Nanowires and Fabrication of High Performance Nanosensors Based on a Single Fe2 O3 Nanowire, *Small (Weinheim an der Bergstrasse, Germany)*. **13** (2017), doi:10.1002/smll.201602868.
69. V. Cretu *et al.,* Synthesis, characterization and DFT studies of zinc-doped copper oxide nanocrystals for gas sensing applications, *J. Mater. Chem. A*. **4**, 6527–6539 (2016), doi:10.1039/C6TA01355D.
70. J. P. Cheng, B. B. Wang, M. G. Zhao, F. Liu, X. B. Zhang, Nickel-doped tin oxide hollow nanofibers prepared by electrospinning for acetone sensing, *Sensors and Actuators B: Chemical*. **190**, 78–85 (2014), doi:10.1016/j.snb.2013.08.098.
71. X. Zhou *et al.,* Nanosheet-assembled ZnFe2O4 hollow microspheres for high-sensitive acetone sensor, *ACS applied materials & interfaces*. **7**, 15414–15421 (2015), doi:10.1021/acsami.5b03537.
72. L. Chow, O. Lupan, H. Heinrich, G. Chai, Self-assembly of densely packed and aligned bilayer ZnO nanorod arrays, *Appl. Phys. Lett.* **94**, 163105 (2009), doi:10.1063/1.3118583.
73. O. Lupan *et al.,* Influence of CuO nanostructures morphology on hydrogen gas sensing performances, *Microelectronic Engineering*. **164**, 63–70 (2016), doi:10.1016/j.mee.2016.07.008.
74. O. Lupan *et al.,* Silver-doped zinc oxide single nanowire multifunctional nanosensor with a significant enhancement in response, *Sensors and Actuators B: Chemical*. **223**, 893–903 (2016), doi:10.1016/j.snb.2015.10.002.
75. J.-D. Kim *et al.,* Investigation of analog memristive switching of iron oxide nanoparticle assembly between Pt electrodes, *Journal of Applied Physics*. **114**, 224505 (2013), doi:10.1063/1.4846759.
76. J.-D. Kim *et al.,* Resistive Switching of Iron Oxide Nanoparticles in Patterned Array Structure on Flexible Substrate, *ECS Transactions*. **50**, 27–31 (2013), doi:10.1149/05004.0027ecst.
77. E. Gale, TiO 2 -based memristors and ReRAM, *Semicond. Sci. Technol.* **29**, 104004 (2014), doi:10.1088/0268-1242/29/10/104004.
78. S. Carrara *et al.,* Memristive-biosensors, *Sensors and Actuators B: Chemical*. **171-172**, 449–457 (2012), doi:10.1016/j.snb.2012.04.089.

79. D. Sacchetto, M.-A. Doucey, G. de Micheli, Y. Leblebici, S. Carrara, New Insight on Bio-sensing by Nano-fabricated Memristors, *BioNanoSci.* **1**, 1–3 (2011), doi:10.1007/s12668-011-0002-9.
80. J. Smits, Controlled Deposition and Applied Field Alignment of Single Walled Carbon Nanotubes for CNT Device Fabrication, *Mat. Res. Soc. Symp. Proc.* **739** (2003), doi:10.1557/PROC-739-H7.11.
81. D.-m. Sun *et al.,* Flexible high-performance carbon nanotube integrated circuits, *Nature nanotechnology*. **6**, 156–161 (2011), doi:10.1038/nnano.2011.1.
82. N. Patil *et al.,* Wafer-Scale Growth and Transfer of Aligned Single-Walled Carbon Nanotubes, *IEEE Trans. Nanotechnology*. **8**, 498–504 (2009), doi:10.1109/TNANO.2009.2016562.
83. Y. Li, Q. Yang, M. Li, Y. Song, Rate-dependent interface capture beyond the coffee-ring effect, *Scientific reports*. **6**, 24628 (2016), doi:10.1038/srep24628.
84. R. D. Deegan, Capillary flow as the cause of ring strains from dried liquid drops, *Nature*. **389**, 827–829 (1997), doi:10.1038/39827.
85. P. J. Yunker, T. Still, M. A. Lohr, A. G. Yodh, Suppression of the coffee-ring effect by shape-dependent capillary interactions, *Nature*. **476**, 308–311 (2011), doi:10.1038/nature10344.
86. R. Abdelaziz *et al.,* Green chemistry and nanofabrication in a levitated Leidenfrost drop, *Nature communications*. **4**, 2400 (2013), doi:10.1038/ncomms3400.
87. M. Elbahri *et al.,* Underwater Leidenfrost nanochemistry for creation of size-tailored zinc peroxide cancer nanotherapeutics, *Nature communications*. **8**, 15319 (2017), doi:10.1038/ncomms15319.
88. M. Li, Parallel measurement of conductive and convective thermal transport of micro/nanowires based on Raman mapping, *Appl. Phys. Lett.* **106**, 253108 (2015), doi:10.1063/1.4923189.
89. Q.-J. Lu, Influence of Temperature on the Conductivity of Multi-walled Carbon Nanotube Interconnects, *Chinese Phys. Lett.* **32**, 47305 (2015), doi:10.1088/0256-307X/32/4/047305.
90. S. Yamashita, Multiwavelength erbium-doped fibre laser using intracavity etalon and cooled by liquid nitrogen, *Electron. Lett.* **32**, 1298 (1996), doi:10.1049/el:19960832.
91. K. Singh, *World Congress on Engineering and Computer Science*, *WCECS 2016 proceedings : conference period and venue: 19-21 October 2016 : Clark Kerr Campus, UC Berkeley, San Francisco Bay Area, USA* (IAENG International Association of Engineers, Hong Kong, 2016).
92. K. Singh, Performance and analysis of temperature dependent multi-walled carbon nanotubes as global interconnects at different technology nodes, *J Comput Electron*. **14**, 469–476 (2015), doi:10.1007/s10825-015-0667-3.
93. V. Datsyuk, Chemical oxidation of multiwalled carbon nanotubes, *Carbon*. **46**, 833–840 (2008), doi:10.1016/j.carbon.2008.02.012.
94. I. D. Rosca, Oxidation of multiwalled carbon nanotubes by nitric acid, *Carbon*. **43**, 3124–3131 (2005), doi:10.1016/j.carbon.2005.06.019.

95. J. Lee, Measurement of the dispersion stability of pristine and surface-modified multiwalled carbon nanotubes in various nonpolar and polar solvents, *Meas. Sci. Technol.* **18**, 3707–3712 (2007), doi:10.1088/0957-0233/18/12/005.
96. F. Xin, Decoration of carbon nanotubes with silver nanoparticles for advanced CNT/polymer nanocomposites, *Composites Part A: Applied Science and Manufacturing*. **42**, 961–967 (2011), doi:10.1016/j.compositesa.2011.03.024.
97. E. J. Sandouk, Multistate resistive switching in silver nanoparticle films, *Science and technology of advanced materials*. **16**, 45004 (2015), doi:10.1088/1468-6996/16/4/045004.
98. C. C. Kuo *et al.,* Galvanic Effect of Au–Ag Electrodes for Conductive Bridging Resistive Switching Memory, *IEEE Electron Device Lett.* **36**, 1321–1324 (2015), doi:10.1109/LED.2015.2496303.
99. M. Zohrabi, M. R. Mohebbifar, Electric Field Enhancement Around Gold Tip Optical Antenna, *Plasmonics*. **10**, 887–892 (2015), doi:10.1007/s11468-014-9876-z.
100. I. Valov *et al.,* Nanobatteries in redox-based resistive switches require extension of memristor theory, *Nature communications*. **4**, 1771 (2013), doi:10.1038/ncomms2784.
101. S. K. Saha, Observation of giant dielectric constant in an assembly of ultrafine Ag particles, *Phys. Rev. B*. **69** (2004), doi:10.1103/PhysRevB.69.125416.
102. A. Vahl, Single target sputter deposition of alloy nanoparticles with adjustable composition via a gas aggregation cluster source, *Nanotechnology*. **28**, 175703 (2017), doi:10.1088/1361-6528/aa66ef.
103. S. Tappertzhofen, Generic relevance of counter charges for cation-based nanoscale resistive switching memories, *ACS nano*. **7**, 6396–6402 (2013), doi:10.1021/nn4026614.
104. B. Mohammad *et al.,* State of the art of metal oxide memristor devices, *Nanotechnology Reviews*. **5** (2016), doi:10.1515/ntrev-2015-0029.
105. O. Lupan *et al.,* Single and networked CuO nanowires for highly sensitive p-type semiconductor gas sensor applications, *Phys. Status Solidi RRL*. **10**, 260–266 (2016), doi:10.1002/pssr.201510414.
106. S.-J. Choi, P. Bennett, D. Lee, J. Bokor, Highly uniform carbon nanotube nanomesh network transistors, *Nano Res.* **8**, 1320–1326 (2015), doi:10.1007/s12274-014-0623-8.
107. S. Kim, J. Yoon, H.-D. Kim, S.-J. Choi, Carbon Nanotube Synaptic Transistor Network for Pattern Recognition, *ACS applied materials & interfaces*. **7**, 25479–25486 (2015), doi:10.1021/acsami.5b08541.